2013-12-18

Advanced Fiber Reinforced Composites as Confining Systems for RC Columns

Adane Z. Abegaz
University of Miami, adane.zeleke@gmail.com

UNIVERSITY OF MIAMI

ADVANCED FIBER REINFORCED COMPOSITES AS CONFINING SYSTEMS FOR RC COLUMNS

By

Adane Z. Abegaz

A DISSERTATION

Submitted to the Faculty
of the University of Miami
in partial fulfillment of the requirements for
the degree of Doctor of Philosophy

Coral Gables, Florida

December 2013

UNIVERSITY OF MIAMI

A dissertation submitted in partial fulfillment of
the requirements for the degree of
Doctor of Philosophy

ADVANCED FIBER REINFORCED COMPOSITES AS CONFINING SYSTEMS FOR RC COLUMNS

Adane Z. Abegaz

Approved:

_____ Wimal Suaris, Ph.D. Associate Professor, Dept. of Civil, Architectural, and Environmental Engineering	_____ Francisco De Caso, Ph.D. Lecturer, Dept. of Civil, Architectural, and Environmental Engineering
_____ Antonio Nanni, Ph.D. Professor, Dept. of Civil, Architectural, and Environmental Engineering	_____ Matthew Trussoni, Ph.D. Assistant Professor in practice, Dept. of Civil, Architectural, and Environmental Engineering
_____ Mohamed Fahmy, Ph.D. Lecturer, Dept. of Industrial Engineering	_____ M. Brian Blake, Ph.D. Dean of the Graduate School

ABEGAZ, ADANE (Ph.D., Civil Engineering)
Advanced Fiber Reinforced Composites as Confining Systems for RC Columns (December 2013)

Abstract of a dissertation at the University of Miami.

Dissertation supervised by Associate Professor Wimal Suaris.
No. of pages in text. (160)

Composite materials are becoming more frequently used in civil engineering structures. One of the most practical applications of these materials is strengthening of reinforced concrete columns by means of confinement with fiber composite sheets with principal advantages of high strength-to-weight ratio, good fatigue properties, non-corroding characteristics, and the easier installation procedure. Over the past few decades a number of composites have emerged as viable solutions to address the issue of potential durability problems in the use of steel as a retrofitting and strengthening system, among which Fiber Reinforced Polymer (FRP) and Fabric Reinforced Cementitious Matrix (FRCM) are the most widely used ones. The maximum efficiency of confining systems using composite materials is reached in case of columns with circular cross-section and is explained by the fact that the entire section of the column is confined uniformly while rectangular sections are less efficient as the confinement action is mostly limited to the corners.

In the first study of this research work, a total of 27 square and rectangular Glass Fiber Reinforced Polymer (GFRP) jackets were tested under hydrostatic load conditions using the Investigation of Circumferential strain Experimental (ICE) methodology, to better understand the behavior of GFRP jackets' properties including the study of the influence

of cross-section aspect ratio, and laminate thickness on the strain properties of GFRP composite laminates. The ICE methodology was used to understand the variations in strains developed and lateral deformations in GFRP jackets due to cross-sectional shape (aspect ratio), and laminate thicknesses. Tests conducted with two, four and six plies of rectangular and square GFRP jackets showed considerably smaller values of hoop strains when compared with the flat coupon specimens.

The second part of this research work reports results of experimental investigations on eight column specimens, into the use and application of glass fiber reinforced polymers. In this study the effect of GFRP confinement on the axial strength and axial deformation of small reinforced concrete (RC) columns with different cross-sectional shapes was investigated. The effect of GFRP wrapping was more significant in enhancing axial deformability (i.e. axial strain) than axial strength. The GFRP confinement was also more effective in square columns than rectangular columns.

In the third study, polyparaphenylene-benzobisethiazole (PBO) - FRCM was studied. A total of 27 columns were tested to investigate and quantify the enhancement in strength and ductility as a function of cross-sectional shapes and number of layers. Rectangular, square, and circular specimens with the same cross-sectional area and slenderness ratio were considered to properly isolate the effect of shape on the confinement effectiveness. In addition to the cross-sectional shape, columns with one and four layers of PBO-FRCM wrapping were tested to investigate their effect.

Experimental results indicate that PBO-FRCM wrapping can significantly enhance the load bearing capacity and ductility of RC columns subjected to a monotonic axial compressive load, with the highest improvement obtained for circular cross-sections. Similar to study 2, the increase in axial deformation due to confinement was found to be greater than the increase in axial strength for all cross sections and PBO-FRCM layers.

Acknowledgments

Undertaking this Ph.D. research has truly been a life-changing experience for me and it would not have been possible without the support that I received from many people. There are no proper words to convey my deep and sincere gratitude and respect for the people who contributed to the completion of this dissertation report, to only some of whom it is possible to give particular mention here. I would like to first say a big "Thank you" to my advisor, Dr. Wimal Suaris, for the support and encouragement he extended to me throughout this long journey. This thesis would not have been possible without his help, support, and patience. I am very grateful to him for believing in me and allowing me to work under his supervision. I am grateful to Dr. Rodrigo Mora for believing in me and allowing me to embark on a Ph.D. journey at the University of Miami in the first place.

My sincere thanks must also go to Dr. Antonio Nanni, Dr. Francisco De Caso, and Dr. Mohamed Fahmy for their kindness and serving on my dissertation committee.

I am most grateful to Dr. Antonio Nanni, for his help and encouragement from start to finish of my journey. He was generous in extending his support at both good and not so good times. He was always there helping me overcome every challenge. I truly can't thank him enough for being more than a professor to me. All the materials and human power needed for the experimental work done were made available because of him. I am very thankful to him for lending me his expertise every step of the way during the research work. He was there to help when I needed a professor assigned; to pick a topic of research and encouraging me to stick to my interests; for collecting components/materials and developing test matrices for each of the studies; during the

experiment, commenting and helping in developing the test methodologies; helping me understand the data processing phase; and through his meticulous reading, helping to make my report better. In short, Dr. Nanni contributed to every part of this research work; for that I am truly grateful.

Apart from being a member of my dissertation committee, Dr. Francisco De Caso has extended his support to this research work both in the lab and outside the lab. He graciously helped me extend the idea of using the ICE methodology he developed in his research for non-cylindrical GFRP jackets. I am very grateful to him for extending his expertise in the matter, for helping me develop the test matrix, and for his help in making sure I had the necessary components of the ICE methodology rig on time. His help made this study possible. I also thank him for reviewing my data analysis and dissertation report.

I am also thankful to Dr. De Luca for his unlimited help inside and outside of the lab in the GFRP and FRCM studies. He was also helpful in the writing process.

To the graduate students, and those who have already graduated since, at the University of Miami: Hany, Steven, Derek, Dr. Loreto, Diego, Diana, and the many more whose names are not listed here, thank you for offering me advice, and supporting me through this entire process. I am also grateful for the help I received from undergraduate students at the University of Miami, and transfer graduate students from Spain. I am most grateful to the laboratory technicians at the Structures lab at the University of Miami for lending me their expertise and intuition to my scientific and technical problems in the lab. Maria and Lizett, you were so generous in your help throughout the years. Thank you so much.

A big “Thank you” to my friend Dr. Agerneh Dagnew for his support and encouragement. I also thank him for hosting me during my stay in Boston, and for his generous support.

I gratefully acknowledge the funding received to undertake this Ph.D. research from the University of Miami, the NSF through the support provided to the Industry/University Center CICI, and its industrial member Ruredil S.p.A. of San Donato Milanese, Italy.

A very special “Thank you” to my friends Sisay Techan and Asrat Techan for their love and unlimited support throughout my stay in Miami and New Jersey. They opened their home and were more than friends to me. Chero and Asre you were too nice and I am sorry that I am not able to thank you enough, for there is no way to describe your generosity. Stay blessed!

And finally, I am greatly indebted to my Parents, two brothers and two sisters to their love and guidance, without which I would not have made it through. To my friends back in Ethiopia, friends in New Jersey and all over the US thank you for your help and encouragement throughout the years.

Adane Z. Abegaz

Table of Contents

List of Tables

List of Figures

Nomenclature

Symbol	Definition
A_c	net cross-sectional area of the compression member,
A_e	area of the effectively confined concrete
A_f	area of grid reinforcement by unit width
A_g	gross cross-sectional area of the compression member
A_s	area of longitudinal steel reinforcement
b	short side dimension of the compression member with rectangular cross section
D	diameter of the compression member
E_c	modulus of elasticity of concrete
E_f	tensile modulus of elasticity of the cracked FRCM composite material specimen
f'_c	specified compressive strength of concrete
f_c	compressive stress in concrete
f'_{cc}	maximum compressive strength of confined concrete
f'_{co}	compressive strength of unconfined concrete
f_l	maximum confining pressure due to FRCM jacket
f_s	Tensile stress in the reinforcement steel
f_y	steel tensile yield strength
h	long side dimension of the compression member with rectangular cross section
K_a	efficiency factor for FRCM reinforcement in the determination of f'_{cc}

K_b	efficiency factor for FRCM reinforcement in the determination of ε_{ccu}
n	number of layers of reinforcement
P_{peak}	Peak load
Δ_{peak}	Axial deformation at peak load
ε_{ccu}	ultimate compressive strain of confined concrete
ε_{fe}	effective tensile strain level in FRCM composite material attained at failure
ε_{fi}	FRCM tensile strain at i^{th} data point
ε_{fu}	ultimate tensile strain of the FRCM composite material
ε_t	tensile strain in the reinforcement
ε_s	Tensile strain in the reinforcement steel
ε_{sy}	Yield tensile strength of the reinforcement steel
$\sigma_{c,peak}$	Concrete axial stress at peak load
σ_{fu}	Standard deviation of the ultimate tensile strength of the FRCM composite material
Ψ_f	additional strength reduction factor for FRCM confined concrete
ϕ_m	Strength reduction factor for flexure
ρ_g	Ratio of the area of longitudinal steel reinforcement to the cross-sectional area of a compression member (A_s/bh).

CHAPTER I

INTRODUCTION

Background

In the past two hundred or so years, structural steel and reinforced concrete have emerged as leading construction materials, and most modern urban landscapes are now defined largely by these two materials. Engineers are looking for new materials that can be used to prolong and extend the service life of existing structures while also enabling the design and construction of durable new structures. Over the past few decades, different kinds of composites have emerged as practical materials for a number of structural engineering applications. Since the early 1990's, interest in the use of FRP materials for structures has increased steadily, and there are currently many field applications of FRPs in structures around the world. Some of the more common FRP applications in civil engineering structures include: Externally-bonded FRP plates, sheets, and wraps for strengthening of reinforced concrete, steel, aluminum, and timber structural members; FRP bars, rods, and tendons for internal reinforcement of concrete structures; all-FRP structures; and FRP hybrid structures. The high tensile strengths of FRP composites makes them an ideal alternative to longitudinal reinforcing elements, for structural concrete members subjected mainly to flexure (Taranu Nicolae et al., 2008).

Composites are defined as materials created by the combination of two or more materials, on a macroscopic scale, to form a new material with enhanced properties that are superior to those of the individual constituents alone. The term composite could mean almost

anything if taken at face value, since all materials are composed of dissimilar subunits if examined at close enough detail. In modern engineering materials, the term usually refers to a matrix material that is reinforced with fibers. The focus in the present work is on those composite materials that are currently used in structural engineering applications: Fiber Reinforced Polymer (FRP) and Fabric Reinforced Cementitious Matrix (FRCM) systems.

Currently, composites have gained wide application in flexural strengthening, shear strengthening and confining reinforcement as external reinforcements of reinforced concrete structures. Existing RC structures may require strengthening for a variety of reasons. For example, it is often desirable to increase the loading to which a structure is subjected, as when a bridge must carry heavier traffic or when a building must be used for purposes other than those for which it was originally intended. It may also be necessary to strengthen old RC structures as a result of new code requirements or because of damage to the structure as a result of environmental stresses. Within the framework of the general problem of strengthening RC structures, there exists the issue of strengthening RC columns.

The strengthening of RC columns represents an engineering challenge, which, like all engineering challenges, involves several solutions, each having its own advantages and disadvantages and its own limits to its applicability and practicality. For instance, it is possible to remove deficient columns and construct new ones in their place. Another solution is to place reinforcing steel and formwork around a column and pour additional concrete (i.e. cross-section enlargement) (Picher et al., 1996). Yet another solution is to use a jacketing scheme wherein the column is encased by some reinforcing material.

Traditionally, steel has been used to jacket RC columns, but recently FRP has become a viable alternative to steel jacketing for it has high resistance to corrosion, high strength-to-weight ratio, easier installation procedure, and is electromagnetically transparent, a behavior desirable in some applications. The polyparaphenylene-benzobisethiazole (PBO)-FRCM composite system considered in the present study offers the following advantages over an epoxy-resin based FRP system: low cost, high fire resistance, resistance to humidity, recyclability, applicability on wet substrate; being a cement-based product, easier application even on rough or irregular surfaces; easy handling; workability; and easy cleanup of tools used for application with water. Composites like other construction materials come with their disadvantages like: high initial cost (compared to steel reinforcement); susceptibility to mechanical damage; susceptibility to fire (FRP without intumescent insulation); longer load transfer (lap) lengths, poor shear strength, low strain to failure, and poor bond between fiber and cement based matrix. Below each of the advanced composite systems are defined.

Fiber Reinforced Polymer (FRP)

An FRP is a specific type of two-component system consisting of high strength fibers embedded in a polymer matrix. The fibers provide the strength and stiffness of an FRP while the matrix is the binder that plays many important roles like binding the fibers together; protecting the fibers from harsh environment; transferring forces between the individual fibers. The matrix phase can be made of polyesters, vinyl esters, or epoxies and the fiber phase can be of glass, carbon or aramid. The FRP considered in the present study has unidirectional glass fibers embedded in epoxy resin manufactured through a wet lay-up process.

Glass fibers are the most inexpensive, and consequently one of the most commonly used fibers in structural engineering applications. There are several different grades available, but the most common are E-glass and the more expensive, but stronger, S-glass. Glass fibers are characterized by their high strength, moderate modulus of elasticity and density, and by their low thermal conductivity and high strain compared to carbon. They are often chosen for structural applications that can tolerate the larger deflections resulting from the comparatively low elastic modulus of the glass fibers. Fig. 1-1 presents the stress-strain curves for the different continuous fibers used in making FRP for engineering applications compared to steel products.

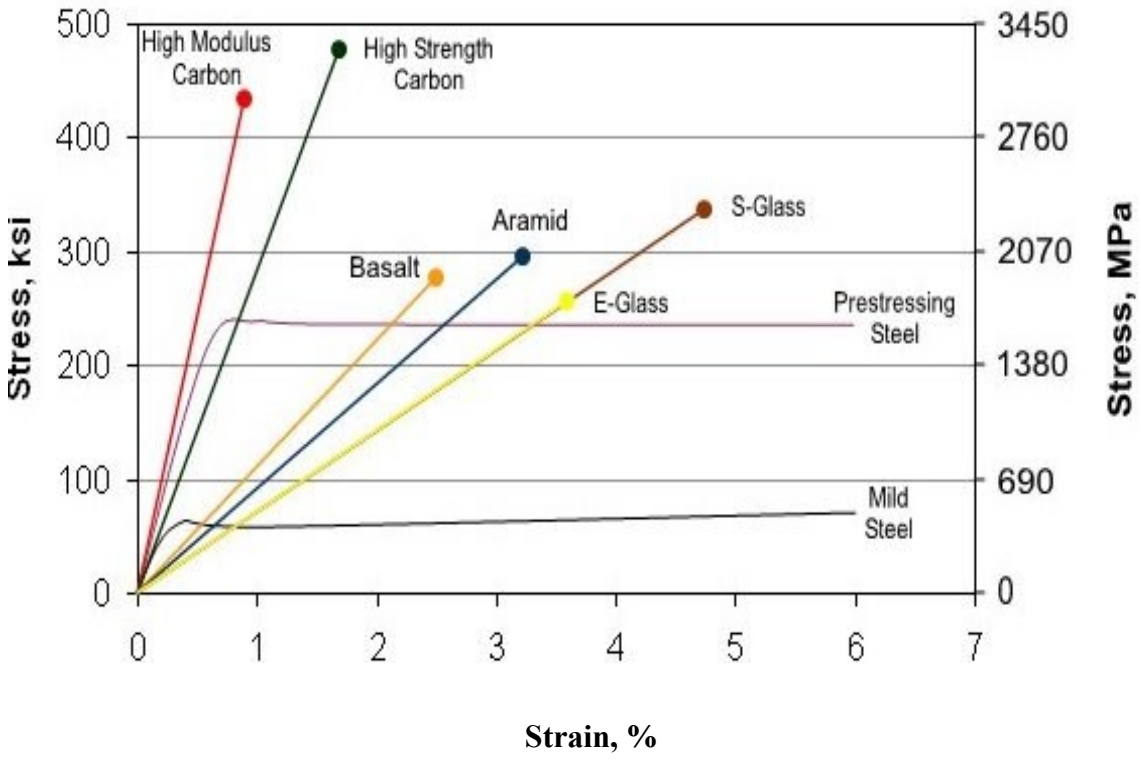

Fig 1-1: Typical stress-strain curves for common fibers (Taerwe, 1995)

Apart from the type of constituent materials used, the overall material properties depend also on the mechanical properties of the matrix, the fiber volume fraction, the fiber cross-sectional area, the orientation of the fibers within the matrix, and the method of manufacturing [ACI 440]. Fig. 1-2 shows typical stress-strain curves for fibers, matrices, and the FRP materials that result from the combination of fibers and matrix.

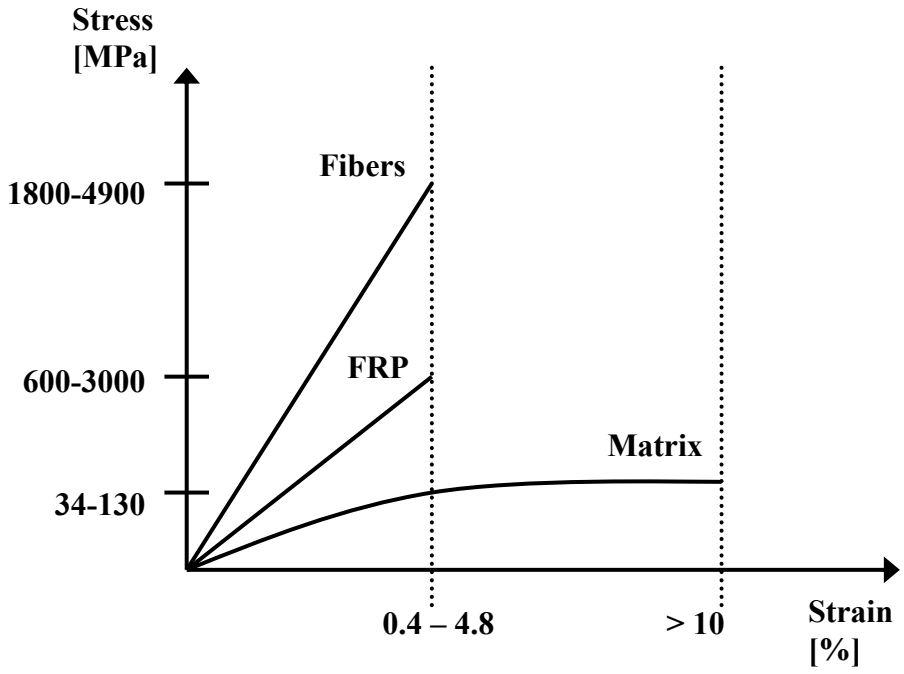

Fig. 1-2: Stress-strain relationships for typical fibers, matrix, and FRP (ISIS 2006)

Fabric Reinforced Cementitious Matrix (FRCM)

Fabric Reinforced Cementitious Matrix (FRCM) was proposed as an alternative material to FRP, by replacing the organic resin with inorganic cement based mortar. FRCMs are composite systems composed of two different phases with different physical and mechanical properties, so as to give the composite different properties than those of its

constituents. The reinforcement phase is an anisotropic material whilst the cementitious matrix can be considered, at least in the most common cases, a continuous isotrope. Thus FRCMs are composite materials, heterogeneous and anisotropic, having prevalently slip behaviors until collapse but with high durability in the face of high temperatures, and fire exposure (Arboleda et al., 2012). The matrix phase in FRCM systems is cement based inorganic binder which consists of fine-grained aggregate, with chemical additives for better workability and mechanical properties. The present research work uses a stabilized cementitious mortar matrix.

FRCM can be reinforced by using ultra-high-strength fabrics, such as the polyparaphenylene-benzobisethiazole (PBO), shown in Fig. 1-3 which was used in the present study.

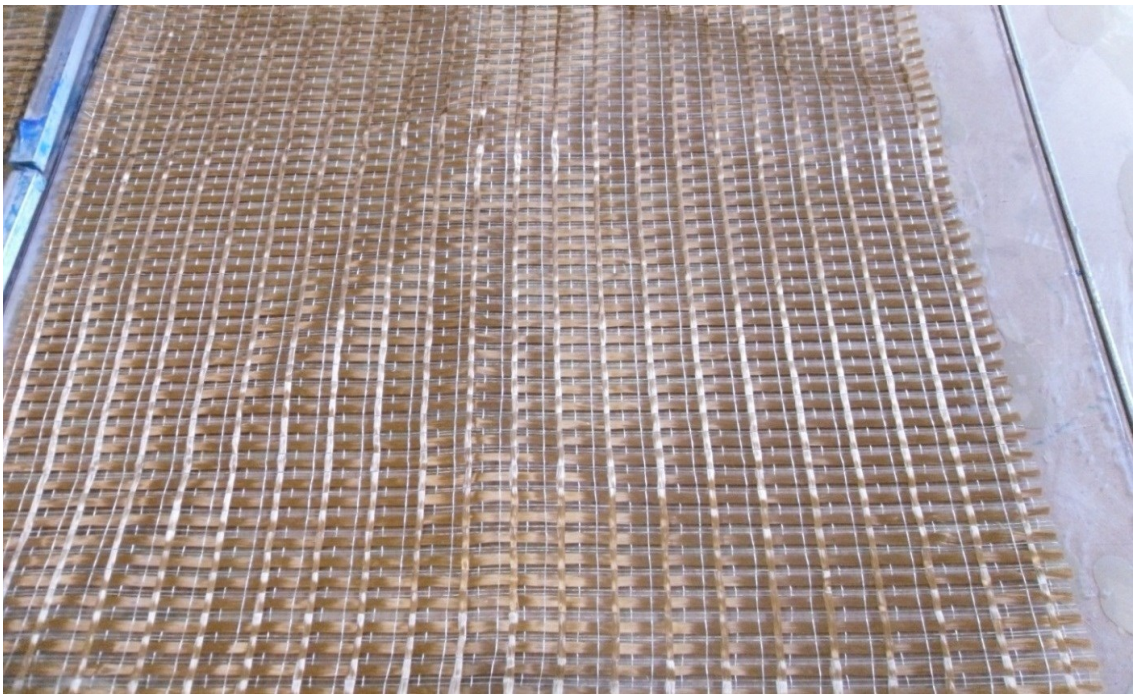

Fig. 1-3: PBO fabric

The PBO fabric used in this study is made of 10 mm and 20 mm spaced roving. The free space between rovings is roughly 5 mm and 15 mm, respectively, and the nominal thickness of the fibers in each direction is 0.046 mm and 0.011 mm, respectively. Fig. 1-4 shows the tensile strength vs. strain property of the high strength zylon (PBO) fabrics, in comparison with other structural fibers. The plot demonstrates that the PBO fabrics have the highest strength among all the widely used fibers and comparable stiffness to carbon fibers.

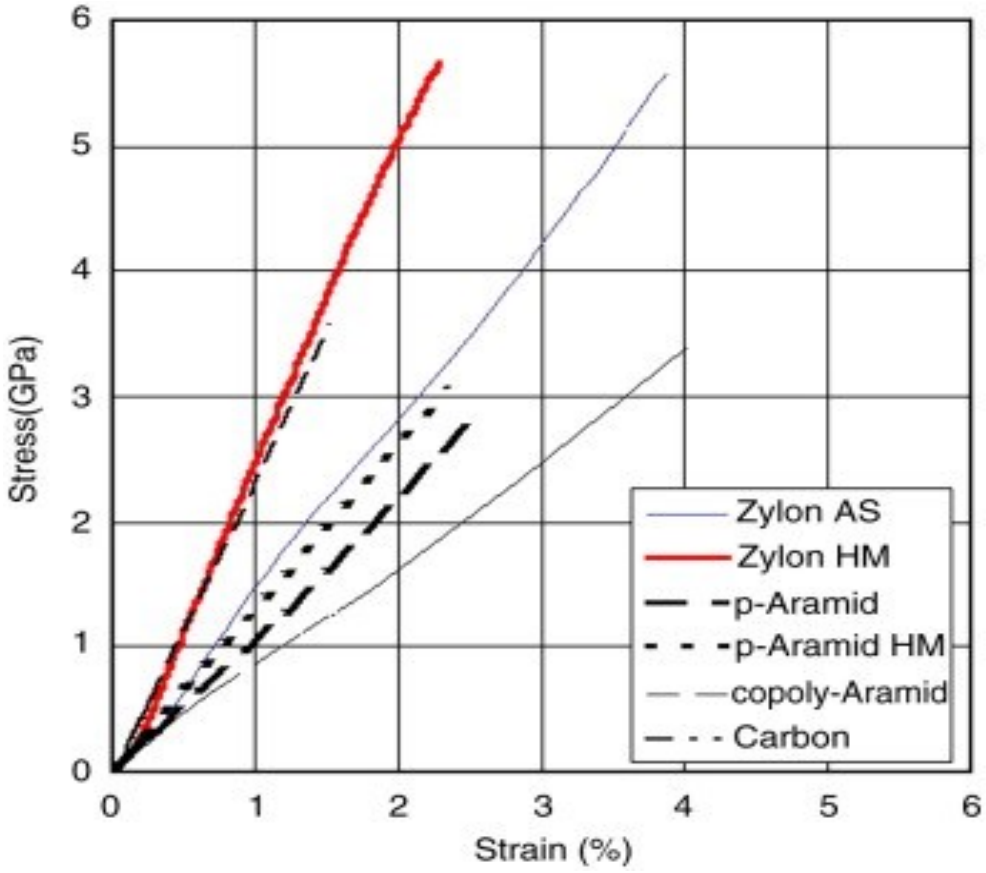

Fig. 1-4: Tensile strength vs. elongation relationships of zylon (PBO), aramid and carbon fibers (Toyobo, 2005)

The stress-strain graph for the PBO coupons by Arboleda et al. (2012) in Fig. 1-5 shows the variability of behavior we see over the sample size, but indicates a merging trend of

some of the characteristic quantities. Where GT 1 to GT 5 are different test repetitions of the same coupon specimens. An idealized tensile stress versus strain curve of PBO-FRCM coupon specimens is provided in Fig. 1-6 which was used for analyzing the performance of PBO-FRCM confined RC columns, presented in chapter IV of this dissertation.

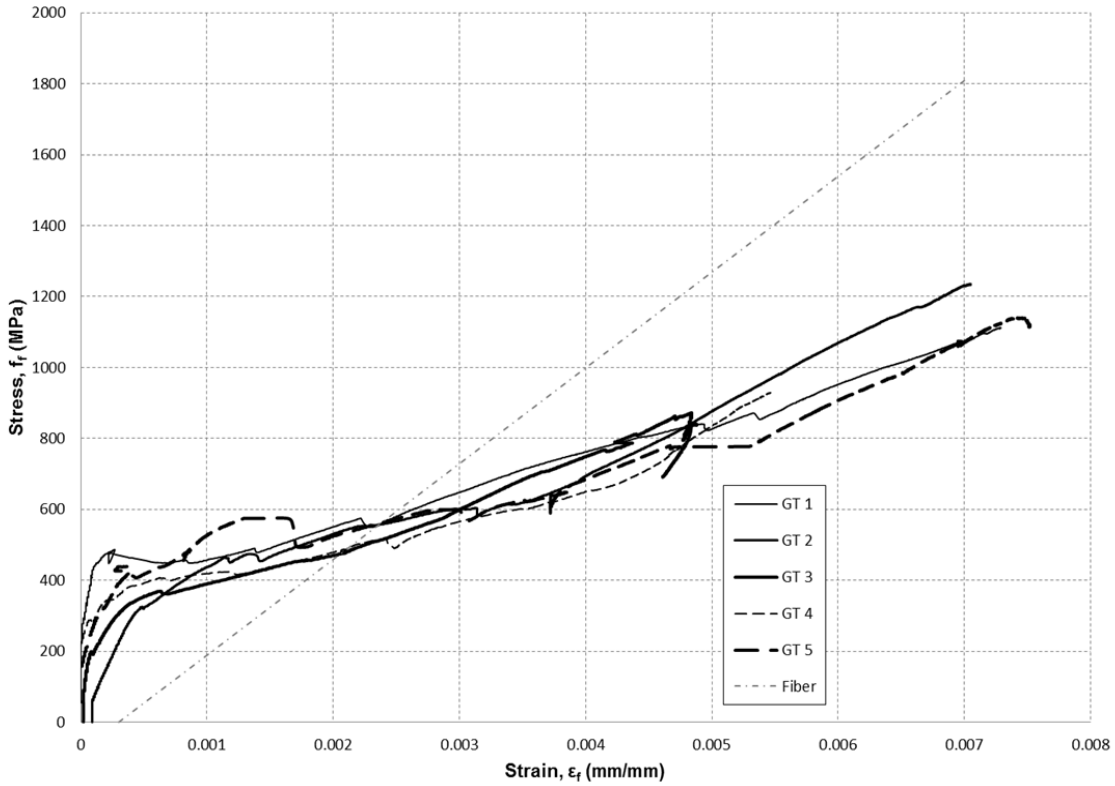

Fig. 1-5: Stress-strain curves for PBO-FRCM tension specimens

(Arboleda et al., 2012)

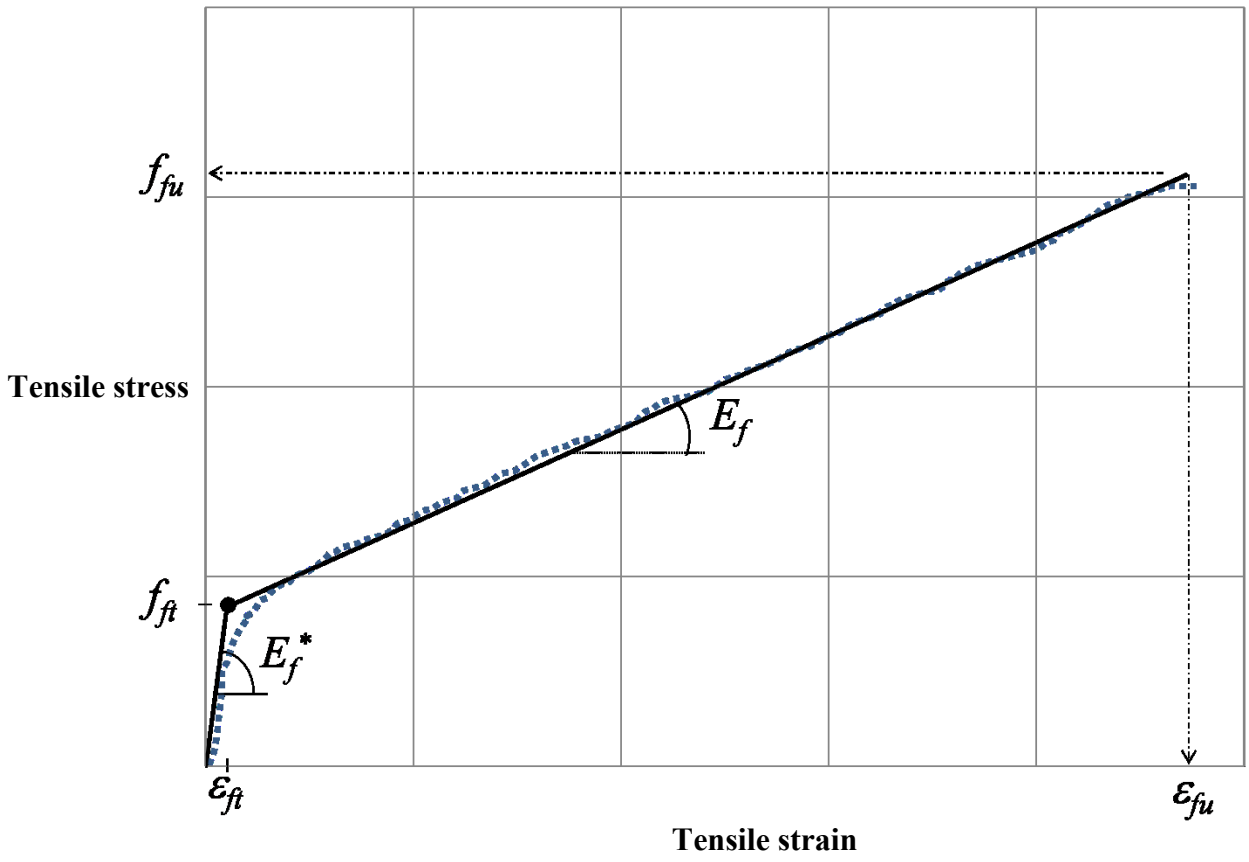

Fig. 1-6: Idealized bi-linear tensile stress vs. strain curve of an PBO-FRCM coupon specimens (Arboleda et al., 2012)

Passive confinement action of FRP jacket

Wrapping RC columns to confine the concrete is referred to as jacketing. Jacketing an RC column with FRP primarily improves column performance, not because the jacket itself carries some fraction of the axial load applied to the column, but rather because it provides passive lateral confining pressure to the column (Nanni et al., 1995). When a concrete cylinder confined by an FRP jacket is subjected to an axial compressive stress, it expands laterally. This expansion is confined by the FRP jacket which is loaded in tension in the hoop direction. The confining pressure provided by the FRP jacket increases continuously with the lateral strain of concrete because of the linear elastic

stress–strain behavior of FRP, in contrast to steel-confined concrete in which the confining pressure remains constant when the steel is in plastic flow. Failure of FRP confined concrete generally occurs when the hoop rupture strength of the FRP jacket is reached. The confining action in FRP-confined concrete can be schematically illustrated in Fig. 1-7.

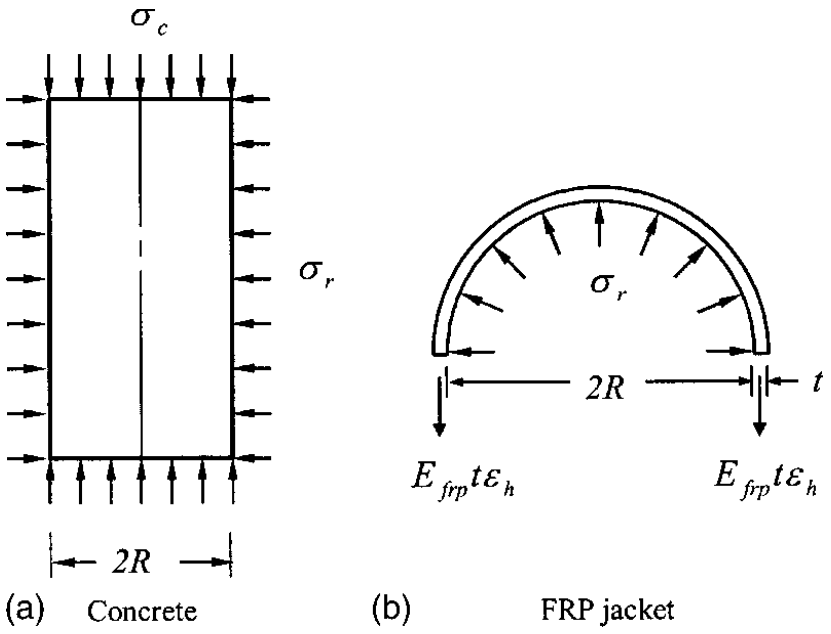

Fig. 1-7: Confinement action of FRP

The lateral confining pressure can be derived using the stress equilibrium and radial displacement compatibility considerations between the concrete core and the jacket.

The ultimate lateral confining pressure exerted by the FRP is given by:

$$f_l = 2\frac{E_{frp}*\varepsilon_{frp,rup}*t}{D} \qquad \text{(equation 1.1)}$$

Where $\varepsilon_{frp,rup}$ is hoop strain of FRP at rupture; t is the total FRP thickness; R is the radius of the confined concrete column; and E_{frp} is the young's modulus of elasticity of the FRP laminate.

For non-circular cross-sections, f_l corresponds to the maximum confining pressure of an equivalent circular cross-section with diameter *D* equal to the diagonal of the rectangular cross-section [ACI 440].

This confining pressure places the concrete in a tri-axial state of stress, altering the load - deformation characteristics of the concrete. High levels of confining pressure enable concrete to sustain both greater axial loads and greater ultimate axial strain (Toutanji et al. (2010)). FRP jackets have shown to enhance both strength and ductility of concrete columns by providing confinement to the concrete core (Nanni et al. (1995)).

Dissertation Outline

This dissertation is presented in five sections. The introductory chapter is followed by chapter II which presents the characterization of non-circular GFRP laminates through Investigation of Circumferential strain Experimental (ICE) methodology. Chapter III presents the study on strengthening of RC columns with GFRP jackets. Chapter IV describes the experimental work done on RC columns wrapped with PBO-FRCM composite systems. Finally, chapter V lists the conclusions drawn from each study, and the proposed recommendations for future work.

Dissertation Objectives

A number of researchers have conducted both numerical and experimental investigations on characterizing the behavior of GFRP strengthened circular columns subjected to pure axial compression. The results of such research works have wide applicability with regard to circular bridge piers but, there is a greater need to understand the behavior of GFRP-wrapped rectangular and square columns, as the vast majority of existing columns in buildings have either rectangular or square cross-sections. Such research will help the industry address the retrofitting and strengthening need to preserve the integrity and functionality of building infrastructures.

The present research focuses on this very idea of understanding the effect of passive confinement to columns with different cross-sectional shapes through the application of GFRP and PBO-FRCM composite systems, when subjected to pure axial compressive loads. The main objectives of the study are:

- Understand strain in FRP jackets;
- Validate FRP confinement strengthening of non-circular columns;
- Provide numerical data for the proposed PBO-FRCM composite system.

The study was designed under three phases to achieve the aforementioned objectives, where specific objectives for each phase include:

Study 1:

- understand the behavior of non-circular GFRP jackets under hydrostatic loading;
- study the influence of cross-section geometry;
- study the effect of laminate thickness (i.e. multiple layers of strengthening) on the behavior of non-circular GFRP jackets under hydrostatic loading.

Study 2:

- understand the effect of cross-sectional shape on the confinement effectiveness of GFRP wrapped RC columns;
- understand the size effect on the confinement effectiveness of GFRP wrapped RC columns;
- compare existing models of GFRP confinement with the present experimental results, for non-cylindrical columns.

Study 3:

- explore the effectiveness of the external PBO-FRCM confinement on improving the axial strength and axial deformation of RC columns;
- understand the effect of cross-sectional shape on the confinement effectiveness of the PBO-FRCM on RC columns;
- understand the effect of number of PBO-FRCM layers on the confinement effectiveness of the PBO-FRCM on RC columns.

Research Significance

Reinforced concrete columns support a variety of structures, for example bridge decks and floor slabs, and can act as piers or piles. Columns also vary in cross-sectional shape depending on their application within a situation, although typically they are either circular or rectangular. Damage to reinforced concrete columns may occur due to a variety of reasons including aggressive environments, and the damages incurred may include slight cracks without damage to reinforcement, superficial damage in the concrete without damage to reinforcement, buckling of reinforcement or rupture of ties. Based on the degree of damage, jacketing of the columns may be recommended as a viable solution

to strengthen and/or retrofit RC columns. Confinement of non-cylindrical columns using composites enhances concrete strength and ultimate strain, but its effectiveness is not as effective as that of a circular cross-section. Far few studies have been done to understand the effect of cross-sectional shape and size on confinement effectiveness of FRP composites in RC columns. In this study an attempt is made to understand the effect of shape and size on confinement effectiveness of GFRP composites. A new approach, ICE methodology, to understand the tensile strain behavior of non-cylindrical GFRP jackets under hydrostatic pressure is also presented.

The construction industry is still in continuous search of innovative composite systems for confining RC columns. For the industry to use advanced composites, like PBO-FRCM strengthening systems for civil infrastructure, it is important to also understand how they behave in their respective applications. This research sheds light on the application of PBO-FRCM composite systems, and its effectiveness in enhancing the axial strength and strain of RC columns with different cross-sectional shapes. It also presents an opportunity to look in to ways of improving the confining system.

CHAPTER II

STUDY 1: STRAIN CHARCTERIZATION OF NON-CIRCULAR GFRP JACKETS USING ICE METHODOLOGY

Background

Jacketing confines concrete, and hence increases the strength and ductility of jacketed columns, as reported in a number of studies (Wang et al. (2008), Mirmiran et al. (1998), Rocca et al. (2008), Toutanji et al. (2009), Saadatmanesh et al. (1994)). When a concrete cylinder confined by an FRP jacket is subjected to axial compression, it expands laterally. This expansion is confined by the FRP jacket which is loaded in tension in the hoop direction. The confining pressure provided by the FRP jacket increases continuously with the lateral strain of concrete because of the linear elastic stress–strain behavior of FRP, in contrast to steel-confined concrete in which the confining pressure remains constant when the steel is in plastic flow. Failure of FRP confined concrete generally occurs when the hoop rupture strength of the FRP jacket is reached (Teng et al. (2009)).

The results of earlier research conducted by Mirmiran et al. (1998) and subsequent studies by a number of researchers (Wang et al. (2008), Yang et al. (2004)) suggest that the confinement effectiveness of FRP jackets in concrete columns depends on several parameters which include cross-sectional shape, corner radius (chamfer), and number of FRP layers (jacket thickness). A significant amount of research has been devoted to circular columns that have been retrofitted with FRP, but much less is known about non-circular FRP-confined RC columns in which the concrete is non-uniformly confined and

the effectiveness of confinement is much reduced (Rochette et al. (2000)), Tan (2002), Wang et al. (2008)).

Design of FRP confined concrete columns requires an accurate estimate of the performance enhancement due to the confinement mechanism, which in turn requires a relatively accurate understanding of the behavior of the confining material and the effect of a number of parameters on the confining behavior of the material used. A number of studies (Nielsen et al. (1994), Teng et al. (2004), Fam et al. (2001)) have been conducted to better understand the properties of confining materials, but most of them involve the use of concrete. In the present study, a total of 27 square and rectangular GFRP jackets (nine 127 mm. by 127 mm.; nine 101.6 mm by 152.4 mm; and nine 101.6 mm by 203.2 mm) were tested under hydrostatic loading conditions using the ICE methodology, to better understand the behavior of GFRP jackets' properties by including the study of the influence of aspect ratio, and total jacket thickness. The research uses the ICE methodology developed by previous researchers at the University of Miami for FRP characterization, which was based on the research presented in a study which was developed to characterize a new type of Fiber Reinforced Cement-based matrix (FRC) composite system for confinement applications. It concluded that composites with brittle matrices are not adequately characterized with the existing tensile flat coupon test method, and the ICE methodology was presented as a candidate test method (De Caso et al. (2011)). The ICE methodology uses the unique behavior of water, which expands when it changes its state from liquid to solid, to understand the variations in strains and lateral deformations in GFRP, by avoiding a number of factors like, uneven pressure exerted by the concrete resulting from its cracking, which are believed to cause premature

failures. The characterization technique provided a chance for a relatively accurate prediction of the characteristics of the confining material in the previous work done by De Caso et al. (2011) on circular specimens, in terms of predicting the actual rupture ultimate strain.

The ICE methodology proposed and validated for circular FRP jackets by De Caso et al. (2011) possesses compelling features, including simplicity of test configuration in terms of machining and minimum number of parts, no undesirable end conditions, and readily available equipment. Its novelty originates from the lack of moving parts or complex fixtures to transfer load to the specimen, and simultaneously has the ability to apply a truly hydrostatic load and thus avoids the uncertainties we might have from the concrete technique. The work presented here sets the first stage of understanding property of non-cylindrical GFRP jackets under hydrostatic loading condition extending the work done by De Caso et al. (2011); and if applicable, understand how much of the reduction in confining capability of the GFRP Jacket is a contribution of the effect of the shape of confined cross-section and the number of plies.

Methodology

A number of researchers (Teng et al. (2004), Spoelstra et al. (1999), Tautanji et al. (1999)), who have FRP confined concrete columns agree on the fact that properties of the confining material determines the failure of the confined column. The difference in the ultimate strain between FRP tensile coupons and FRP jackets confining concrete are also well established but a number of uncertainties exist. All researches before De Caso et al. (2011) are tests on GFRP confined concrete columns, and are therefore unable to assess the causes in the difference of the ultimate condition of GFRP jackets confining concrete.

Ordinary ice, one of the 15 known crystalline phases of water as seen from the phase diagram in Fig. 2-1, reduces its density upon freezing (Fletcher (1970)). The ICE methodology helps create a uniform radial strain of the GFRP cylindrical jackets and it also helps to avoid some of the causes of uncertainties, and enables the effect of an isolated parameter on the confinement effectiveness, reproducing the confinement action as previously shown in Fig. 1-7. The unique property of water that expands when it changes state of matter from liquid to solid, as shown in Fig. 2-2, is the key to this method. This unique property of reduction in density upon freezing attributed to the inherent strong intermolecular interaction making ordinary ice capable of exerting a hydrostatic pressure up to 700 MPa in the presence of restraints (De Caso et al. (2011)).

The ICE methodology test rig consists of four high-strength and high-stiffness steel studs with threaded ends, aluminum rectangular and square end-plates with rectangular and square grooves machined in the inner surface of each plate to accommodate open-ended non-cylindrical specimens of varying thickness, high strength steel stiffening, and bolts. Two aluminum "C" sections were used to make the molds to manufacture rectangular/square jackets of GFRP which were fitted in to the grooves of aluminum end plates. The jackets were then filled with water and vertically restrained by metal plates joined with threaded steel studs. Then this assembly was instrumented and put in a freezer, which provided appropriate conditions for the water to change its state from liquid to solid state. As the water changes its state, it expands and exerts an outward hydrostatic pressure on the inner walls of the hollow GFRP, simulating the confining action as previously discussed. The ends of the water filled GFRP jackets were fully restrained by the end plates and longitudinal bars to guarantee the hydrostatic pressure

generated from the water/ice was fully exerted in the radial direction, stressing the GFRP jacket in the hoop direction. This restraining of the ends ensured that the GFRP was subjected only to a uni-axial stress. The test matrix presented in Table 2-1 was designed and used for the present study.

The three different geometric cross-sections: square (127 mm. x 127 mm x 381 mm), rectangular (101.6 mm x 152.4 mm x 304.8 mm), and rectangular (101.6 mm x 203.2 mm x 304.8 mm), with corner radii of 12.7 mm were considered in the present research to better understand the effect of shape on the properties of GFRP jackets with two, four or six plies under hydrostatic loading conditions. A four part designation is used to identify each specimen. The first letter stands for cross-sectional shape; the second part indicates the aspect ratio while the digit in the third part indicates the number of plies. The final letter indicates the repetition number.

Materials

Water/ordinary ice was used as a loading system subjecting the jacket to a gradually increasing hydrostatic pressure due to its change of volume while it undergoes phase change due to freezing as described in Fig. 2-2. The material specifications used in this study, as provided by the manufactures, are presented in Table 2-2. The epoxy was a gelatinous solvent-free epoxy resin, which was made up of two pre-measured components (a resin component A and a hardener component B). The components were mixed together, at a mix ratio of 4:1 (component A: component B) used as the matrix phase. The mix remained workable for approximately 40 minutes at +23^{o}C after mixing. Typical values for properties of the epoxy mix are presented in Table 2-3. Composite properties were computed experimentally, from direct tensile testing of flat coupons, as

presented in Table 2-4, following ASTM C3039 "standard test method for tensile properties of polymer matrix composite materials" (2008).

GFRP Jackets

A two part epoxy resin coupled with unidirectional glass fiber sheet was used to produce the GFRP jackets in a wet lay-up process, as shown in Fig. 2-3. A pair of aluminum "C" molds were used to manufacture the 27 open ended GFRP jackets. After fabrication, the specimens were left on a horizontal frame in the air to cure for a period of 48 hours. The aluminum molds were then released after the specimens were fully cured, and they were then cut to length using a high precision horizontal band saw. GFRP jackets had a reinforcement length equal to the number of layers times the perimeter of the jacket and an additional half perimeter for an overlap to avoid slip and force failure on "no-lap" zone, where the no-lap zone represented two sides of the non-circular GFRP jackets.

Flat Coupons

In addition to the cylindrical hand lay-up manufactured GFRP specimens tested, a total of nine GFRP flat coupon specimens with two-, four-, and six-plies, were tested with the purpose of determining the tensile strength and ultimate rupture strain for use as a control. Coupons were manufactured and tested in accordance with standard ASTM D 3039 with identical constituent materials as in the square and rectangular GFRP jackets.

The flat coupon specimens were prepared using a horizontal panel mold of overall width dimensions 500 by 330 mm length (in the fiber direction), following a wet lay-up technique. The GFRP panel was released after 48 hours from the mold and individual coupons were cut by means of a water-lubricated precision diamond circular saw, to their respective final dimensions. The preparation process ended by bonding aluminum tabs,

using a commercially available high strength adhesive, at the ends of the flat coupon specimens. Tabs were pre-stamped to create small dents on the surface to improve the mechanical grip between the tab and the sanded surface of the GFRP coupons, allowing better load transfer to engage the GFRP laminate during testing.

Testing

The GFRP jackets were instrumented with strain gauges and potentiometers. All the 27 specimens were instrumented with three strain gauges each located at mid-height (1/2H) for the no-lap sides, and the corner between them. Three specimens (one from each cross-section) were instrumented with additional strain gauges at quarter-height from the ends to study the strain distribution along the height of the jackets, and three others (one from each of the cross-sections) were instrumented with strain gauges at their inner and outer faces. Nine specimens were instrumented with two potentiometers to measure lateral deformation at a side and corner at the no-lap zones.

The specimens were then fitted in to grooves of the end plates prepared for each cross-section type, closing the gap between the jacket and the groove edge with water resistant sealant to avoid leaks during testing. After filling the end plate ended jacket with tap water, the top end plate was fitted similarly in to the water filled jacket, and the end plates were finally strengthened with stiffening studs. The whole set-up was then placed in to a freezer, as presented in Fig. 2-4. Thermocouples were used to measure air temperature throughout each test. The test set up and instrumentation is shown in Fig. 2-5.

GFRP flat coupon specimens were tested according to ASTM D 3039 loaded at a displacement rate of 0.025 mm/min using a 22 Kips MTS universal test frame. Mechanical wedge-type grips were used to engage the specimens by applying a uniform pressure on aluminum tabs. The load was measured via an internal load cell, while strains were recorded using a strain gauge adhesively bonded at the center of each specimen. An extensometer was also used to measure longitudinal deformation to verify the strain gauge readings. Direct tensile test set-up is shown in Fig. 2-6.

The vertical bars used for ensuring a lateral radial pressure to be applied on the jacket was found to be successful in restraining the jacket from experiencing pressure in the longitudinal direction as intended. They showed almost negligible axial deformation as described in Fig. 2-7, due to the restraining frame provided by the end plates, stiffening plates and bars. Therefore, the longitudinal strain on the GFRP jackets is negligible due to the restriction in this axis.

Results and Discussion

Modes of failure

Most of the GFRP jacket specimens with a low number of plies experienced rupture of the jacket within the middle third section, while the remaining specimens went through splitting of the GFRP jacket within the middle third section on the longer side (for rectangular jackets). The ruptures and splitting observed in the jackets are presented in Fig. 2-8. It should also be noted that leaking of water was a major problem observed in the experiment, making the methodology unable to produce enough pressure to fail most of the jackets. Therefore the results reported were not able to capture the maximum

tensile strain of the GFRP jackets and ultimate capacity was not captured. Average circumferential strain (με) experimental results observed is presented in Table 2-5.

Circumferential strains and lateral deformations

All the GFRP jackets tested in the present study have consistently shown a linear strain versus time relationship till the end. Fig. 2-9 presents the circumferential strain and temperature versus time relation for a representative rectangular (aspect ratio = 2.0) two-layer GFRP jacket. It shows that the long side of the jacket attained the highest strain first while the outer face of the corner experienced negative strain. Strain was observed to remain constant after the 14th hour, which may be due to leaking of the water and/or the frozen ice incapable of applying any more increased pressure thus keeping the already deformed jacket in its new shape until the end. This has been observed in many specimens and therefore may not have reached the ultimate capacity. Fig. 2-10 presents typical rectangular GFRP jackets perimetral strain versus time relations for four plies; here we can observe how the strain on the side-L reaches a maximum value. Fig. 2-11 shows a typical perimetral strain and temperature versus time relation for a square two-layer GFRP jacket. It shows that the sides experienced equivalent perimetral strains, as the corner show negative strain at its corner outer face. This consistent observation prompted the instrumentation of the jackets with strain gauges at their inner faces so that a more clear understanding of the jackets' cross-sectional stress distribution may be studied. Strain gauges were then applied at the inner face, and the readings shown a strain distribution across the thickness of the jackets, with positive strain at the outer face for the sides and negative strain at their inner faces as shown in the typical result presented in Fig. 2-12. The square columns have shown similar property, but failure

occurred predominantly at the mid-height corner zone. The maximum strains obtained in these tests conducted on two, four and six plies of rectangular and square GFRP jackets have shown considerably smaller values in comparison with their respective flat coupon specimens. This may be because the inability of the pressure developed to fail the GFRP jackets. The behavior observed made the corners to register negative strains at outer face.

The behavior of the GFRP jackets was further studied by instrumenting the jackets with potentiometers to measure the lateral movement of the sides and corners. Fig. 2-13 presents the lateral deformation experienced by a typical rectangular GFRP jacket throughout the test until maximum strains. It shows that a typical rectangular (101.6 x 152.4 mm) GFRP jacket bulges outward at its sides while it moves in-ward at the corners when it is subjected to a hydrostatic pressure. The lateral deformation versus time relation shown in Fig. 2-14 for a typical rectangular (101.6 x 203.2 mm) GFRP jacket shows similar kind of behavior as in the ones described above, except that the lateral deformations observed for both the corner and side is higher. The square GFRP jackets also show similar characteristics, Fig. 2-15, except that the corner didn't move much (0.5 mm) when compared with their rectangular counterparts. The non-cylindrical GFRP jackets are trying to take cylindrical shape as they are being pushed outward by the hydrostatic pressure the freezing water produced. All the jackets failed at their middle third section, as the perimetral strains studied shown in Fig. 2-16 for a typical jacket.

The maximum strains attained by square jackets (14363 με for two-plies, 13728 με for four-plies and 13350 με for six-plies) were considerably higher than those for rectangular jackets. Rectangular jackets with aspect ratio of 1.5 have, at the middle third section, attained average strains of 6272 με for two-plies; 13229 με for four-piles; and 14363 με

for six-plies. The rectangular jackets with aspect ratio of 2.0 have shown a maximum strain reading 6274 με for two-plies; 6809 με for four-plies; and 8898 με for six-plies, which are smaller than the ones observed with rectangular jackets with 1.5 side aspect ratio.

Results of the GFRP flat coupon tensile tests are summarized in Table 2-4 including: ultimate tensile strength, f_{fu}; tensile chord modulus, E_{chord}; measured ultimate strain, ε_{fu}, and computed ultimate tensile strains, $\varepsilon^*_{fu.}$ The average, standard deviation (*SD*), and coefficient of variance (*CV*) for the aforementioned values based on three specimens per design are also provided. The axial stress versus strain response was linear elastic to failure as illustrated in Fig. 2-17, where GFRP coupons failed suddenly rupturing in tension. Representative failed GFRP flat coupons are shown in Fig. 2-18. The six-ply direct tensile test was not able to reach failure because of the grip problems experienced.

Volumetric expansion and lateral deflection

Based on the observations from the experimental study, a numerical computation of the lateral deflection of a representative square and rectangular jackets subjected to hydrostatic pressure was carried out, for comparison purposes.

A numerical analysis was done on a square cross-section jacket based on Fig. 2-19.

Relationship between lateral deflection and volumetric expansion, ε_v can be computed as follows, assuming that the deformed shape can be described by:

$$y = \Delta \sin(\frac{\pi x}{b}) \qquad \text{(equation 2.1)}$$

Since the jacket can deform freely, no length change is expected, hence:

$$a = \int_0^b \sqrt{(1 + y'^2)}\, dx \qquad \text{(equation 2.2)}$$

$$a = b + \frac{\pi^2}{4}\frac{\Delta^2}{b} \qquad \text{(equation 2.3)}$$

The area confined within the deformed shape is equal to the undeformed area (a^2) plus its expansion ($\varepsilon_v a^2$) assuming that no vertical deformation is permitted.

$$a^2(1+\varepsilon_v) = b^2 + 4\int_0^b \Delta \sin\left(\frac{\pi x}{b}\right) dx \qquad \text{(equation 2.4)}$$

$$a^2(1+\varepsilon_v) = b^2 + \frac{8b\Delta}{\pi} \qquad \text{(equation 2.5)}$$

But $a - b = \delta$

These set of equations may be simplified and solved as:

$$\Delta = \frac{\pi\varepsilon_v a}{8} \qquad \text{(equation 2.6)}$$

$$\delta = \frac{(\frac{\pi\Delta}{2})^2}{b} \qquad \text{(equation 2.7)}$$

The potentiometer readings (where the readings are considered to be perpendicular to the surface of the GFRP jacket) are:

$$\delta_1 = \Delta - (\frac{\delta}{2}) \qquad \text{(equation 2.8)}$$

$$\delta_2 = (\frac{\sqrt{2}}{2})\delta \qquad \text{(equation 2.9)}$$

The maximum strain can be computed as:

$$\varepsilon_{max} = \frac{nt}{(2b^2/\pi^2\Delta)} \qquad \text{(equation 2.10)}$$

Where *n* is the number of layers, *t* is the thickness of one layer of GFRP.

Similarly for a representative rectangular jacket, Fig. 2-20, the lateral deformations can be found from:

$$\delta_h = \frac{(\frac{\pi\Delta 1}{2})^2}{b} \text{ and } \delta_v = \frac{(\frac{\pi\Delta 2}{2})^2}{a} \qquad \text{(equation 2.11)}$$

$$\Delta_1 = \frac{\pi\varepsilon_v b}{4} \text{ and } \Delta_2 = \frac{\pi\varepsilon_v a}{4} \qquad \text{(equation 2.12)}$$

The potentiometer readings (where the readings are considered to be perpendicular to the surface of the GFRP jacket) are:

$$\delta_1 = \Delta_1 \qquad \text{(equation 2.13)}$$

$$\delta_3 = \Delta_2 \qquad \text{(equation 2.14)}$$

$$\delta_1 = \delta_h \sin(tan^{-1}\left(\frac{\delta_v}{\delta_h}\right)) \qquad \text{(equation 2.15)}$$

The analysis results for the square GFRP jackets are shown in Fig. 2-21. The numerical results for the rectangular GFRP jackets are shown in Figs. 2-22 and 2-23.The maximum volumetric expansion used for the analysis was $\varepsilon_v = 0.10$. The ICE methodology showed that the lateral deformation concentrated at the mid-height with expansion up to 33 percent, thus the experimental lateral deformations were much higher than the 10 percent expansion assumed in the analysis. All the lengths are given in mm.

Conclusions

- Rupture of the fibers was observed in two- and four-plies of GFRP jackets in all the cross-sections considered. In square jackets rupture occurred at the middle third section of the corners, and the rectangular jackets ruptured at the middle third section of their long sides.
- Maximum circumferential strains recorded were consistently lower when compared to GFRP flat coupons;
- The ice was unable to rupture jackets with six plies due to incapability to develop enough pressure, and water leaking was an issue;
- The ICE methodology to characterize GFRP presented an opportunity to instrument the inner face of the jackets and observe how they behave across their

thickness. A behavior was observed, where the jackets have experienced tension and compression on opposite faces, contraction at the corners.

Further Research

- More research need to be done on non-cylindrical jackets to provide more data base and verify the properties observed and reported in the present research, and more is needed to be understood about the failure mechanisms;
- Pressure developed due to the ice freezing needs to be measured and the leaking problem should be addressed to develop enough pressure to strain the jackets till ultimate capacity;
- For better comparison the temperature during testing for both the jackets and flat coupon specimens should be taken in to consideration;
- Characterization properties of other FRP materials, such as Carbon FRP (CFRP) or Aramid FRP (AFRP);
- Evaluating the behavior of hybrid-fiber sheets due to the recently increase in the use of hybrid-FRP. When using different materials with significantly different properties in the same fiber sheet, currently it is unclear what design parameters ought to be used;
- Assessing the behavior of externally bonded FRP made from different fiber orientations, such as sheets with fibers in the 0, ±45 and 90 º directions.

Table 2-1: Test Matrix

Cross-section Geometry	No. of GFRP plies	No. of Repetitions	Specimen Designation
Square (127 x 127 mm)	2	3	S_1.0_2_A,B,C
	4		S_1.0_4_A,B,C
	6		S_1.0_6_A,B,C
Rectangular (101.6 x 152.4 mm)	2		R_1.5_2_A,B,C
	4		R_1.5_4_A,B,C
	6		R_1.5_6_A,B,C
Rectangular (101.6 x 203.2 mm)	2		R_2.0_2_A,B,C
	4		R_2.0_4_A,B,C
	6		R_2.0_6_A,B,C

Table 2-2: Glass fiber properties (manufacturer's values)

Fiber Type	Filament			Sheet	
	Tensile modulus (MPa)	Tensile strength (MPa)	Tensile strain (%)	Ply thickness (mm)	Weight (kg/m^2)
Glass Fiber	76,948.20	3,399.24	4.7	0.503	0.596

Table 2-3: Epoxy properties (Manufacturer's values)

Property	Value
Specific Gravity (Kg/m^3)	1,060
Tensile Strength (N/mm^2)	40
Tensile Elongation: after 28 days (%)	1.80
Compressive Strength (N/mm^2)	70
Flexural Strength (N/mm^2)	70
Modulus of elasticity under compression (N/mm^2)	1,400

Table 2-4: Flat coupon tensile testing result

Specimen ID	Ultimate tensile strength f_{fu} (MPa)	Tensile chord modulus E_{chord} (GPa)	Last measured tensile strain ε_{fu} (με)	Computed ultimate tensile strain $\varepsilon^* f_u = f_{fu} / E_{chord}$ (με)
2 - Ply				
2P-A	431	23	19708	18739
2P-B	468	24	23852	19500
2P-C	443	21	21215	21095
Average	447	23	21592	19778
SD	19	2	2098	1202
CV (%)	4.25	8.70	9.72	6.08
4 - Ply				
4P-A	408	23	19265	17739
4P-B	377	25	23122	15080
4P-C	343	26	23146	13192
Average	376	25	21844	15337
SD	33	2	2234	2284
CV (%)	8.78	8.00	10.23	14.90
6 - Ply				
6P-A	n/a	22	n/a	--
6P-B	n/a	26	n/a	--
6P-C	n/a	23	n/a	--
Average	--	--	--	--
SD	--	--	--	--
CV (%)	--	--	--	--

Table 2-5: Maximum circumferential strain (με) experimental results

Cross-section	No. of Plies	Maximum strain	Side - L	Side - S	Corner
Rectangular (101.6 x 203.2 mm)	2	Average	6274	6116	-6135
		SD	856	698	-795
		COV (%)	13.6	11.4	12.9
	4	Average	6809	3838	-6615
		SD	474	259	-655
		COV (%)	6.9	6.7	9.9
	6	Average	8898	5758	-6102
		SD	356	465	-546
		COV (%)	4.0	8.1	8.9
Rectangular (101.6 x 152.4 mm)	2	Average	6272	909	-2216
		SD	664	103	-283
		COV (%)	10.5	11.3	12.7
	4	Average	13229	5647	-5946
		SD	1025	845	-616
		COV (%)	7.7	14.9	10.3
	6	Average	14363	7909	-11545
		SD	1592	1087	-1063
		COV (%)	11.1	13.7	9.2
Square (152.4 x 152.4 mm)	2	Average	8802	5735	-13728
		SD	752	351	-1782
		COV (%)	8.5	6.1	12.9
	4	Average	7365	7061	-13350
		SD	963	436	-1679
		COV (%)	13.1	6.1	12.5
	6	Average	8475	8476	-13158
		SD	606	483	-1208
		COV (%)	7.1	5.7	9.1

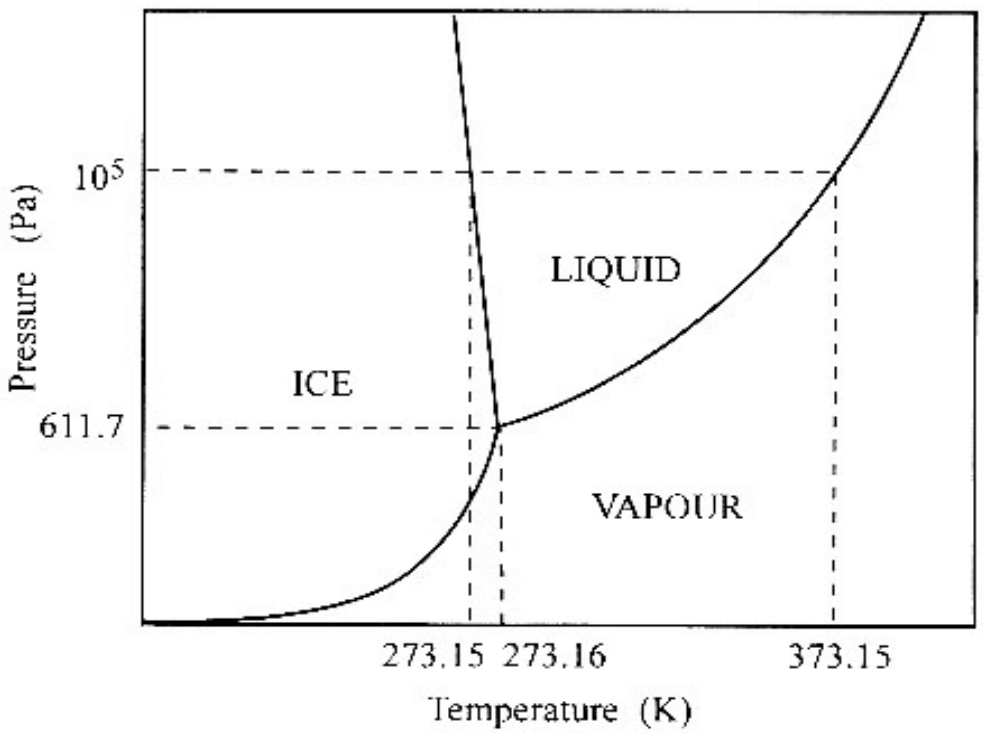

Fig. 2-1: Phase diagram of water (Fletcher (1970))

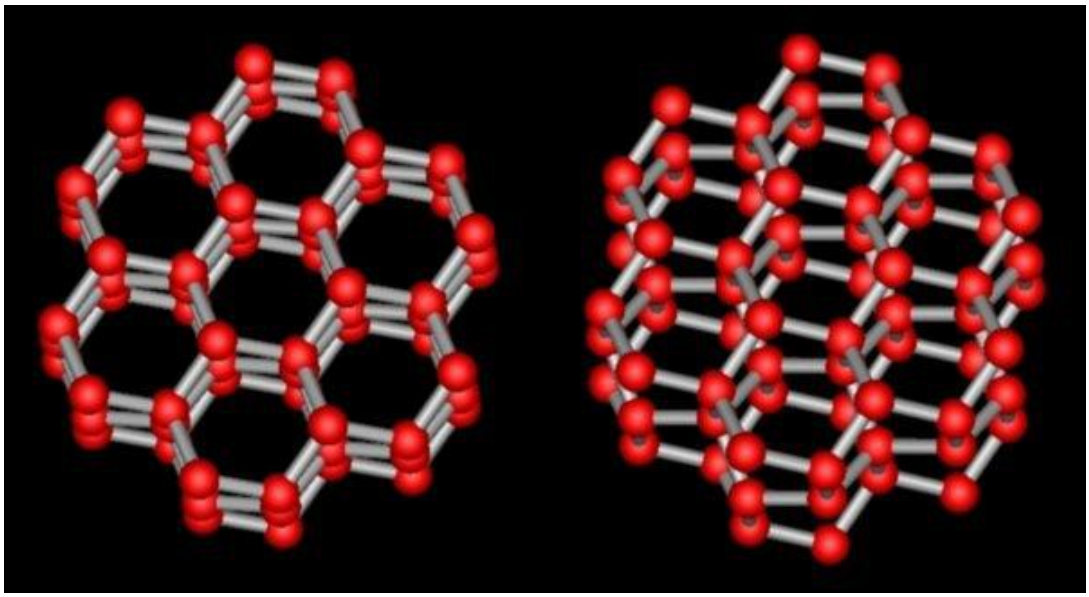

a)

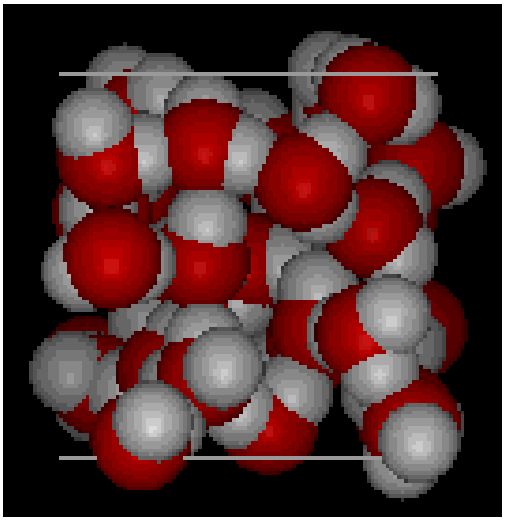

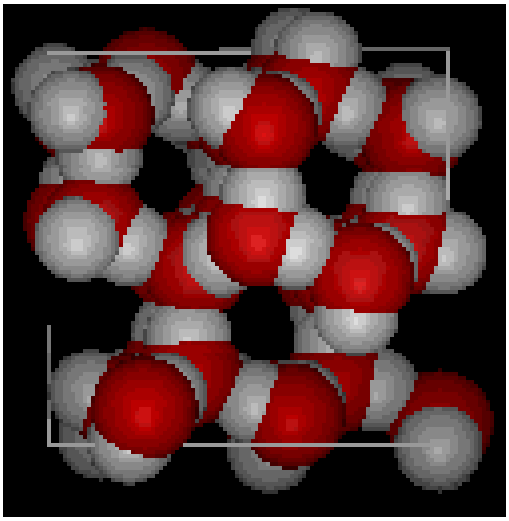

b) c)

Fig. 2-2: a) ordinary ice crystal structure, b) ice prior freezing, c) ice after freezing (Chaplin (2007))

Fig. 2-3: Wet lay-up impregnation of glass fibers and wrapping of the aluminum "C" section

Fig. 2-4: Instrumented GFRP jacket inside the freezer

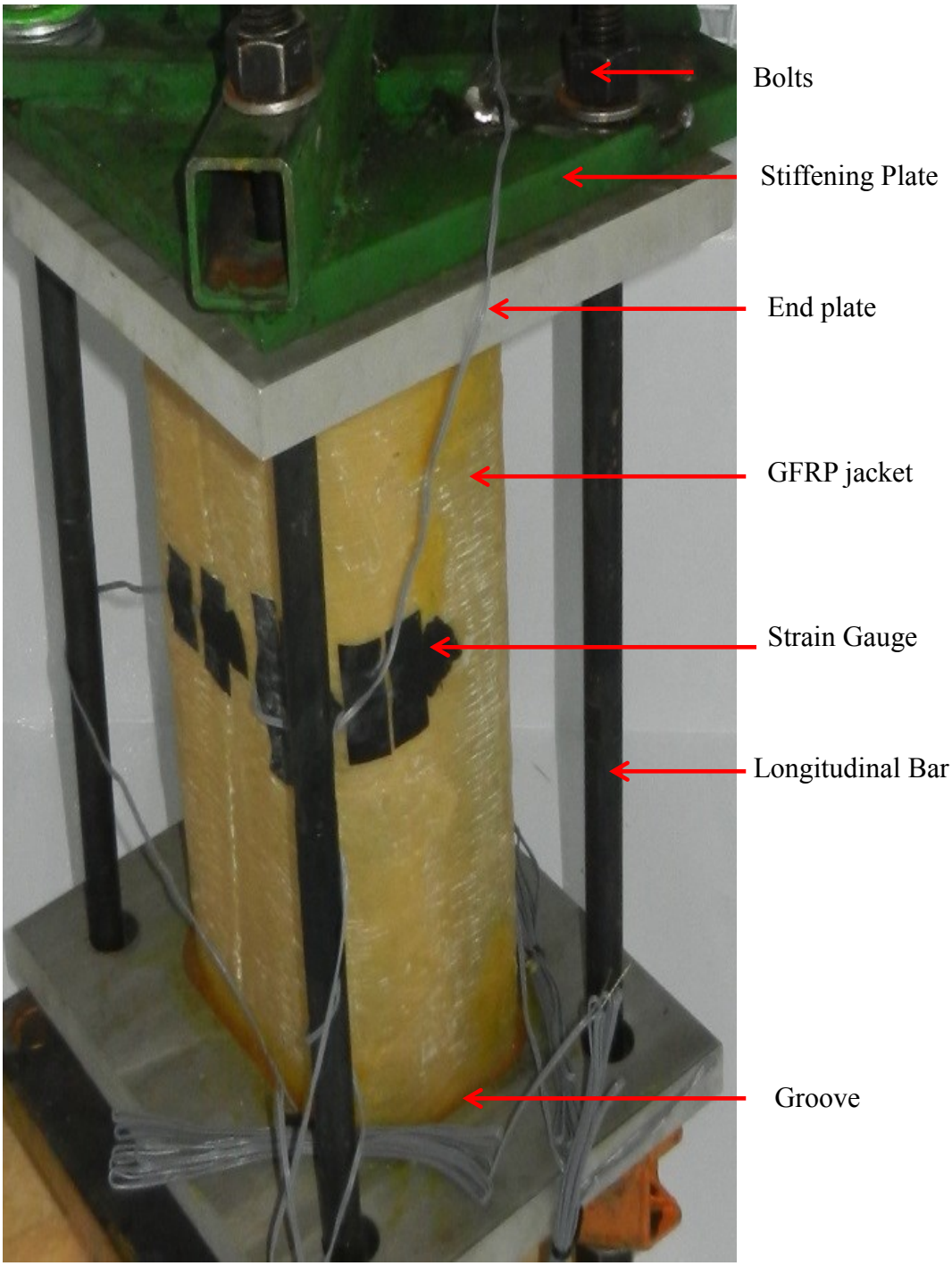

Fig. 2-5: Test setup and instrumentation

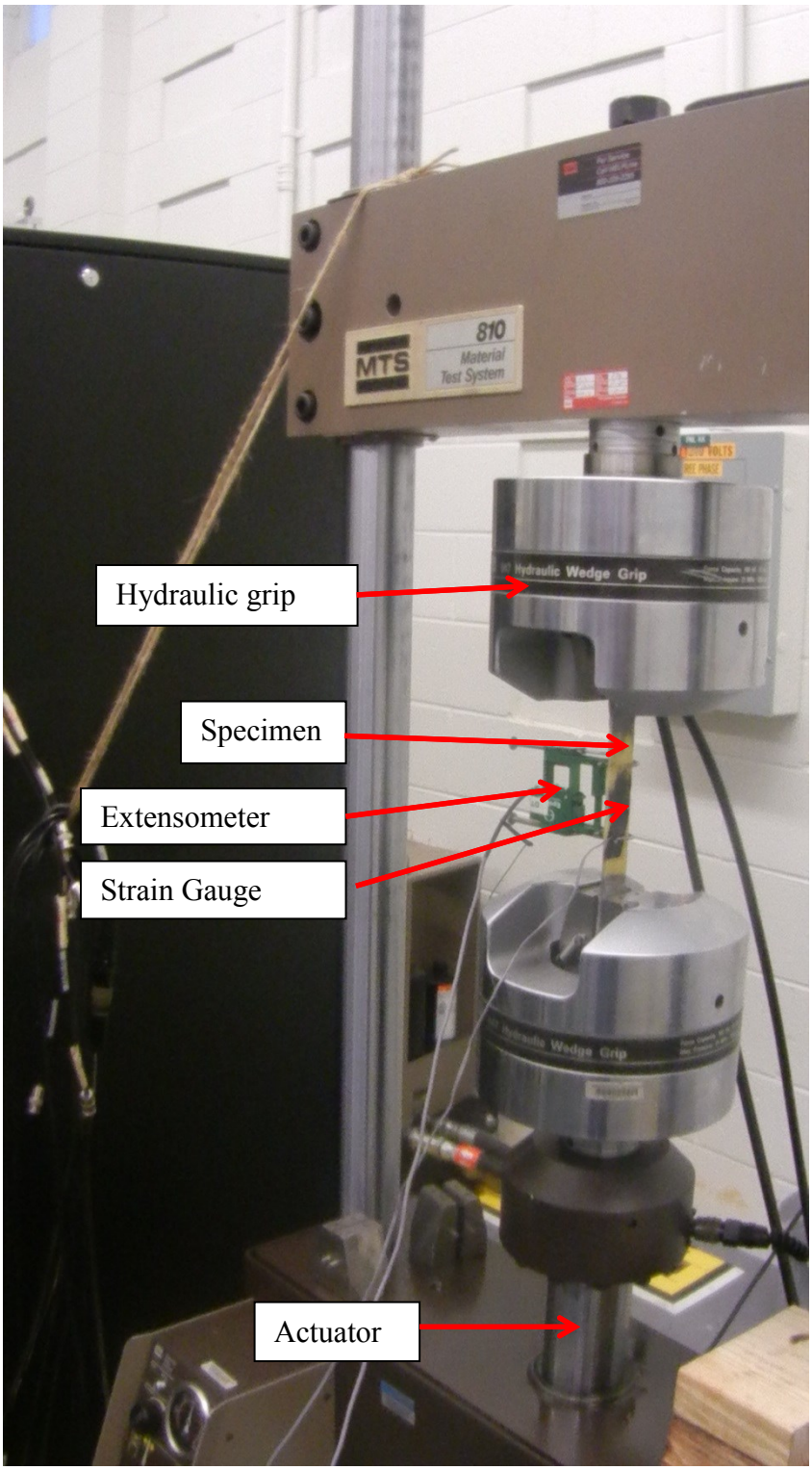

Fig. 2-6: Direct tensile testing of GFRP flat coupons

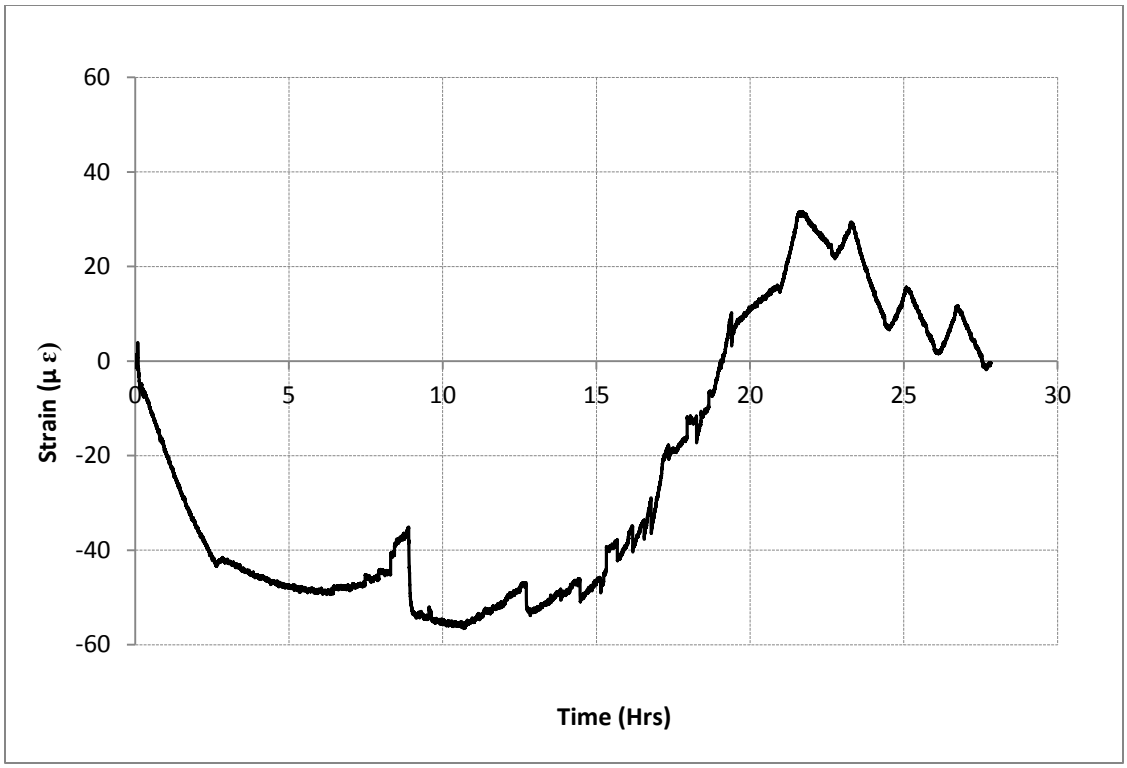

Fig. 2-7: Strain vs. time (longitudinal bar)

a) R_1.0_2_A **b) R_1.5_6_B** **c) R_2.0_4_B**

Fig. 2-8: Representative square and rectangular jackets post test

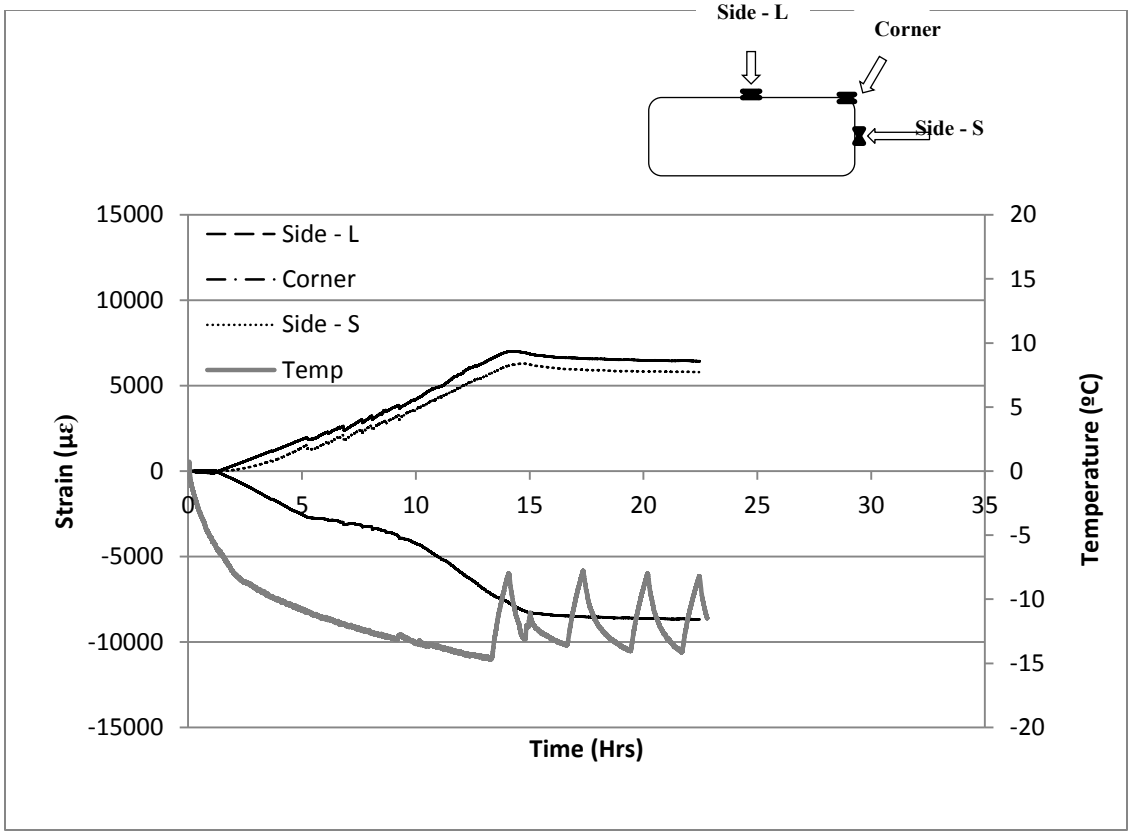

Fig. 2-9: Circumferential strain and temperature vs. time relation (R_2.0_2_B)

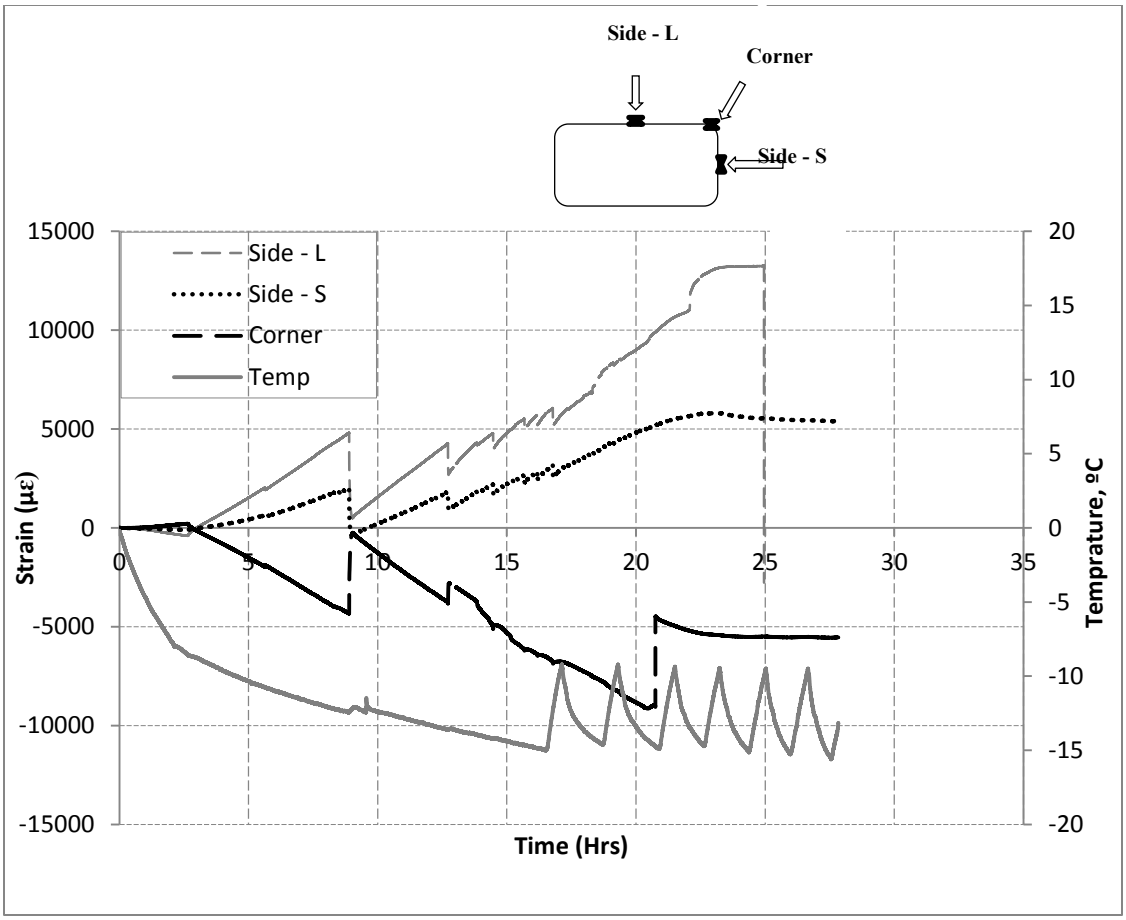

Fig. 2-10: Circumferential strain and temperature vs. time (R_1.5_4_A)

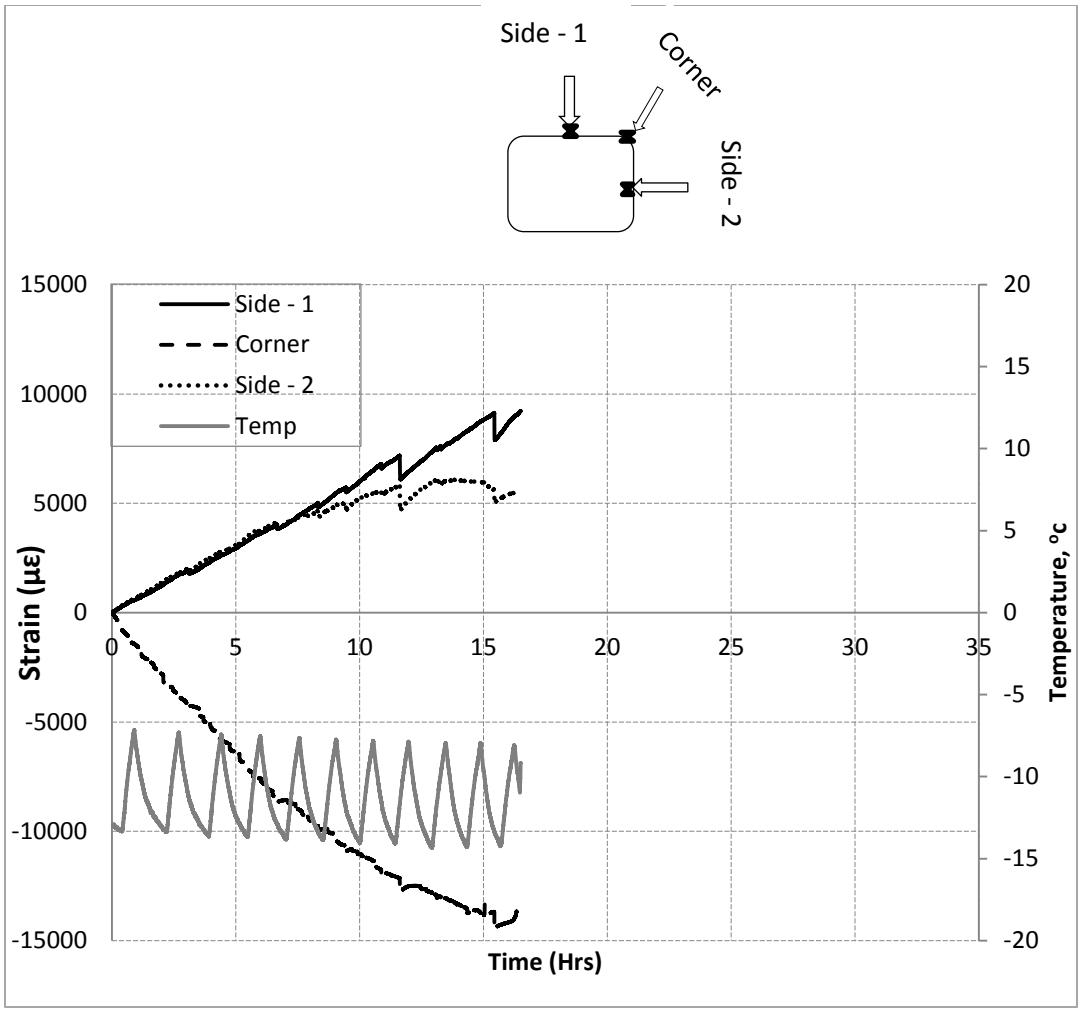

Fig. 2-11: Circumferential strain and temperature vs. time relation (R_1.0_2_B)

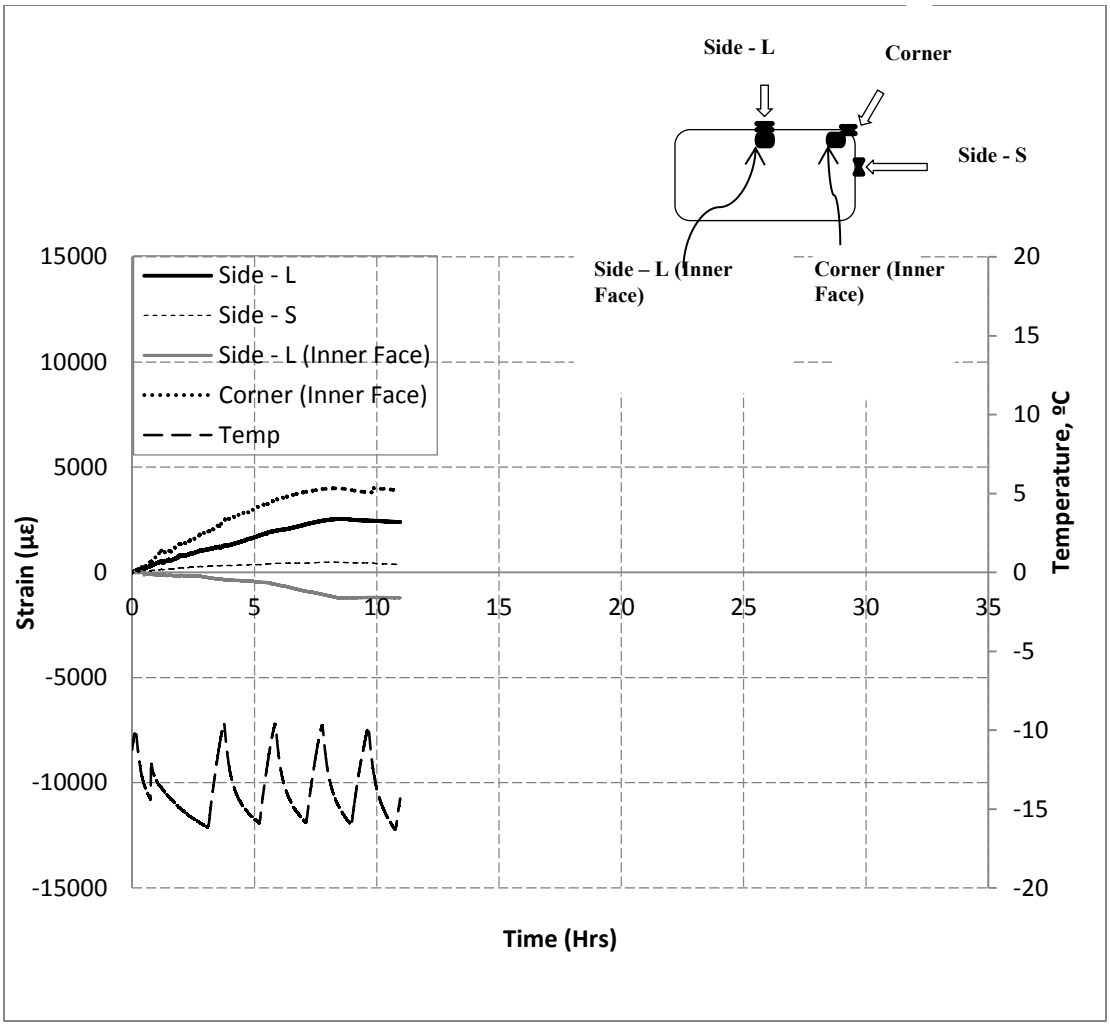

Fig. 2-12: Circumferential strain and temperature vs. time relation

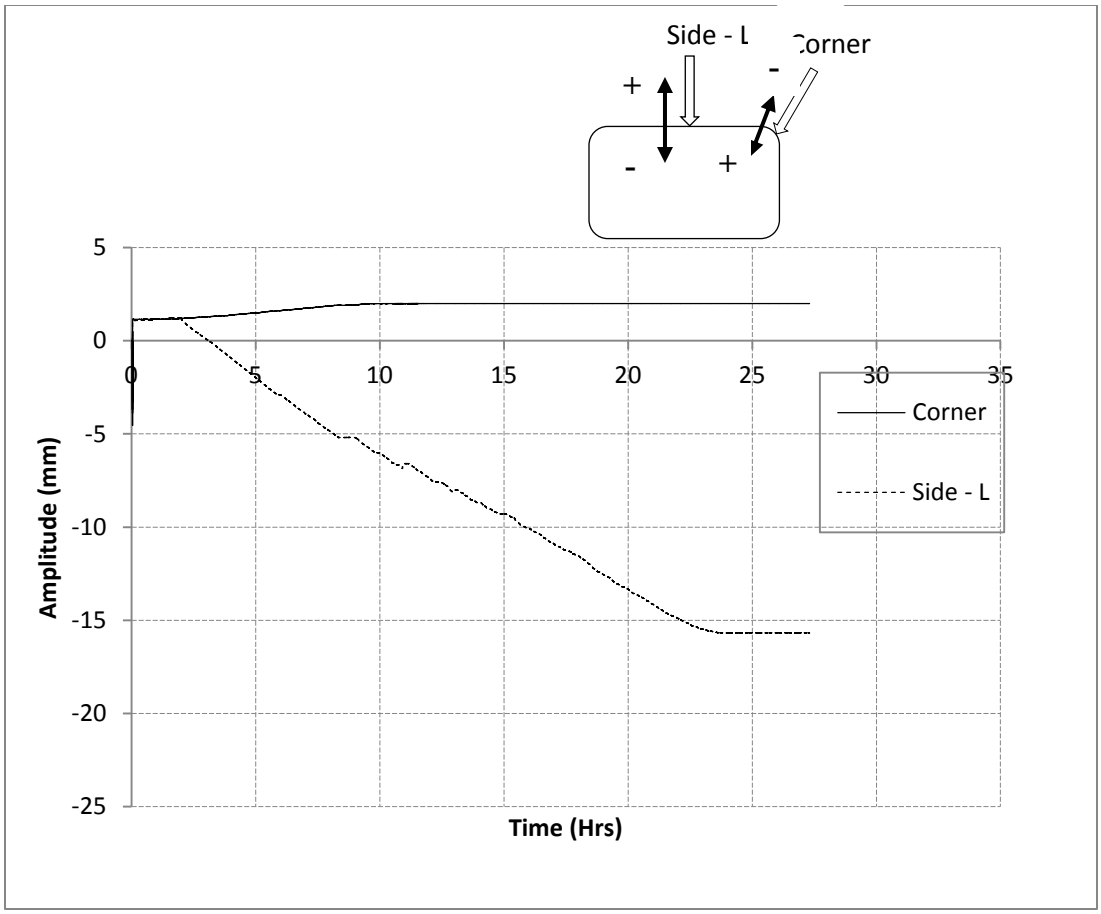

Fig. 2-13: Lateral deformation vs. time (rectangular, 101.6 x 152.4 mm)

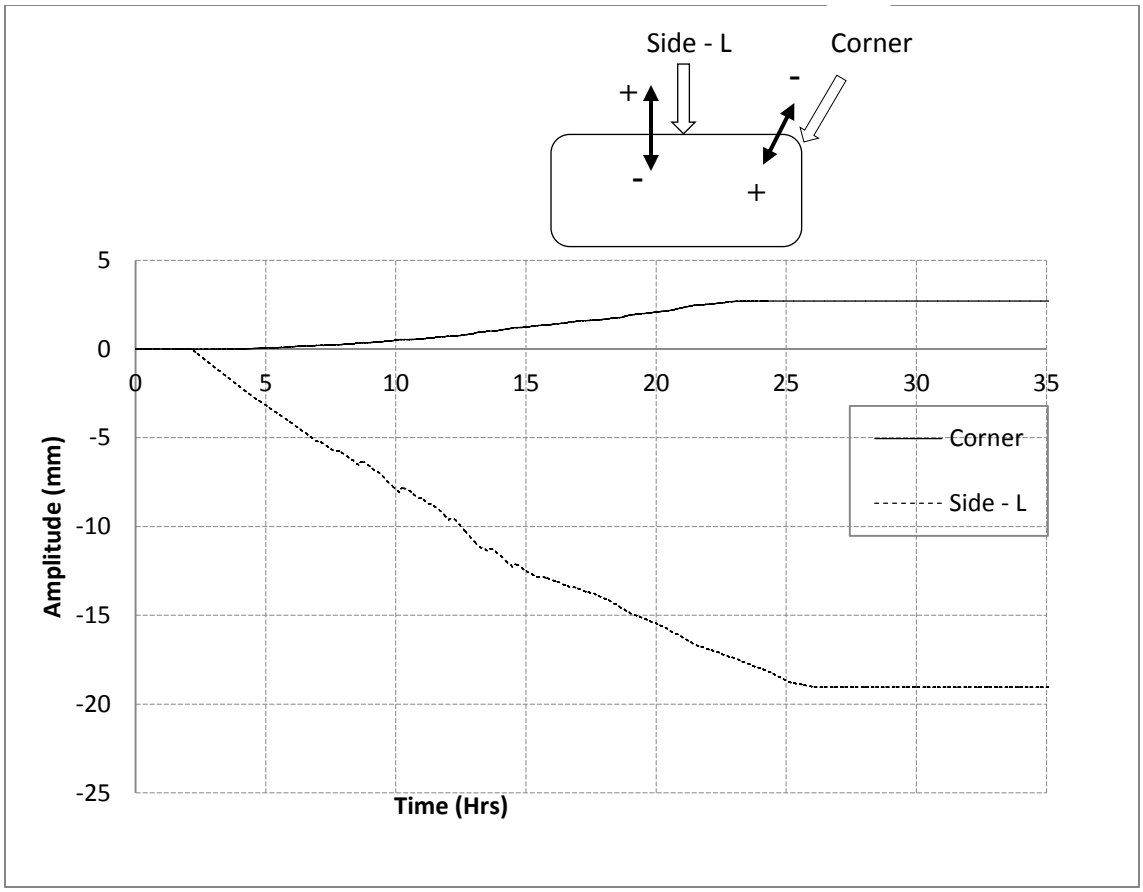

Fig. 2-14: Lateral deformation vs. time (rectangular, 101.6 x 203.2 mm)

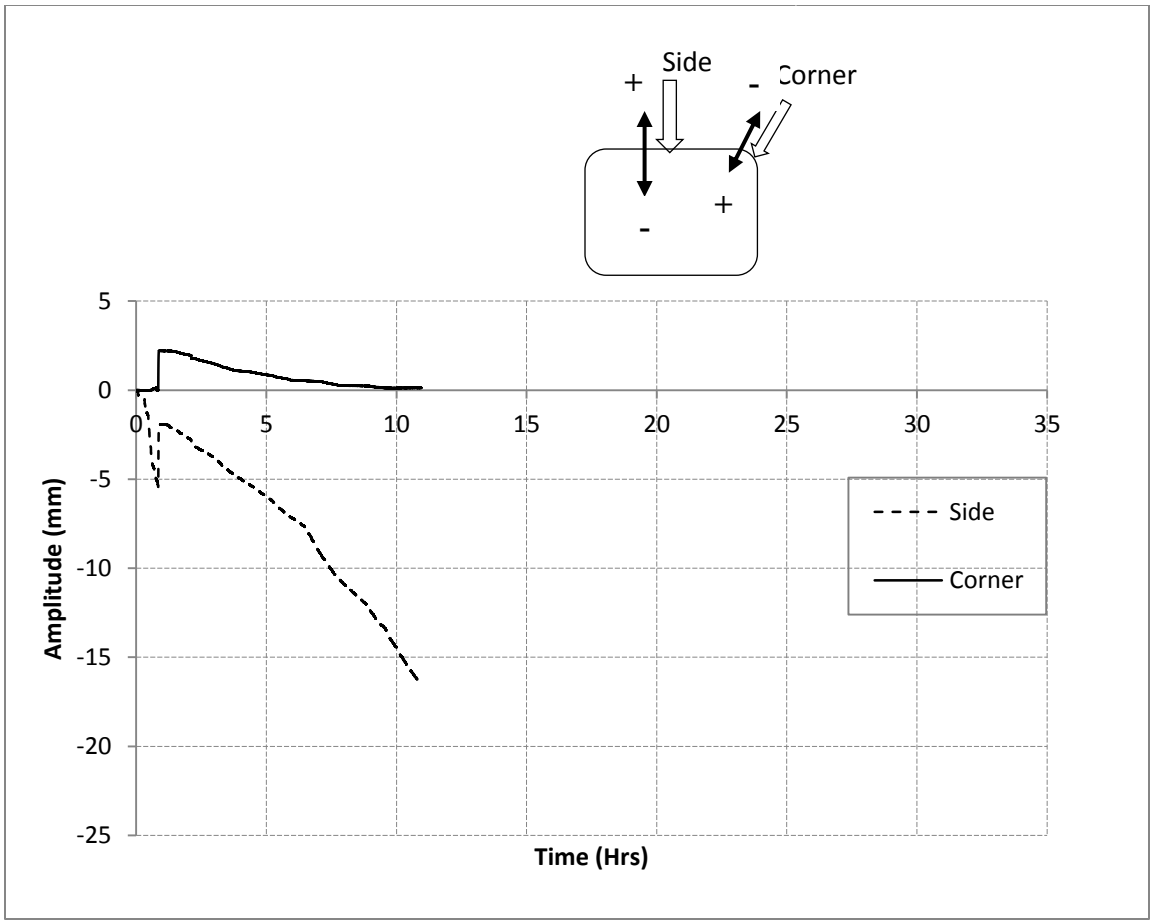

Fig. 2-15: Lateral deformation vs. time (square, 127 x 127 mm)

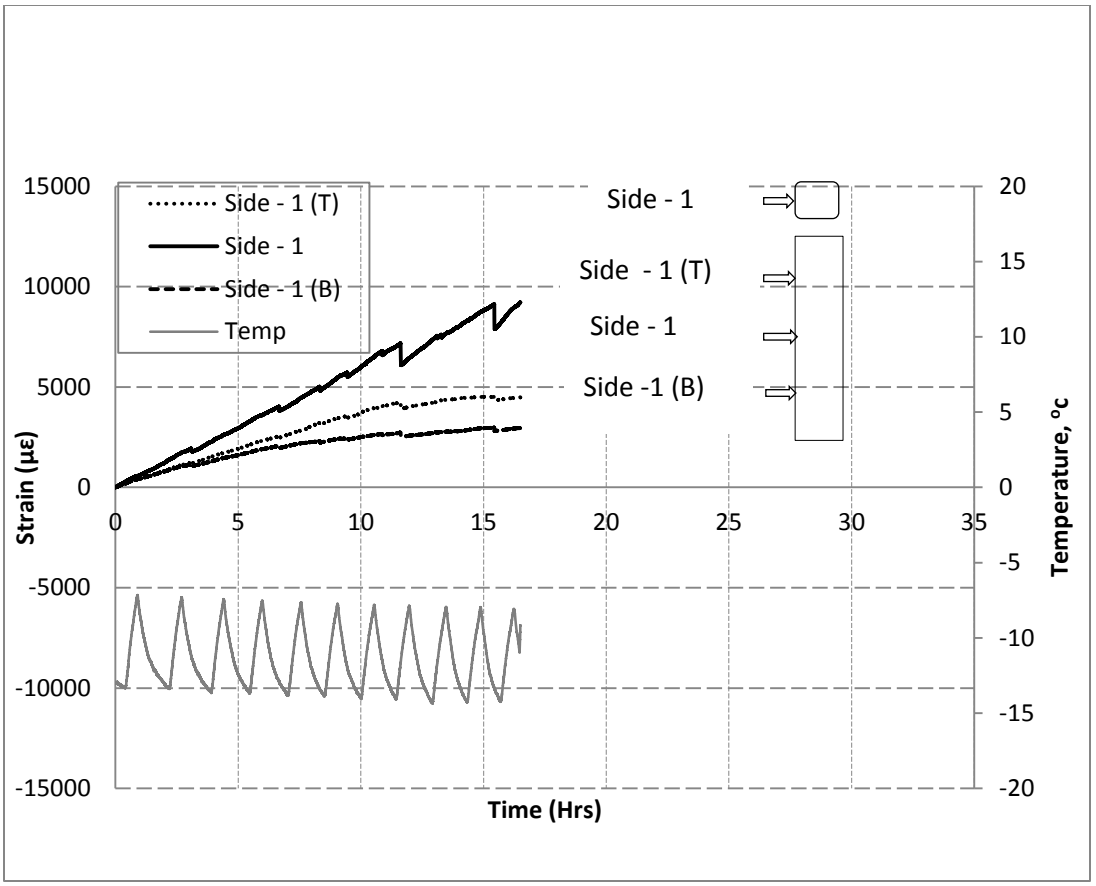

Fig. 2-16: Circumferential strain and temperature vs. time relation along the height of GFRP jackets

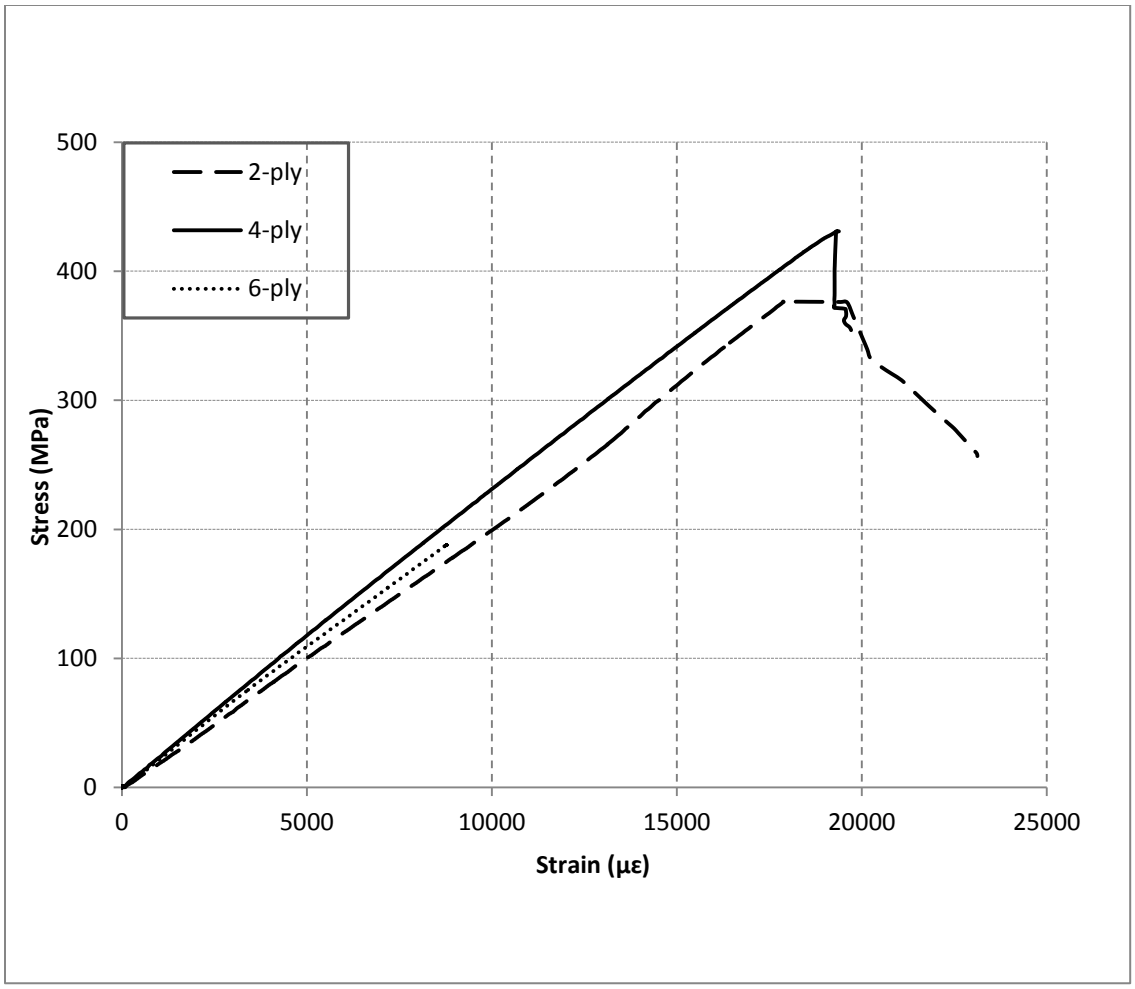

Fig. 2-17: Flat coupon stress vs. strain relation

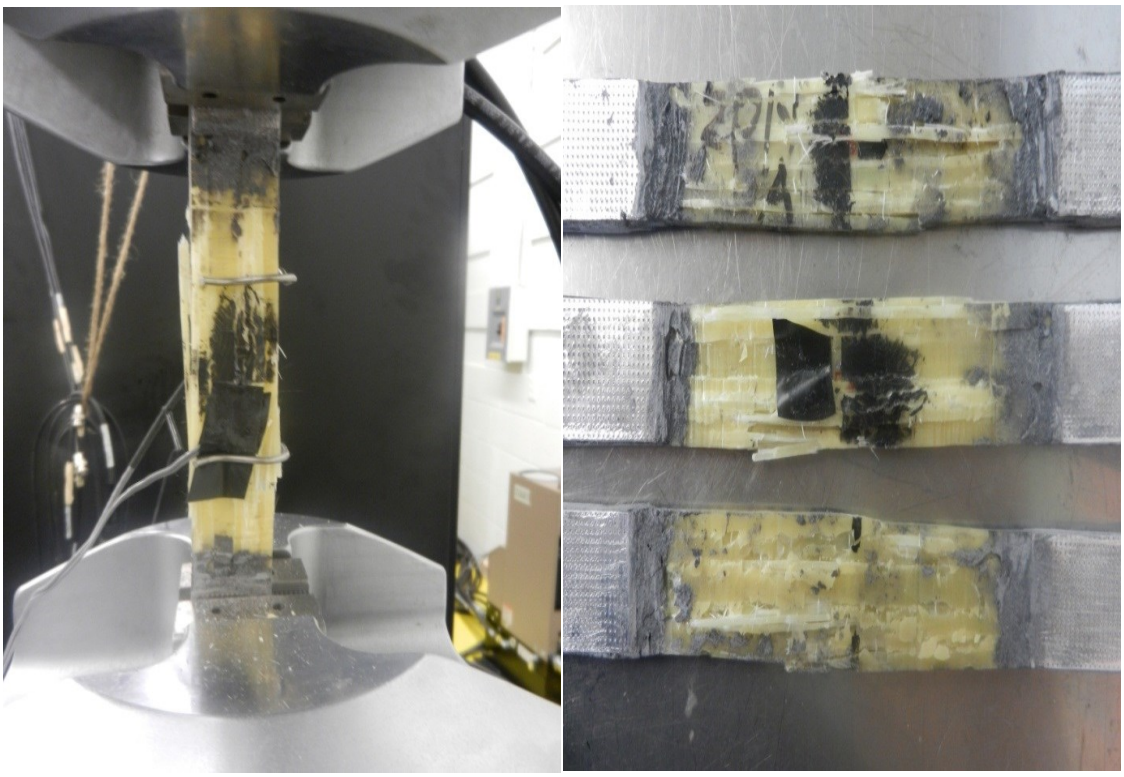

Fig. 2-18: Failed GFRP tensile flat coupons

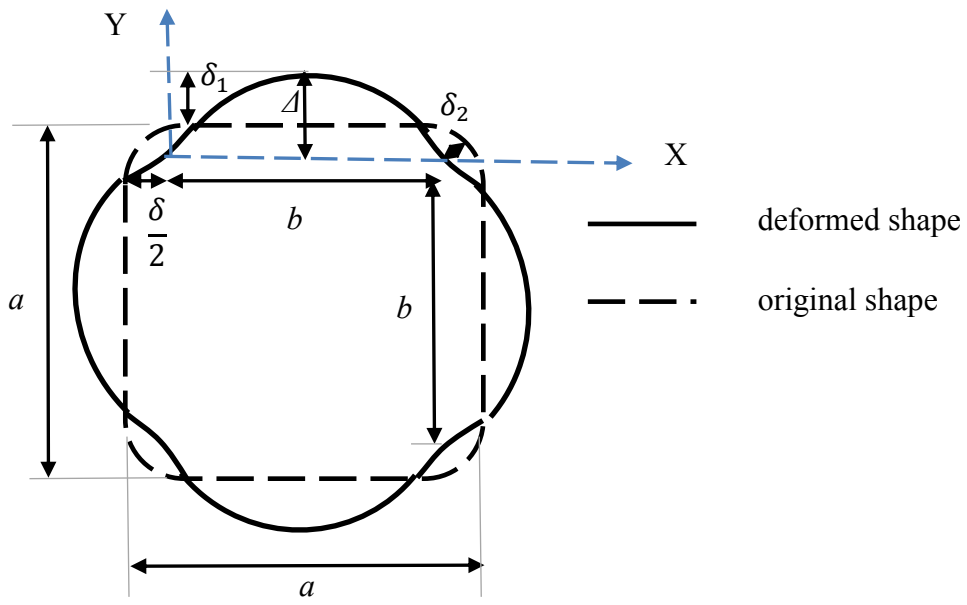

Fig. 2-19: Lateral deformations of square GFRP jackets

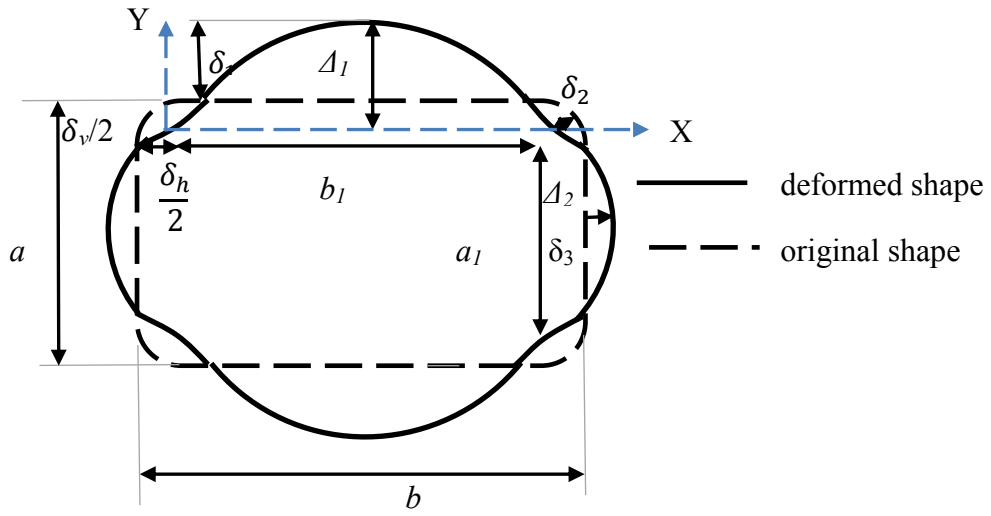

Fig. 2-20: Lateral deformations of rectangular GFRP jackets

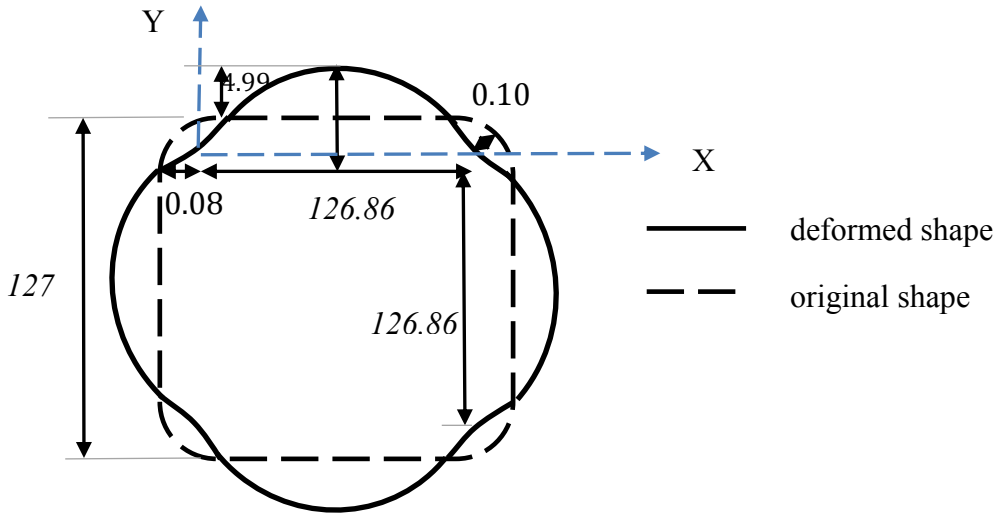

Fig. 2-21: Lateral deformations of square GFRP jackets (numerical analysis)

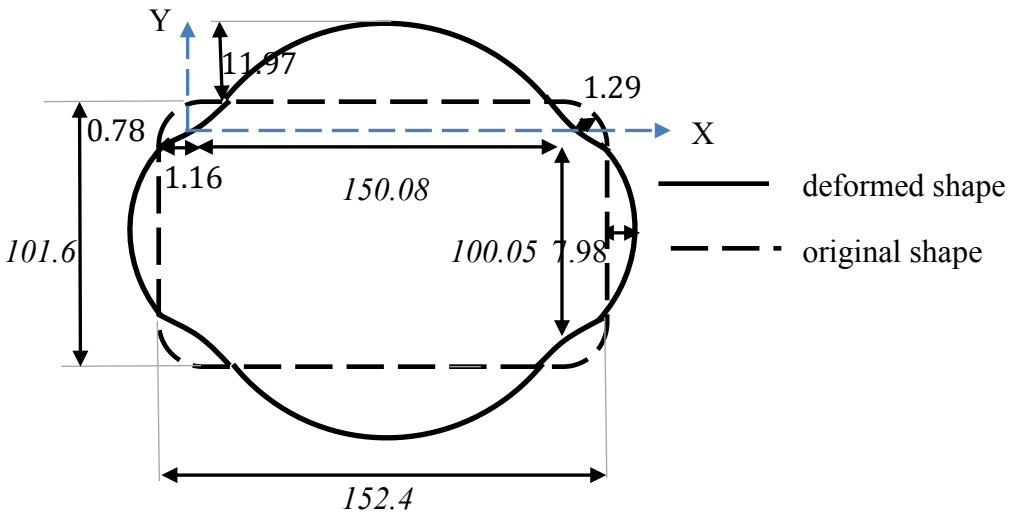

Fig. 2-22: Lateral deformations of rectangular (aspect ratio = 1.5) GFRP jackets (numerical analysis)

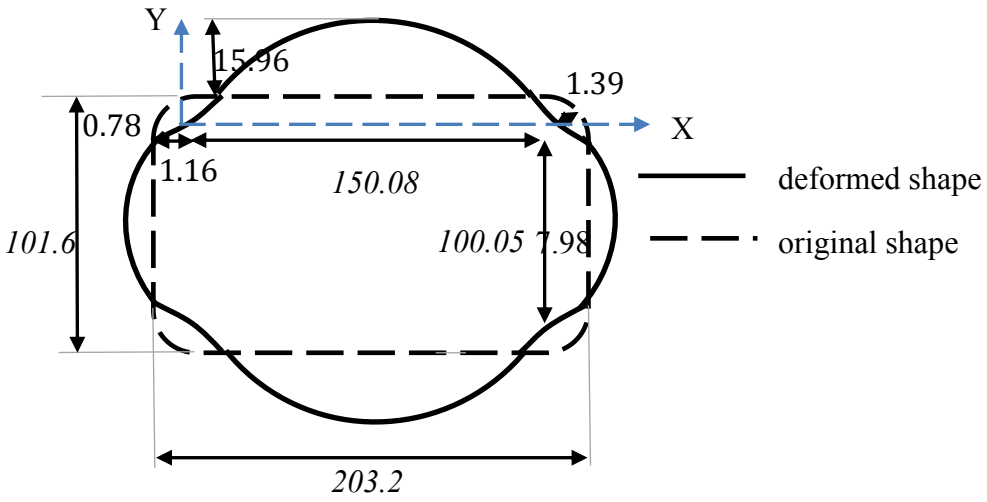

Fig. 2-23: Lateral deformations of rectangular (aspect ratio = 2.0) GFRP jackets (numerical analysis)

CHAPTER III

STUDY 2: EFFECT OF SIZE AND CROSS-SECTIONAL GEOMETRY ON CONFINEMENT EFFECTIVENESS OF GFRP WRAPPED RC COLUMNS

Background

A number of alternative techniques are available in the literature for the retrofitting of RC structures, which are based on different principles of retrofitting: strengthening of structure; completion of load path and removal of structural irregularity; and enhancing deformation capacity of structure. Each of the listed techniques for retrofitting RC columns has its own advantages and disadvantages. Removing deficient columns and constructing new ones, placing reinforcing steel and formwork around a column and pouring additional concrete are few of the techniques that can be used. Jacketing scheme wherein the column is encased by some reinforcing material is another way of retrofitting RC columns. FRP is one of the most widely used jacketing schemes, and many researches has been done to better understand their behavior, and provide models for analysis and design purposes.

Although most studies on fiber-wrapped concrete columns have been conducted in the past three decades, the first attempt at such a confinement mechanism was made in late 1970's. Kurt (1978) suggested using commercially available plastic pipes filled with concrete. His experimental studies indicated that plastic pipes were more effective than steel pipes in confining concrete. For a slenderness ratio of less than 20, plastic-encased concrete showed a 45° shear failure, both in the concrete core and in the plastic pipe,

resulting from the combination of axial compression and hoop tension in the pipe. Later, Saadatmanesh et al. (1994) conducted experiments on circular and rectangular concrete columns retrofitted with E-glass fiber fabric to evaluate the increase in strength and ductility due to GFRP wrapping. The parameters such as the compressive strength of concrete, strap thickness and strap spacing were investigated. The authors concluded that (i) the rate of increase in ultimate axial load, ductility and maximum moment carrying capacity decreases with increase in concrete compressive strength and (ii) the rate of increase of ductility decreases with increase in strap spacing.

Seible et al. (1997) conducted experiments to investigate effect of seismic retrofit of RC columns with carbon fiber fabric. The authors found that (i) the carbon fiber fabric retrofitted specimens showed better deformation capacities as that of steel retrofitted specimens and (ii) the increase in stiffness and load carrying capacity were less with carbon fiber fabric as compared to those of the steel jacket retrofit.

Rochette and Labossiere (2000) conducted tests on RC columns retrofitted with carbon and aramid fiber fabric under uniaxial loading. The parameters like the cross-sectional shape and confinement stiffness were investigated. Tests were carried on 22 square columns, seven cylinders and five rectangular columns. The authors concluded that the compressive strength of the specimen increases with increase in the thickness of the fabric and the specimens with rounded corners increased the confinement effect.

Hadi (2005) conducted tests on eccentrically loaded columns wrapped with two types of materials. Half of the columns were wrapped with GFRP and the other half with CFRP. All his test columns were tested by applying an axial load at 50 mm eccentricity. Based

on his study, he concluded that considerable gain in strength and ductility is obtained when reinforcing the columns with CFRP (straps horizontally wrapped).

In terms of column confinement, glass fibers are particularly attractive. First, they have the highest ultimate strain of any "relative high-modulus" fiber; second, their low fatigue and creep-rupture resistance are not a detrimental factor in this type of application. In addition, the shortage of carbon fiber supplies, as well as the development of high-performance glass fibers with lower manufacturing costs has made GFRP cost-competitive when compared to CFRP laminates, thereby inducing an important increase in the demand of glass fibers over the last years.

A number of studies have demonstrated that the use of GFRP wrapping in particular is effective in confining small cylindrical plain and RC columns. Limited studies are found for the cases of non-cylindrical members especially of large size, and subsequently there are limited research studies on size and shape effect on confinement effectiveness of GFRP wrapping of non-circular RC columns. Prior to the work of De Luca et al. (2011), there was little experimental evidence on full-scale RC rectangular and square columns externally confined by GFRP. The study by De Luca et al. was aimed at investigating the effectiveness of the GFRP confinement in relation to different cross-sectional geometries; and studying the deformability enhancement due to GFRP confinement; and the present study extends these investigations to small scale specimens of both rectangular and square cross-sections. De Luca et al. (2011) concluded that the presence of the GFRP jacket allows a "growth" in volume of the concrete core by offsetting buckling of the longitudinal bars and by delaying unstable crack propagation, leading to an improvement in the concrete axial deformation but not an increase in axial strength; the shape of the

cross-section influences the effectiveness of the confinement; and existing semi-empirical prediction models do not converge to the same prediction for the ultimate axial capacity of full-scale GFRP-confined prismatic concrete columns. This study is thus meant to build upon these findings to further understand the behavior of non-cylindrical GFRP-wrapped RC columns.

Cross-sectional shape is one of the many parameters that affect strength and ductility of GFRP confined concrete columns (Lam and Teng (2003)). This is attributed to the non-uniform pressure developed in FRP confined non-cylindrical concrete columns. When a rectangular or square column is wrapped with FRP laminates, the confining pressure developed due to concrete dilation is high at the corners where stress concentration is present (Mirmiran et al. (1998)).

A test matrix was designed to isolate the cross-sectional shape and size to study their effect on the effectiveness of GFRP wrapping of non-cylindrical RC columns. The present study compares confinement in small scale columns with the full scale RC columns that were investigated in the research work done by De Luca et al. (2011).

Methodology

The present experimental study consists of eight (four square and four rectangular) small scale concrete columns, from which half were confined with one layer of GFRP with the remaining half left unconfined to be used as control specimens, as presented in Table 3-1.

The two different cross-sections used in this study were square and rectangular with dimensions: 127 mm x 127 mm x 609.6 mm and 101.6 mm x 152.4 mm x 609.6 mm.

The cross-section sizes of the column specimens in the present study were chosen such that the side aspect ratio is kept equivalent to the full scale specimens tested by De Luca et al. (2011), to study the effect of cross-sectional size on confinement effectiveness of GFRP composite system. The square and rectangular specimens' cross-sections were selected so that they have equivalent cross-sectional area to study the effect of shape on confinement effectiveness.

A two-part designation is used to identify each specimen. The first part identifies whether the specimen is wrapped or not: "W" for wrapped specimens, and "U" for the control specimens. The second part indicates cross-sectional geometry: "S" stands for square (127 mm x 127 mm) and "R" for rectangular (101.6 mm x 152.4 mm).

Materials

The concrete mix used to cast the RC column specimens had a 28 day compressive strength of 36 MPa. Concrete strength was based on the results of compression tests on 6 by 12 in. (152.4 mm diameter by 304.8 mm) cylinder samples, as per ASTM C 39. All the columns were longitudinally reinforced with eight No. 2 G-60 (420 MPa) steel non-deformed bars, and steel with the same grade was used for tie reinforcement, as shown in Fig. 3-1. Properties of steel reinforcement used in the present study are presented in Table 3-2. Unidirectional continuous glass fiber sheets were used for the GFRP systems, where the properties of the fiber sheets as provided by the manufacturers are summarized in Table 3-3.

Specimen Preparations

The column specimens were designed using the ACI 318-63 code-mandated minimum amount of longitudinal reinforcement and minimum tie area at maximum spacing. The control square and rectangular RC columns have design capacities of 36.11 MPa and 35.95 Mpa, respectively. ACI 318-63 requires that the total area of longitudinal bars be larger than 1.0% of the gross section area, A_g; and that the vertical spacing of the ties be the smallest of 16 times longitudinal bar diameters, 48 times tie diameters, and the least lateral dimension of the column.

Preparation of the eight RC columns consisted of making the forms, preparing the steel cages, casting the concrete, capping the top and bottom ends of the columns, surface preparation which consisted of cleaning the concrete surface through light sand blasting, and application of primer throughout the surface of the columns for good bond between the concrete surface and the GFRP system, and application of the GFRP. Formwork for the rectangular and square cross-section columns were made as per the dimensions and steel reinforcement as seen in Fig. 3-1. Steel cages for each specimen were then prepared using eight no. 2 longitudinal steel bars with ties at 101.6 mm spacing. The RC columns were demolded after three days and the specimens were left to cure for 28 days before applying the GFRP laminates. High strength grout capping was applied to each specimen to ensure that columns remained plumb with parallel ends.

Wrapping of the RC columns with GFRP required cutting the glass fiber sheet as per the specimen geometry, and mixing the two parts of epoxy (as recommended by the manufacturer). Before applying the fiber sheet reinforcement, the corners of the square

and rectangular cross-section concrete columns were beveled with a chamfer radius of approximately 9 mm to prevent damage to the fabric at the corners, and improve the overall confining effect of the GFRP as suggested in ACI 440. After the concrete surface preparation was completed, the already cut-to-dimension continuous dry glass fiber sheet was laid down horizontally to impregnate it manually following a wet-layup technique where a ribbed roller was used throughout the process to improve fiber impregnation. GFRP was then applied over the concrete column, keeping it impregnated and providing an overlap of 101.6 mm to prevent slip. The GFRP-wrapped RC columns were left to cure at room temperature for more than 48 hours before testing began. A total of four RC columns were wrapped with one layer of GFRP. Fig. 3-2 shows a sample GFRP wrapped RC column.

Testing

Pure axial compression load test was set-up for all the specimens. Each of the eight concrete specimens, both wrapped and control RC columns, were tested to failure under monotonically increasing concentric load at a displacement control rate of 0.5 mm/min (0.02 in/min). The test was performed using a displacement controlled 889 kN (200 Kip) capacity universal test frame. The top loading plate, together with the high strength grout capping at the top and bottom ends of the specimens, helped ensure concentric loading was applied. Each specimen was instrumented with linear variable differential transformer (LVDT) sensors on the external surface to measure the vertical displacement of the specimen, as shown in Fig. 3-3. An external load cell of 889.64 kN capacity was also used in the test set-up. All data were gathered using a National Instruments data acquisition system.

Results and Discussion

A number of researchers carried out studies on the possible parameters that affect strengthening of RC columns using FRP jacketing. Mirmiran et al. (1997) studied dilation characteristics of confined concrete, and concluded that effectiveness of the jacket on ultimate values is dependent on stiffness of the jacket. Cross-sectional geometry, and jacket parameters like rupture strain and ultimate stress of the jackets affect the stress-strain behavior of FRP confined concrete. Corner radius, number of FRP layers (thickness of FRP), modulus of elasticity of FRP, grade of concrete, and FRP volumetric ratio are some of the parameters that affect the confinement of FRP wraps (Toutanji et al. (2010), Seible et al. (1997), Rochette and Labossiere (2000)). The present study focuses on two of the aforementioned parameters that affect confinement of GFRP wraps namely, cross-sectional shape and size (i.e. scale of the RC columns).

The test results of the present study are summarized in Table 3-4. Maximum load applied, P_{peak}; axial deformation when the maximum load (peak) was reached, δ_{peak}; and ratio of concrete axial stress at peak, $\sigma_{c,peak}$, normalized with respect to the average concrete compressive strength, f_c', between confined and unconfined specimens are reported.

Failure of the control specimens initiated with vertical cracks followed, first, by lateral displacement of the longitudinal bars that contributed to the splitting of the concrete cover and, finally, by crushing of the concrete core and buckling of the longitudinal bars, as shown in Fig. 3-4. All GFRP-confined columns failed due to rupture of the GFRP jacket; cracking of the concrete core developed after the maximum load was attained, and

longitudinal bar buckling was visible after the removal of the ruptured GFRP jacket and concrete cover, as shown in Fig. 3-5. In evaluating the increment in concrete strength due to GFRP confinement, the strength of the control column specimen normalized with respect to f'_c was used as presented in Table 3-4.

The normalized concrete axial stress versus axial deformation plot for the four specimens from each category of the test specimens is shown in Fig. 3-6. The GFRP confined specimens behaved similarly with respect to each other with the load steadily decreasing after reaching the peak load while the axial deformation continued increasing due to the confining action of the GFRP wrap. Failure occurred by rupture of the FRP laminates. Fiber rupture always initiated in the proximity of a corner and then propagated towards the sides. From the experimental results, it was observed that the axial load carrying capacity of reinforced concrete columns under pure axial compression was increased due to GFRP application for both the rectangular and square specimens, but not by the same amount. The load carrying capacity of the reinforced concrete columns with rectangular cross-section without and with GFRP confinement was 450.16 kN and 530.05 kN, respectively under pure axial loading, showing 17.74% increase due to one ply of GFRP wrapping. This increment in load carrying capacity was increased to 30.58% for reinforced concrete column with square cross-section, keeping all the other parameters the same. An even greater improvement was observed in the axial deformation experienced by the confined specimens, it increased by a factor of 3.63 and 4.08 in the rectangular and square specimens, respectively. The specimens with square cross-section experienced higher deformation before failure than the rectangular columns. Thus from the test results it can be concluded that, the GFRP wrapping was more effective in

increasing the axial load carrying capacity of square specimens than the rectangular specimens and GFRP confinement had a greater impact in enhancing the axial deformation than the axial load bearing capacity for both the square and rectangular columns.

Size effect

The size effect on structural strength is an important phenomenon with a historical background. In any case, this phenomenon is still not considered in most specifications of the design codes for concrete structures, as well as the design practices for polymer composites. A size effect study was done through the comparison of strength confinement effectiveness in the small scale specimens (present study) with the confinement effectiveness in the full scale columns by De Luca et al. (2011). A 0.503 mm thick GFRP laminate was used in wrapping small scale specimens, while 2.515 mm thick GFRP of the same mechanical behavior was used in confining the full scale specimens, providing equivalent confining pressure. The strength confinement effectiveness (f'_{cc}/f'_{co}) and confining pressure (f_l) for small scale and full scale columns are summarized in Table 3-5. The strength confinement effectiveness in enhancing axial strength was 1.31 for small scale square specimens while it was 1.15 for the full scale square columns. It was 1.17 and 1.13 for rectangular small scale and full scale specimens, respectively. Based on this, it was concluded that the GFRP jacket was more effective in enhancing load bearing capacity in columns with smaller cross-sections.

Comparison between present experimental results and existing models

Concrete confinement is a very important design factor when designing concrete columns under axial compression. Studies have shown that effective transverse confinement can cause a large improvement in axial strength and ductility of the concrete member (Mirmiran et al. (1999)). The increased ductility is a desired attribute, allowing warning of structural failure in the member.

Different researchers proposed models for concrete confined with different types of reinforcement, beginning with traditional reinforced concrete. The most widely accepted model for reinforced concrete is by Mander et al (1988). This model was originally used as a starting point for FRP modeling, but it was found to over-estimate the strength of the FRP reinforcement (De Lorenzis and Tepfers (2003)). Spoelstra and Monti (1999) developed a confinement model not only for FRP reinforcement but also for steel jackets or other transverse reinforcement. Their model uses an iterative approach. The model keys on the interaction between the dilating concrete and the confining device, in this case the FRP. Saadatmanesh et al. (1994) noted that the rate at which the ultimate parameters of the concrete are reached can be slowed with a higher concrete compressive strength. Also, ductility can be increased with an increase in the thickness of the FRP wrap.

Most of the available models for evaluating the compressive strength of FRP-confined concrete columns are based on the confinement model that was derived experimentally by Richart et al. (1928) for specimens under active hydrostatic pressure:

$$\frac{f'_{cc}}{f'_{co}} = 1 + k_1 \frac{f_l}{f'_{co}} \qquad \text{(equation 3.1)}$$

Where: f'_{cc} *and* f'_{co} are the compressive strengths of confined and unconfined concrete, respectively; f_l is the lateral hydrostatic pressure, and k_1 is the confinement effectiveness coefficient.

This is the general form adopted by the majority of the existing strength models for FRP confined concrete. Numerous strength models have been developed by fitting experimental data to the general form of equation 3.1, and the confinement effectiveness coefficient k_1 is derived as a constant, as a function of the effective lateral confining pressure f_l. Five existing models for FRP-confined non-cylindrical columns are summarized below.

Samaan et al. (1998)

Samaan et al. (1998) proposed a confinement model for an FRP-encased concrete, which is given by:

$$\frac{f'_{cc}}{f'_{co}} = 1 + k_1 k_s \frac{f_l}{f'_{co}} \qquad \text{(equation 3.2)}$$

Where k_s is the shape factor that accounts for the effect of non-uniform confinement and is defined as $k_s = 2r/D$, in which *r* denotes the corner radius, and *D* is the diameter of an equivalent circular column and equated to the side length of a square column or the longer side length in the case of a rectangular section. The confinement effectiveness

coefficient k_1 in the model is adopted as $k_1 = 6.0 f_l^{-0.3}$. Therefore, its final form is given by:

$$\frac{f'_{cc}}{f'_{co}} = 1 + 6.0\left(\frac{2r}{D}\right)\frac{f_l^{0.7}}{f'_{co}} \qquad \text{(equation 3.3)}$$

Lam and Teng (2003)

This model takes the form

$$\frac{f'_{cc}}{f'_{co}} = 1 + 3.3\left(\frac{A_e}{A_c}\right)\frac{f_l}{f'_{co}} \qquad \text{(equation 3.4)}$$

Where the value of the confinement effectiveness coefficient k_l of 3.3 is obtained by calculating the confining pressure f_l in Equation 3.1 with $\varepsilon_j = \varepsilon_{h,rup}$ and replacing d with an equivalent diameter D that is defined as the diagonal distance of the section, i.e., $D = \sqrt{h^2 + b^2}$, where h and b are the depth and breadth of the column section, respectively.

The shape factor is taken into account by the effective confinement area ratio of A_e/A_c that is given by

$$\frac{A_e}{A_c} = 1 - \left[\left(\frac{b}{h}\right)(h - 2R_c)^2 + \left(\frac{h}{b}\right)(b - 2R_c)^2\right]/3A_g \quad \text{(equation 3.5)}$$

Where A_g is the gross area of the column section, i.e. $A_g = bh - (4 - \pi)r^2$.

Challal et al. (2003)

In this model, the compressive strength of FRP strengthened concrete is given by:

$$f'_{cc} = f'_{co} + 412000k \qquad \text{(equation 3.6)}$$

Where the stiffness coefficient k is:

$k = \frac{E_f A_f}{E_f A_f}$, Where A_f is the area of 1 inch-wide FRP sheet.

Mirmiran and Shahawy (1997)

In the model proposed by Mirmiran and Shahawy (1997), the shape factor k_e is expressed as a function of the diameter of an equivalent circular column, D, and the corner radius *r* as:

$$k_e = \frac{2r}{D} \qquad \text{(equation 3.7)}$$

The compressive strength of FRP strengthened concrete is computed as follows:

$$f'_{cc} = f'_{co} + kf'_l \qquad \text{(equation 3.8)}$$

Where $f'_l = k_l f_l$ and $k_l = 6f_l^{-0.3}$

ACI committee 440

The model in ACI 440 predicts the maximum confined compressive strength as in Lam and Teng's model (2003) with the inclusion of a reduction factor, $\varphi_f = 0.95$:

$$f'_{cc} = f'_{co} + \varphi_f 3.3 k_a f_l \qquad \text{(equation 3.9)}$$

The confining pressure is given by:

$$f_l = \frac{2E_f n t_f \varepsilon_{fe}}{D} \qquad \text{(equation 3.10)}$$

Where $\varepsilon_{fe} = k_\varepsilon \varepsilon_{fu}$

Strain efficiency factor, $k_\varepsilon = 0.55$ (ACI 440)

The shape factor, k_a for non-circular columns is given by:

$$k_a = \left(\frac{A_e}{A_c}\right)\left(\frac{b}{h}\right)^2 \qquad \text{(equation 3.11)}$$

Where: $$\frac{A_e}{A_c} = \frac{1 - \frac{\left[\left(\frac{b}{h}\right)(h-2r_c)^2 + \left(\frac{h}{b}\right)(b-2r_c)^2\right]}{3A_g} - \rho_g}{1-\rho_g} \qquad \text{(equation 3.12)}$$

The confinement effectiveness of the specimens in the present study is compared with the predictions of the existing confinement models. Two of the existing models (Lam and

Teng (2003) and ACI 440) have over-predicted the confinement effectiveness of the GFRP confined columns, while the models by Samaan et al. (1998), Mirmiran and Shahawy (1997) and Challal et al. (2003) under-predicted the maximum confined concrete compressive strength, as shown in Table 3-6. This inconsistency among the existing models highlights the importance of further study on non-cylindrical GFRP confined concrete.

Conclusions

- The predominant failure mode observed was rupture of the glass fiber, which shows that the matrix phase was able to fully impregnate the continuous glass fibers. Design of GFRP wrapped columns can be based on the rupture strength of the glass fibers used in the FRP system, as it is supported by the present study;
- Strength and deformability of RC columns of both rectangular and square columns were enhanced due to the passive confining action of the GFRP composite system applied. Deformability enhancement observed was much more significant than the strength enhancements. The confinement effectiveness of GFRP composite in enhancing deformability and axial load carrying capacity was greater in the case of square columns that their rectangular equivalents.
- GFRP composites were found to be more effective in enhancing the axial strength of small scale specimens than the full scale columns.
- Models by Lam and Teng and ACI 440 overestimated the confined concrete axial strength, while models by Mirmiran and Shahawy, Samaan et al., and Challal et al. underestimated the confined concrete strength.

Table 3-1: Test matrix

Specimen ID	Cross-section geometry	Description
UR-1	101.6 mm x 152.4 mm	control rectangular
UR-2	101.6 mm x 152.4 mm	control rectangular
WR-1	101.6 mm x 152.4 mm	rectangular with one layer of GFRP-wrap
WR-2	101.6 mm x 152.4 mm	rectangular with one layer of GFRP-wrap
US-1	127 mm x 127 mm	control square
US-2	127 mm x 127 mm	control square
WS-1	127 mm x 127 mm	square with one layer of GFRP-wrap
WS-2	127 mm x 127 mm	square with one layer of GFRP-wrap

Table 3-2: Internal steel reinforcement properties

Description	Steel
Specified yield strength (f_y)	413.26 MPa
Yield tensile strain (ε_{sy})	0.002 mm/mm
Tensile modulus of elasticity(E_s)	199950 MPa

Table 3-3: GFRP system properties (manufacturer's values)

Filament yarn properties	**Value**
Ratio in volume (%)	100
Tensile modulus (MPa)	76,948.20
Tensile strength (MPa)	3,399.24
Tensile strain (%)	4.7
Sheet properties	**Value**
Ply thickness (mm)	0.503
Weight (kg/m^2)	0.596

Table 3-4: Confinement effectiveness, $\frac{f'_{cc}}{f'_{co}}$ (experimental results)

Specimen ID	P_{peak} **(kN)**	δ_{peak} **(mm)**	$(\sigma_{c,peak}/f_c)/(\sigma_{c,peak}/f_c)_{control}$
UR	450.14	1.85	1.00
WR	530.03	6.89	1.17
US	323.18	2.30	1.00
WS	422.02	7.98	1.31

Table 3-5: Comparison of confinement effectiveness (small scale vs. full scale)

Cross-section		Confinement effectiveness (f'_{cc}/f'_{co})	Confining pressure (f_l) (Mpa)
Square	127 mm x 127 mm (Small scale)	1.31	20.17
	609.6 mm x 609.6 mm (Full scale)	1.15	21.16
Rectangular	101.6 mm x 152.4 mm (Small scale)	1.17	19.86
	355.6 mm x 508 mm (Full scale)	1.13	20.32

Table 3-6: Confinement effectiveness, $\frac{f'_{cc}}{f'_{co}}$ (existing models and present study)

Cross-section	Mirmiran et al. (1997)	Samaan et al. (1998)	Challal et al. (2003)	Lam and Teng (2003)	ACI 440	Present study (Exp.)
Rectangular	1.03	1.16	1.16	1.53	1.22	1.17
Square	1.04	1.21	1.16	1.53	1.49	1.31

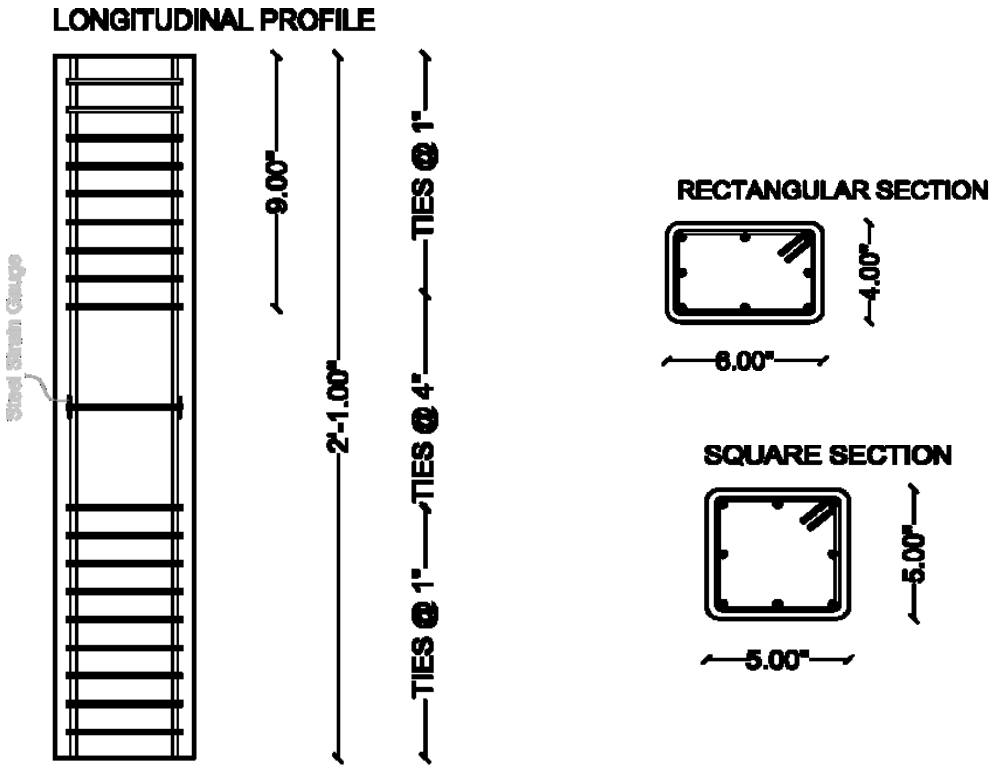

Fig. 3-1: Reinforcement layout of RC column specimen

Fig. 3-2: Sample GFRP wrapped column

Fig. 3-3: Sample instrumentation and test set up

Fig. 3-4: Sample of failed control RC columns

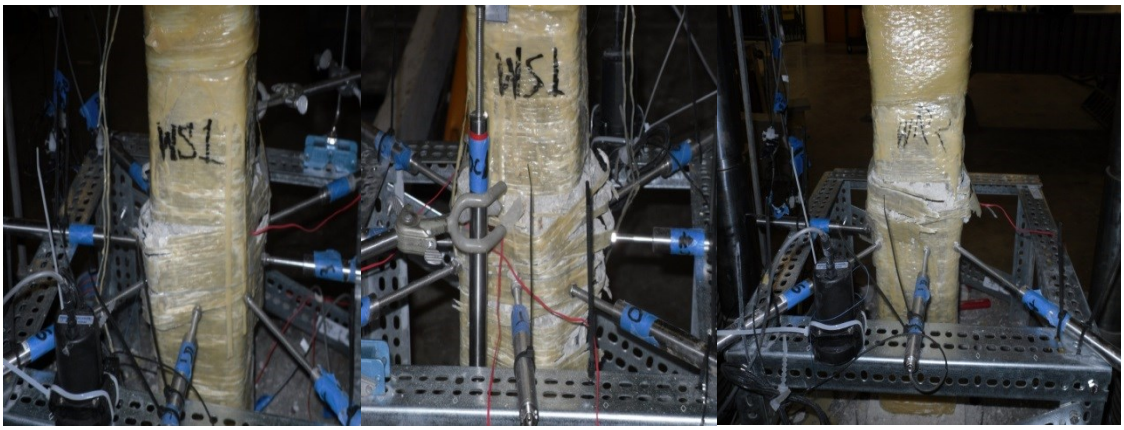

Fig. 3-5: Sample of failed GFRP wrapped concrete columns

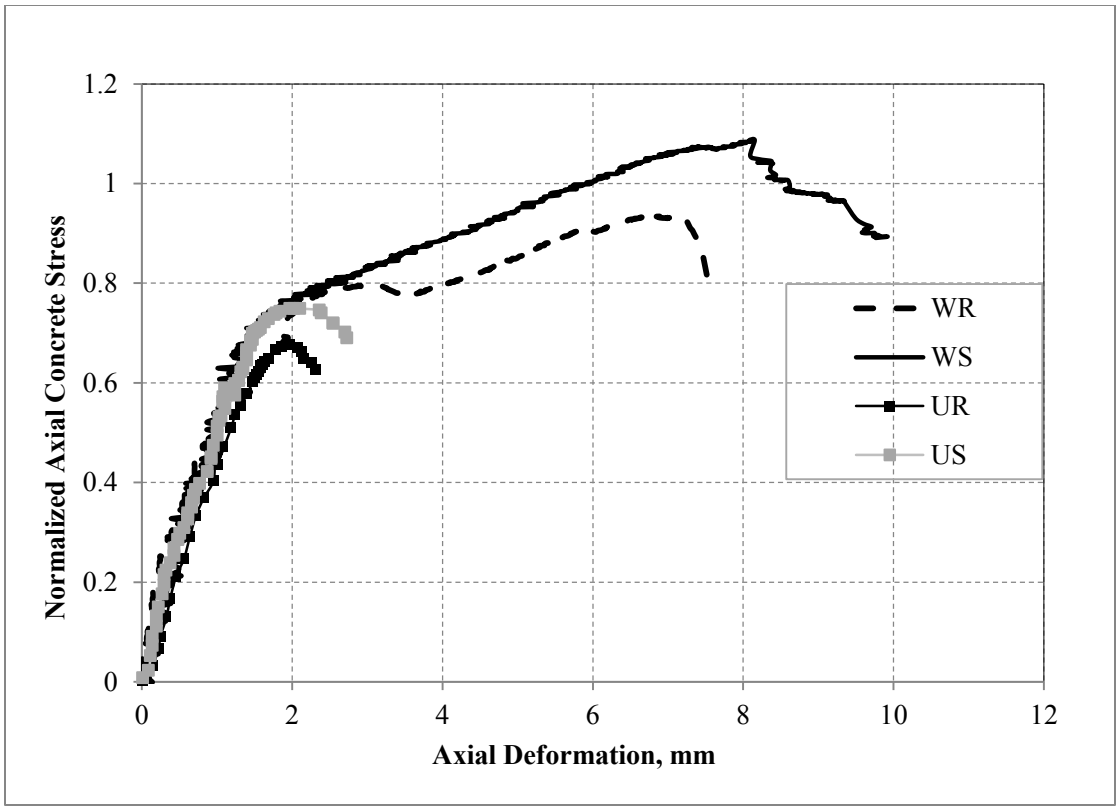

Fig. 3-6: Normalized concrete axial stress vs. axial deformation

Where: WR - GFRP confined rectangular RC column; UR - Unconfined rectangular RC column; WS - GFRP confined square RC column; and US - Unconfined square RC column.

CHAPTER IV

STUDY 3: FABRIC REINFORCED CEMENTITIOUS MATRIX (FRCM) COMPOSITES AS CONFINING SYSTEMS FOR RC COLUMNS

Background

A number of alternative techniques are available for retrofitting and strengthening of RC structures, based on different principles of such as: maintaining continuity of load path, removal of structural irregularities; strengthening; and, enhancing deformation capacity. The use of fiber reinforced polymer (FRP) wraps to confine concrete columns is one form of such strengthening or ductility enhancement that has received much attention from the research community and has found significant use in practice, as discussed in detail in studies 1 and 2 of this report.

Similar to other strengthening materials, FRP has some disadvantages when used in hot, humid, or other aggressive environments mainly due to the loss in the bonding effectiveness of the epoxy used (ACI 549). Fabric Reinforced Cement Matrix (FRCM) was proposed as an alternative material to FRP, by replacing the organic resin with inorganic cement based mortar to address the drawbacks of using FRP. Thus FRCMs like FRPs are composite materials, heterogeneous and anisotropic, having prevalently elastic behaviors until collapse but with high durability in the face of high temperatures, and fire exposure. The performance of the FRCM system can be improved by using ultra-high-strength fiber fabrics, such as the polyparaphenylene-benzobisethiazole (PBO), which is evaluated in the present study. Results of research conducted on bond behavior and

flexural, shear and axial strengthening are available in the literature to document the viability of FRCM systems (ACI 549).

D'Ambrisi et al. (2012) conducted an experimental investigation on the bond developed between PBO-FRCM and concrete surface by means of double shear tests. They evaluated different effective anchorage length of 250 mm – 300 mm and found a maximum debonding strain of 0.825 %. They reported that the debonding occurs at the fabric/matrix interface after a considerable fabric/matrix slip.

Experimental results of RC beams strengthened in flexure with various types of FRCM materials confirm the effectiveness of FRCM materials for strengthening RC beams (D'Ambrisi et al., 2011). They reported that the failure of FRCM strengthened beams was caused by the loss of strengthening action consequent to fiber/matrix debonding.

Triantafillou and Papanicolaou (2006) concluded that FRCM jacketing provides substantial gain in shear resistance (up to 70 % for one layer of FRCM) after investigating, experimentally and analytically, the use of FRCM to increase shear resistance of RC members with rectangular cross sections under monotonic and cyclic loading.

Triantafillou et al. (2006) conducted experimental investigation of three different parameters, inorganic mortar versus resin-based matrix, strength of the inorganic mortar, and number of reinforcement layers, using cylindrical specimens. They also performed testing on rectangular prisms aimed at investigating the use of inorganic mortar versus resin-based matrix, number of reinforcement layers, and effectiveness of bonded versus unbonded confinement and concluded the following: a) FRCM confining jackets provide

substantial gain in compressive strength (25 % and 49 % for two and three layers, respectively) and deformation capacity (by a factor of 4.9 and 5.4 for two and three layers, respectively). This gain increases with the number of fabric layers and depends on the tensile strength of the mortar, which determines whether failure of the jacket occurs due to fiber fracture or debonding; b) compared with their resin-impregnated counterparts, FRCM may have slightly lower effectiveness in enhancing axial strength and strain capacity, depending on the type of mortar (strength gain of 25 % for two layers of FRCM versus 53 % for two layers of FRP; ultimate strain gain by a factor of 4.9 for FRCM versus 8 for FRP) ; and, c) failure of FRCM jackets is less brittle compared to organic resin-impregnated systems, due to the slowly progressing failure of individual fiber strands and slippage.

De Caso et al. (2011) conducted experimental investigation plain concrete cylinders confined by fiber reinforced cement-based matrix (FRC) for confinement effectiveness. A total of 18 cylinders (out of 22) confined by one, two or four layers of basalt FRC were tested for compression with the objectives of understanding their confinement effectiveness. The study reported a linear strength enhancement for the different FRC reinforcement: 21 % for one ply, 64 % for two plies and 121 % for four plies. They also reported average increases in axial strain 34 % for one layer, 333% for two layers and 115% for four layers of FRC confinement. Loss of compatibility in the external reinforcement due to fiber-matrix separation was found to be the predominant failure mode.

Even though some interesting field applications have been reported that justify FRCM potential as a strengthening technology (Nanni, 2012), experimental and theoretical research is still needed to fully characterize FRCM and quantify its mechanical effectiveness based on parameters such as type and arrangement of fibers, type of cementitious matrix, and conditions of the substrate (D'Ambrisi and Focacci, 2011).

Previous studies on strengthening (Fam, A. Z. et al., 2001; Harries, K. A. et al., 2002; Mirmiran, A. et al., 1997; De Luca et al., 2011) have shown that the number of layers of wrapping material affects the performance of RC columns. Quantifying the amount of enhancement in load bearing capacity and ductility obtained by additional layers of the confining material is needed for economical strengthening of columns.

This study of the dissertation presents an experimental program of RC columns with various cross-sectional shapes confined with one or four layers of PBO-FRCM composite systems with the objectives of: investigating the effectiveness of PBO-FRCM confinement as it relates to cross-section geometry and number of plies; and providing experimental data to develop analysis and design tools. A total of 27 specimens with equivalent cross-sectional area of 16,129 mm^2 and height of 609.6 mm were tested to investigate and quantify the enhancement in strength and ductility of RC columns of different cross-sectional shapes. Rectangular, square, and circular specimens with constant cross-sectional area and height were considered to properly isolate the effect of shape on the confinement effectiveness. In addition to the cross-sectional shape, columns with one or four layers of PBO-FRCM wrapping were tested to investigate the effect of the number of plies on their performance.

Methodology

The specific objectives of this study were intended to be achieved by testing PBO-FRCM wrapped RC columns of different cross-section, and number of PBO-FRCM layers for pure axial compression. Table 4-1 shows the test matrix of the present experimental study. Three different cross-sectional shapes were considered: circular, 152.4 mm in diameter; rectangular, 101.6 mm x 152.4 mm; and square, 127 mm x 127 mm. All the specimens had an equal height of 609.6 mm with equal internal steel reinforcement. Before applying the fabric, the corners of the square and rectangular cross-section RC columns were beveled to prevent damage to the PBO fabrics at the sharp corners and improve the confining effect of the PBO-FRCM composite material. After the surface preparation was completed, PBO-FRCM was applied over the concrete column in one or four layers following the recommendations provided by the manufacturer. Three specimen types each with three repetitions were considered per cross-section type: one was kept as-built and used as a benchmark, while the other two were wrapped with one and four plies of PBO-FRCM composite material. The specimen notations are as follows. The first letter refers to the size of specimens: S for small scale specimens. The next letter refers to cross-section shape: C for circular, S for square and R for rectangular, followed by the number of PBO-FRCM layers (0, 1 or 4). The last part refers to the repetition number (1, 2 or 3).

Materials

Concrete Mixtures

Two concrete mixtures of equivalent unconfined concrete strength were used for making the RC columns tested in this study. Concrete with compressive strength of 24.64 MPa was used for the square and circular specimens, and concrete with compressive strength of 22.84 MPa was used for the rectangular specimens, as presented in Table 4-2. Mixtures were prepared at Supermix batching plant in Miami using a mechanical mixer. The mechanical characteristics of each concrete mixture were experimentally determined as per ASTM C39 based on eight cylindrical concrete specimens with a nominal diameter of 152.4 mm. Table 4-2 summarizes the batch information and average compressive strengths. Table 4-3 provides detailed information of each compressive strength test from the cylinder compressive tests conducted for the two batches.

Internal steel reinforcement

All the columns were longitudinally reinforced with eight No. 2 G-60 (420 MPa) steel non-deformed bars and steel with the same grade was used for tie reinforcement. Internal steel reinforcement properties used for the present study are shown in Table 4-4.

FRCM composite systems

FRCMs are composite systems composed of two different phases with different physical and mechanical properties, so as to give the composite different properties than those of its constituents. The reinforcement phase used in this study was polyparaphenylene-benzobisethiazole (PBO) fabric, and the matrix was a grout system based on Portland cement and a low dosage of dry organic polymers, less than 5% by weight (Nanni, 2012).

To obtain a composite with good mechanical properties, it is not sufficient to use resistant fabrics, it is also necessary to provide good adhesion between the matrix and the reinforcement. The matrix comprises high-fineness cement, an adhesion promoter, inorganic nanoparticles, micro-aggregates, and a poly-carboxylate water-reducing admixture, and was designed to achieve a chemical bond with the PBO fabric (Nanni, 2012). The manufacturers' values for PBO fiber and fabric characteristics used in this study are presented in Tables 4-5 and 4-6, respectively. The mechanical properties, including the modulus of elasticity and the tensile strength of the PBO-FRCM composite used in this study, were obtained through tensile testing of flat coupons by Arboleda et al., 2012. Flat coupon specimens were tested according to AC434, Appendix A for PBO-FRCM composite systems (Arboleda et al., 2012) and properties found are summarized in Table 4-7. These properties were used for the design calculations.

Specimen Preparation

The experimental program in this study consisted of: 1) nine small columns with rectangular cross-section of 101.6 mm x 152.4 mm and a height of 609.6 mm; 2) nine small columns with square cross-section of 127 mm x 127 mm and a height of 609.6 mm; and 3) nine small cylindrical columns of 152.4 mm in diameter and 609.6 mm of height.

Preparation of the RC columns consisted of making the forms, preparing the steel cages, casting the concrete, capping the top and bottom ends of the columns, surface preparation, and application of the PBO-FRCM. The rectangular, square and circular cross-section columns were made as per the dimensions and steel reinforcement details shown in Fig. 4-1.

Beveling the corners of the square and rectangular columns (to avoid damage to the PBO-fabric) was made possible through the application of 9 mm radius moldings at the four corners of each formwork before casting. Steel cages for each specimen were then prepared using eight no. 2 longitudinal steel bars with ties according to the reinforcement detail presented in Fig. 4-1. A debonding agent was applied to the molds, and the steel cages were put in place allowing for a 10 mm thick concrete cover on all sides. RC column specimens were left to cure for over 28 days as per ASTM C192 before applying the external strengthening PBO-FRCM composite system. The PBO-FRCM installation process followed the methodology described below where the main fabric was oriented at 90° direction with respect of the main axis of the column. Additionally, in order to avoid premature failure at the two ends of the column specimens, glass fiber reinforced polymer (GFRP) plies were applied to stiffen the ends. Sulfur compound caps were applied to each specimen to ensure that columns remained plumb. Surface preparation for PBO-FRCM application consisted of light sand blasting.

PBO-FRCM Composite Material Preparation and Installation

The inorganic matrix product was prepared by mechanical mixing, since hand mixing was not recommended by the manufacturer. The preparation started by adding the dry powder cementitious matrix to 90% of the water needed for the mix. Mixing continued for at least three minutes until creating a homogeneous matrix paste. If necessary, the remaining water was mixed for additional two minutes. Upon completion, the mortar was allowed to rest for two minutes before applying on the substrate surface. The matrix to water ratio for the inorganic matrix used in this study was six liters of water to 25 kg material.

PBO-FRCM composite material Installation

The installation of the PBO-FRCM composite system was performed with the presence of trained personnel on all specimens. The procedure to install the PBO-FRCM strengthening system followed was similar to the wet layup technique used in fiber reinforced polymer (FRP) composite systems as described below, refer to Fig. 4-2.

Step 1: Surface preparation: Preparing the substrate was done using pressurized water to clean the surface of the structural element from dust and other contaminants.

Step 2: The first layer of matrix was applied with a trowel on the structure surface with a thickness of 3 to 4 mm.

Step 3: The pre-cut fabric was laid on top of the first matrix layer and pressed lightly with the bottom of the trowel to embed the fiber in the matrix.

Step 4: A second layer of the matrix was added with the trowel to cover the fabric with a thickness of 3 to 4 mm.

An overlap of 100 mm was used when joining fabrics together at the end of each layer. The environmental temperature for FRCM application specified by the manufacturer was between 5 ºC to 35 ºC, and for the present study PBO-FRCM application was performed at room temperature.

Throughout the processes of preparation and installation of the PBO-FRCM systems applied on the test specimens, quality control evaluations were performed. Quality

control evaluations consisted of: verification checks of the mass prior to mixing the matrix with the water; visual checks on the consistency of the matrix before, during, and after installation; matrix thickness layer verification with a vernier caliper; environmental temperature check before, during, and after installation; and installations performed indoors to shelter from the environment (direct sun and rain). In addition to these measures all the constituent materials were handled based on the manufactures specifications and laboratory internal procedures, to ensure proper use of the PBO-FRCM composite system.

The first layer of matrix was applied on the concrete surface leaving 25.4 mm from bottom and top ends uncovered to avoid direct vertical loading of the PBO-FRCM jacket. The fabric was then wrapped around the column with the main direction perpendicular to the column axis, keeping it impregnated and providing an overlap of 100 mm at the end of each ply. The mesh was pressed into the matrix, and a 3 mm deep layer of mortar was applied at the overlap zone on top of the first layer of the fabric. For specimens with four plies, 3 mm thick layer of mortar was applied on top of the preceding fabric. The PBO-FRCM wrapped specimens were left to cure at room temperature for 28 days before any testing began. A total of 18 RC columns were wrapped with the PBO-FRCM composite, out of which nine were wrapped with one layer and the remaining nine with four layers.

Testing

Pure axial compression tests were conducted for all RC columns. The tests were performed using a displacement controlled universal test frame with a maximum capacity of 889 kN (200 kip). Each of the 27 concrete specimens, both wrapped and control RC

columns, was tested to failure under monotonically increasing load at a rate of 0.51 mm/min. Specimens were centered via the concentric rings of the frame and placed between the loading plates and checked for plumbness in order to avoid any eccentricity. All specimens (including concrete cylinders) were capped with a sulfur compound at their ends to ensure a flat surface of loading against the loading plates of the frame. The top loading plate, together with the sulfur compound capping, helped apply pure concentric (compressive) loading. Axial load was measured via a force transducer in the test frame; axial shortening (vertical deformation) and the frame head displacement was measured via Linear Voltage Displacement Transducers (LVDTs). All data were gathered using a National Instruments data acquisition system. Fig. 4-3 shows a typical column specimen ready for testing.

Results and Discussion

Modes of failure

All the RC column control specimens failed in a manner expected under compression, with steel yielding and crushing of concrete at failure. The dominant failure mode in the PBO-FRCM strengthened RC column specimens in compression was fabric-matrix separation, after substantial dilation, as shown in Fig. 4-4. The incapability of the cementitious matrix to fully impregnate the PBO fabrics was the main drawback in the application of PBO-FRCM composite system for strengthening RC columns. The interfacial bond between the concrete surface and the PBO-FRCM system was also found to be weak. No fabric rupture was observed unlike the GFRP strengthened columns, but rather significant slippage was observed. This is a clear indication that the design criteria should not be based on ultimate strength of the fabric, rather on the bond strength at the

surface of contact between the PBO-fabric and matrix, and concrete and PBO-FRCM. All strengthened specimens experienced buckling of the internal steel reinforcement and crushing of concrete at failure, as discovered from post-test observation of the specimens, as seen in Fig. 4-5.

Stress versus strain curves

Stress versus strain curves to study the effect of PBO-FRCM layers and effect of cross-sectional shapes are presented in Fig. 4-6 and Fig. 4-7 respectively. These figures give the axial stress versus the axial strain for circular, square and rectangular specimens with zero, one or four layers of PBO-FRCM. The stress and strain at failure for the confined specimens of all cross-sections for both PBO-FRCM confinement amounts were higher than those for unconfined ones. These figures also show how the ductility of the concrete specimens was affected by the increase of the degree of confinement.

The stress versus strain graphs in Fig. 4-6 is mostly bilinear. The slope of the initial stages of the stress-strain curves is linear which is essentially identical to that of the unconfined concrete columns. The PBO-FRCM jacket had little effect on this portion of the curves in all the cross-sections, which indicates that no confinement is activated in the PBO-FRCM, except that stiffer jackets (four layers) increased the stress and strain at the transition zone especially for circular cross-sections. After the peak strength of the unconfined concrete was reached, the concrete started to expand rapidly with little increase of the load, leading the concrete to deteriorate in its internal structure and yet experience higher confining pressure from the PBO-FRCM jacket. Since circular columns were fully confined, the stress-strain curves with four layers of PBO-FRCM

have shown a sustainable ascending curve even though the stiffness of curve decreases, showing that the confining pressure developed from the four layers of PBO-FRCM was able to overcome the effect of concrete degradation under the large strains it was experiencing. The one layer of PBO-FRCM confinement didn't have the same strengthening capacity, as it was unable to provide the concrete enough confining pressure to overcome degradation, thus the second stage of the curve was a flat plateau. Rectangular and square cross-sections had their confining action mostly limited at their corners, and thus their second stages didn't show significant increase in strength rather they showed flat plateau. These non-circular columns with low level of confinement (one layer) had a short plateau second stage followed by sudden drop, as enough confining pressure to overcome concrete degradation was not developed.

Strength and ductility

Compression behavior of the PBO-FRCM wrapped specimens was mostly similar in each series in terms of stress-strain curves and failure modes of the columns. From the average experimental results reported in Tables 4-8 and 4-9, it can be seen that the increase in strength and axial strain varied according to the cross section shape and the amount of confinement provided by PBO-FRCM (expressed in number of layers). Table 4-8 summarizes the average axial strength gains for RC columns of different cross-sectional shapes confined one and four layers of PBO-FRCM composite system. Table 4-9 summarizes the average axial deformability gains for RC columns of different cross-sectional shapes confined one and four layers of PBO-FRCM composite system. The test results show that with increase in number of PBO-FRCM layers, strength and ductility of PBO-FRCM wrapped reinforced concrete columns increase. The amounts of these

increases vary depending on the cross-section geometry and the number of PBO-FRCM layers applied. Results of the experimental investigation done by Loreto et al., 2013 were compared with the present study to investigate the effect of size on the confinement effectiveness of PBO-FRCM wrapped RC columns, as presented in Tables 4-10 and 4-11.

Effect of number of PBO-FRCM layers

The test results described in Table 4-8 indicate that PBO-FRCM confinement can enhance the ultimate strengths for the two thicknesses considered. The amounts of these increases varied depending on the number of PBO-FRCM wraps applied. As observed for circular cross-sections, the average increase in strength was 11% for one layer and 33% for four layers, over its unconfined concrete strength. The strength enhancement for square cross-sections was 10% for one layer and 24% for four layers of PBO-FRCM jackets, while rectangular cross-sections gained average strength increases of 6% and 11% for one layer and four layers of PBO-FRCM jackets. From these results, it is evident that four layers of PBO-FRCM confinement increased the confining pressure in all the cross-sections tested in this study, enhancing the axial strength of columns. Fig. 4-8 shows the gain in axial load capacity (%) versus number of PBO-FRCM layers for the three cross-sectional shapes.

The results described in Table 4-9 indicate that PBO-FRCM confinement can improve the ultimate axial strain in RC columns. As in the strength enhancement, the amount of enhancement in axial strain varied depending on the number of PBO-FRCM layers. Circular cross-sections showed average increase in ultimate axial strain of 30% for one layer and 132% for four layers, over the unconfined columns. The ultimate axial strain gain over the unconfined columns for square cross-sections was 21% for one layer and

90% for four layers of PBO-FRCM jackets, while rectangular cross-sections gained an average ultimate axial strain of 18% and 82% for one layer and four layers of PBO-FRCM jackets. From these results, it is evident that four layers of PBO-FRCM confinement increased the confining pressure in all the cross-sections tested in this study, preventing a brittle failure of the columns. The results showed that the improvement in axial deformation was higher than the enhancement in axial strength for all the cross-sections considered. Therefore, it can be concluded that, any level of PBO-FRCM confinement was effective in increasing strength, but more so in enhancing the compressive axial strain sustained by the columns, as presented in Fig. 4-9.

Fig. 4-10 shows the variation of confinement effectiveness (in terms of load bearing capacity, f'_{cc}/f'_{co}) with respect to the number of PBO-FRCM layers for the three cross-sections. As the layers of PBO-FRCM were increased from one to four, confinement effectiveness varied from 1.11 to 1.33 for circular columns, from 1.10 to 1.24 for square columns, and from 1.06 to 1.11 for rectangular columns.

Effect of cross-sectional shape of RC columns

Test results, Tables 4-8 and 4-9, clearly showed that both strength enhancement and ultimate strain capacity enhancement were more significant for circular columns than for square and rectangular columns. This is due to the stress concentrations at the corners of the square and rectangular cross-sectioned columns and consequently to the lower confining pressure and smaller effective confined concrete core areas. Similarly, square columns showed better strength enhancement and ultimate strain capacity enhancement than the rectangular ones. This is also because of smaller effective confined concrete core area in rectangular cross-sections at higher cross-sectional aspect ratios.

Fig. 4-10 presents the confinement effectiveness variation for the three cross-sectional shapes with different number of PBO-FRCM layers. It clearly shows that circular columns have a steepest curve indicating they gain the most out of every additional PBO-FRCM layer applied over the rectangular and square cross-sections. From the limited data, plotted in Fig. 4-10, from the present study, the following observations were made: circular columns showed a gain of 1.41 times the confinement effectiveness (in axial strength) attained by the square columns with equal level of confinement (in terms of number of layers), and 3.21 times the confinement effectiveness attained by the rectangular ones; and the square columns showed a gain 2.28 times the confinement effectiveness attained by the rectangular columns with equal level of confinement (in terms of number of layers).

Fig. 4-7 presents typical stress-strain relationships of the three cross-sections with equal number of PBO-FRCM layers to further understand the effect of cross-section on stress capacity and strain capacity.

Effect of size of RC columns

Summary of small scale versus large scale column specimens' average experimental results for confinement effectiveness in terms of axial load capacity enhancement is presented in Table 4-10. The test results showed that not only was the confinement most effective for circular columns than square columns and least for rectangular sections in enhancing their axial strength, but also PBO-FRCM confinement showed no significant difference between small scale and large sized columns. The large sized columns tested by Loreto et al., 2013 consisted of: 1) circular columns with a diameter of 228.6 mm; and 2) columns with square cross-section of 203.2 mm x 203.2 mm.

The increase in compressive axial strains at the peak loads is compared between the small scale and large scale columns in Table 4-11. The effect of number of PBO-FRCM layers and cross-sectional geometry on enhancing compressive strains at peak loads was observed to be similar except that the small specimens showed much more improvement relative to large sized specimens.

The stress-strain curves for typical small and large specimens are presented in Fig. 4-11. It shows that for both the cross-sections compared, the effect of PBO-FRCM confinement on strength enhancement and axial strains is more significant in the small scale specimens.

Comparison with AC434/ACI 549

The model in AC434 is based on Lam and Tang's stress-strain model presented in 2003 (AC434), which is based on limit state design principles and presented in Table 4-12. The "FRP based" model is used in design calculations for PBO-FRCM wrapped columns, with the modulus of elasticity for PBO-FRCM taken as the slope of the linear portion of its stress-strain curve. Once the FRCM composite system has cracked it behaves in a linear elastic manner, similar to FRP composites, until it fails completely. The values of strength and strain to be used in the design equations of AC434 are defined as the average value minus one times the standard deviation, while the elastic modulus is simply the average value. Table 4-12 shows the equations used for axial load capacity of PBO-FRCM wrapped RC columns. The contribution of the mortar matrix to the compressive strength of the FRCM-confined columns was neglected as per ACI 549.

Fig. 4-12a shows the performance of the AC434 model in predicting the confinement effectiveness for circular columns. The experimental versus theoretical confinement effectiveness is plotted to compare the predictions with respect to the actual values obtained from the experiment. The middle line of 1.0 indicates that the predicted values of $\frac{f'_{cc}}{f'_{co}}$ are equal to those of the tests. AC434 under-predicted the strength confinement effectiveness of all the 12 specimens tested. A similar performance has been observed for non-circular columns as presented in Fig 4-12 b.

Furthermore, Fig. 4-13 is presented to show the difference in stress-strain relationship between AC434 prediction and the experimental results of the present study for circular, square and rectangular columns with one and four layers of PBO-FRCM. AC434 predicts the stress-strain response of PBO-FRCM confined columns under pure axial compression accurately; however it underestimates the performance for all the cross-sections with both one and four layers of PBO-FRCM.

Table 4-13 presents a summary of average theoretical (AC434) versus experimental strength and strains for all the cross-sections with one and four layers of PBO-FRCM composites. AC434 predicts a strength gain of 5 % and 17 % for one and four layer of PBO-FRCM in circular specimens while the experimental values show a much higher strength gain of 11 % and 33 % respectively. Similar under-prediction, by AC434, of strength gains was observed in both square and rectangular cross sections. AC434 predicted the axial strain gain in circular specimens to be 32 % and 121 % compared with the 30 % and 132 % strain gain observed through the experimental investigation for one and four layers of PBO-FRCM wrapping.

Organic versus inorganic composites comparison

Compared with control specimens, GFRP wrapping increased the axial strength of square and rectangular specimens by 31 % and 17 %, respectively. The ultimate strain for square and rectangular cross-sections was enhanced by a factor of 4.08 and 3.63, respectively. The PBO-FRCM jacket also enhanced the axial strength of square and rectangular concrete by 10 % and 6 %, respectively, while the ultimate strain was enhanced by a factor of 1.21 and 1.18. The two composite systems used in the present study were both able to enhance strength and deformability performances of non-cylindrical concrete columns. A comparison of confinement enhancement of GFRP and PBO-FRCM jackets in enhancing axial strength and ultimate strain of square and rectangular specimens was undertaken and presented in Table 4-14. A 10% and 6% strength enhancement were obtained in the PBO-FRCM wrapped square and rectangular columns, while it was 31% and 17% in the case of GFRP confined columns. Deformability of these specimens was also enhanced by a factor of 4.08 and 3.63 in GFRP strengthened square and rectangular columns, respectively. Smaller deformability enhancements of 1.21 and 1.18 with respect to their unconfined counterparts of square and rectangular cross-sections respectively were observed in PBO-FRCM wrapped columns.

Conclusions

The following conclusions can be drawn from the results derived from the 27 PBO-FRCM strengthened and control RC columns tested under pure axial compression in the present study:

- The predominant failure mode was fabric-matrix separation, which is caused by insufficient impregnation of the cementitious matrix in to the structural PBO fabric. This may be remedied by improving the quality of the inorganic cementitious matrix and the PBO mesh to improve impregnation;
- Circular columns gained the most in terms of both axial load carrying capacity and ductility enhancement than their rectangular and square counterparts. The gain in axial deformation capacity was found to be much more significant than axial load carrying capacity enhancement for all the cross-sections. Small and Large columns of the same cross-section shape have shown equivalent strength gain, and the small columns gained more axial deformation capacity than their large counterparts;
- The model proposed in AC434 and ACI 549 was found to predict the behavior, even though it had under-predicted gains in axial strength;
- GFRP jacket provided better strength and deformability enhancements in both the square and rectangular cross-sections. It is worth mentioning that PBO-FRCM jackets didn't rupture in all the specimens tested, indicating the full capacity of the fabric was never used. Thus, improving the bond between the PBO fabric and the binding mortar will greatly improve PBO-FRCM performance.

Table 4-1: Test matrix

Cross-section	Confinement Condition	Specimen Designation	No. of Repetitions
Circular (152.4 mm diameter)	Benchmark	S_C_0_1,2,3	3
	PBO-FRCM – 1 Layer	S_C_1_1,2,3	
	PBO-FRCM – 4 Layers	S_C_4_1,2,3	
Rectangular (101.6 x 152.4 mm)	Benchmark	S_R_0_1,2,3	
	PBO-FRCM – 1 Layer	S_R_1_1,2,3	
	PBO-FRCM – 4 Layers	S_R_4_1,2,3	
Square (127 x 127 mm)	Benchmark	S_S_0_1,2,3	
	PBO-FRCM – 1 Layer	S_S_1_1,2,3	
	PBO-FRCM – 4 Layers	S_S_4_1,2,3	

Table 4-2: Concrete properties

Property	Unit	Batch 1 (B1)	Batch 2 (B2)
Compressive strength (f'_c)	MPa	22.84	24.64
Ultimate compressive strain (ε_{cu}) (assumed)	mm/mm	0.003	0.003
Compressive modulus of elasticity (E_c) (computed)	MPa	22607	23483

Table 4-3: Compressive concrete strength of concrete cylinders (102 mm diameter, 204 mm height)

Specimen ID	Peak Load		Compressive Strength	
	kN	lbf	MPa	psi
B1 - 1	179	40303	22.13	3209
B1 - 2	179	40176	22.06	3199
B1 - 3	184	41414	22.74	3297
B1 - 4	189	42470	23.32	3381
B1 - 5	188	42197	23.17	3360
B1 - 6	188	42161	23.15	3357
B1 - 7	183	41104	22.57	3273
B1 - 8	191	42871	23.54	3413
Average	--	--	22.84	3311
St. Dev.	--	--	0.51	74.65
C.O.V (%)	--	--	2.25%	2.25%
B2 - 1	200	44911	24.66	3576
B2 - 2	197	44219	24.28	3521
B2 - 3	202	45348	24.9	3611
B2 - 4	200	44984	24.7	3582
B2 - 5	194	43654	23.97	3476
B2 - 6	198	44510	24.44	3544
B2 - 7	203	45603	25.04	3631
B2 - 8	204	45803	25.15	3647
Average	--	--	24.64	3573
St. Dev.	--	--	0.37	54.01
C.O.V (%)	--	--	1.51%	1.51%

Where B1 – Batch 1, B2 – Bach 2 (eight cylinders for each batch)

Table 4-4: Internal steel reinforcement properties

Property	Value
Specified yield strength (f_y)	413.26 MPa
Yield tensile strain (ε_{sy}) (assumed)	0.002 mm/mm
Tensile modulus of elasticity (E_s) (computed)	199950 MPa

Table 4-5: PBO fiber characteristics (manufacturer's values)

Property	Value
Density (g/cm^3)	1.56
Tensile strength (GPa)	5.8
Modulus of elasticity (GPa)	270
Ultimate deformation (%)	2.15
Breakdown temperature (°C)	650
Coefficient of thermal dilation (10-6 °C-1)	-6

Table 4-6: Fabric characteristics (manufacturer's values)

Property	Value
Weight of the fabric (g/m^2)	126
Weight of PBO fibers in the fabric (g/m^2)	88
Equivalent dry fabric thickness in the direction of the warp (mm)	0.0455
Equivalent dry fabric thickness in the direction of the weft (mm)	0.0115
Ultimate tensile strength of the warp by width unit (KN/m)	264
Ultimate tensile strength of the weft by width unit (KN/m)	66.5

Table 4-7: PBO-FRCM properties (Arboleda et al. (2012))

Property	Value
Fiber area by unit width (A_f)	47.52 mm^2/m
Ultimate tensile strain (ε_{fu} -$\sigma_{\varepsilon fu}$)	0.005388 mm/mm
Tensile modulus of elasticity of the cracked PBO-FRCM composite material specimen (E_f)	137422 MPa
Ultimate tensile stress* (f_{fu})	898 MPa

* *Where* $f_{fu} = (\varepsilon_{fu} - \sigma_{\varepsilon fu}) * E_f$

Table 4-8: Summary of average axial strength enhancements for PBO-FRCM confined columns

Cross-Section	No. of Layers	$P_{unconfined}$ (kN)	$P_{confined}$ (kip)	$P_{confined}/P_{unconfined}$
Circular	0	495.33 (SD=26.95, COV=5.45%)	--	--
	1	--	550.33 (SD=20.79, COV=3.80%)	1.11
	4	--	659.00 (SD=25.53, COV=3.80%)	1.33
Square	0	455.67 (SD=28.92, COV=6.50%)	--	--
	1	--	500.67 (SD=20.40, COV=4.07%)	1.10
	4	--	566.00 (SD=24.98, COV=4.44%)	1.24
Rectangular	0	407.00 (SD=25.51, COV=6.20%)	--	--
	1	--	431.33 (SD=35.23, COV=8.25%)	1.06
	4	--	451.00 (SD=24.76, COV=5.65%)	1.11

Table 4-9: Summary of experimental results for confinement effectiveness on axial deformation

Cross-Section	No. of Layers	δ (mm)	$\delta_{confined}/\delta_{unconfined}$
Circular	0	1.048 (SD = 0.042, COV = 3.974%)	1.00
	1	1.363 (SD = 0.038, COV = 2.808%)	1.31
	4	2.424 (SD = 0.153, COV = 6.312%)	2.32
Square	0	1.056 (SD = 0.033, COV = 3.085%)	1.00
	1	1.312 (SD = 0.082, COV = 6.240%)	1.21
	4	2.042 (SD=0.127, COV=6.230%)	1.90
Rectangular	0	1.000 (SD = 0.050, COV = 5.020%)	1.00
	1	1.190 (SD = 0.022, COV = 1.875%)	1.18
	4	1.805 (SD = 0.102, COV = 5.642%)	1.82

Table 4-10: Summary of axial load capacity enhancement, small scale vs. large scale columns

Cross-Section	No. of Layers	$P_{unconfined}$ (kN)		$P_{confined}$ (kN)		$P_{confined}/P_{unconfined}$	
		Small	Large	Small	Large	Small	Large
Circular	0	495.33	1036.44	--	--	--	--
	1	--	--	550.33	1143.19	1.11	1.10
	4	--	--	659.00	1365.60	1.33	1.31
Square	0	455.67	1178.05	--	--	--	--
	1	--	--	500.67	1267.74	1.10	1.08
	4	--	--	566.00	1450.12	1.24	1.23

Table 4-11: Summary of ductility enhancement, small scale vs. large scale columns

Cross-Section	No. of Layers	δ (mm)		$\delta_{confined}/\delta_{unconfined}$	
		Small	Large	Small	Large
Circular	0	1.041	2.134	1.00	1.00
	1	1.363	2.286	1.31	1.07
	4	2.424	3.429	2.32	1.61
Square	0	1.056	1.956	1.00	1.00
	1	1.312	2.210	1.21	1.13
	4	2.042	2.616	1.90	1.35

Table 4-12: List of equations used for design (AC434)

Equation	Section (Equation No.)
$f'_{cc} = f'_{co} + 3.3\kappa_a f_l$	Sec. 8.3.2 (16)
$f_l = (2n\ A_f E_f \varepsilon_{fe})/D$ *for circular cross sections*	Sec. 8.3.2 (17a)
$f_l = (2n\ A_f E_f \varepsilon_{fe})/(b^2+h^2)^{1/2}$ *for rectangular cross sections*	Sec. 8.3.2(17b)
$\varepsilon_{fe} = \varepsilon_{fu}$	Sec.8.3.2(18)
$\varepsilon_{ccu} = \left(\varepsilon_c^{'} 1.5 + 12\kappa_b \frac{f_1}{f_c^{'}} \left(\frac{\varepsilon_{fe}}{\varepsilon_c^{'}} \right)^{0.45} \right) \le 0.01$	Sec.8.3.2(19)
$\kappa_a = \frac{A_e}{A_c} \left(\frac{b}{h} \right)^2$	Sec.8.3.2(20)
$\kappa_b = \frac{A_e}{A_c} \left(\frac{b}{h} \right)^{0.5}$	Sec.8.3.2(21)
$\frac{A_e}{A_c} = \frac{1 - \left((b/h)(h-2r)^2 + (h/b)(b-2r)^2 \Big/ (3A_g) - \rho_g \right)}{1-\rho_g}$	Sec.8.3.2(22)

Table 4-13: Summary of percentage gains in axial strength and strain (AC434 vs. Experimental)

Cross-section	No. of PBO-FRCM layers	Axial strength gain (%)		Axial strain gain (%)	
		Experimental	AC434	Experimental	AC434
Circular	1	11	5	30	32
	4	33	17	132	121
Square	1	10	4	21	18
	4	24	13	90	76
Rectangular	1	6	1	18	19
	4	11	6	82	69

Table 4-14: GFRP versus PBO-FRCM confinement

Cross-section	Strength enhancement		Ultimate strain enhancement	
	GFRP	PBO-FRCM	GFRP	PBO-FRCM
Square	1.31	1.10	4.08	1.21
Rectangular	1.17	1.06	3.63	1.18

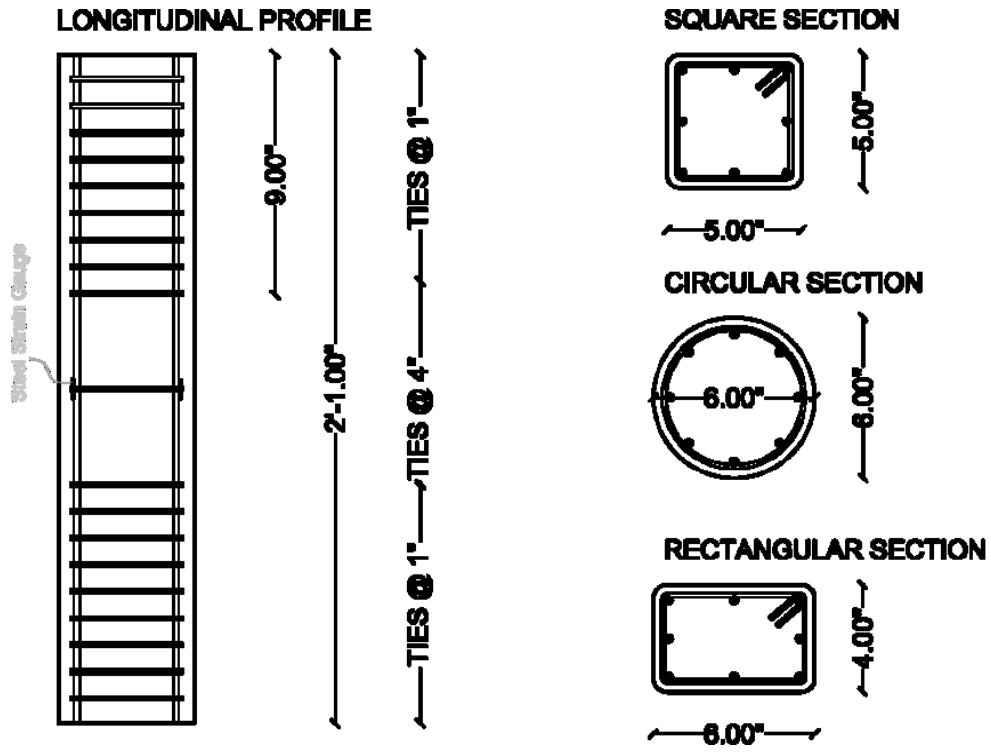

Fig. 4-1: Reinforcement layout of small scale RC column specimens

Fig. 4-2: Demonstration of installation procedure of PBO-FRCM strengthening

Fig. 4-3: Typical RC column specimen (square cross-section) before testing

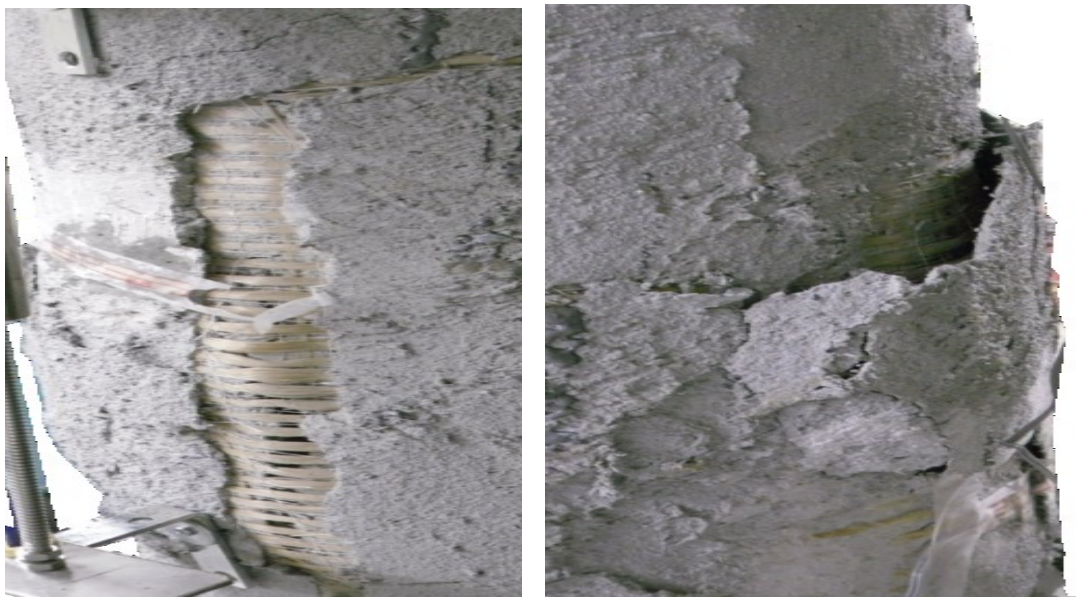

Fig. 4-4: Typical column element after testing

Fig. 4-5: Buckling of the internal steel reinforcement in RC column

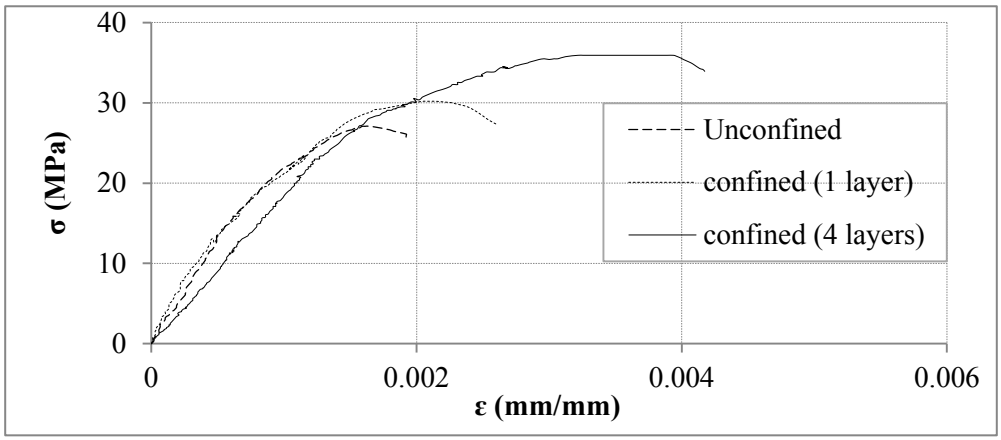

a) Circular

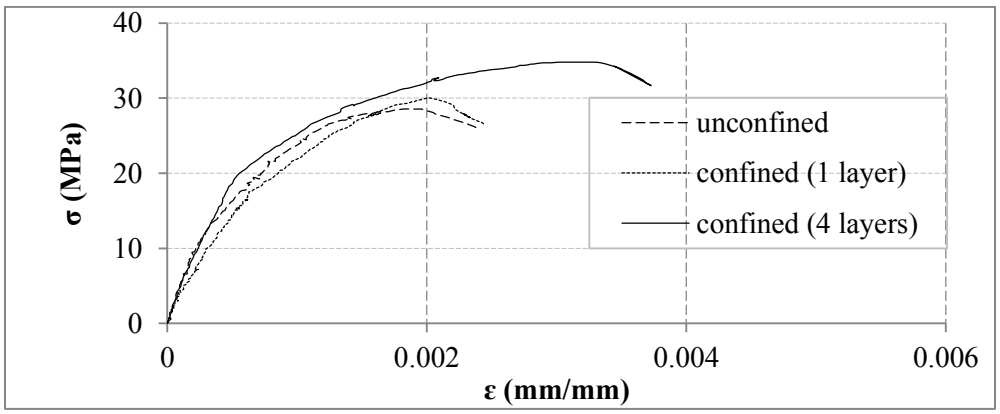

b) Square

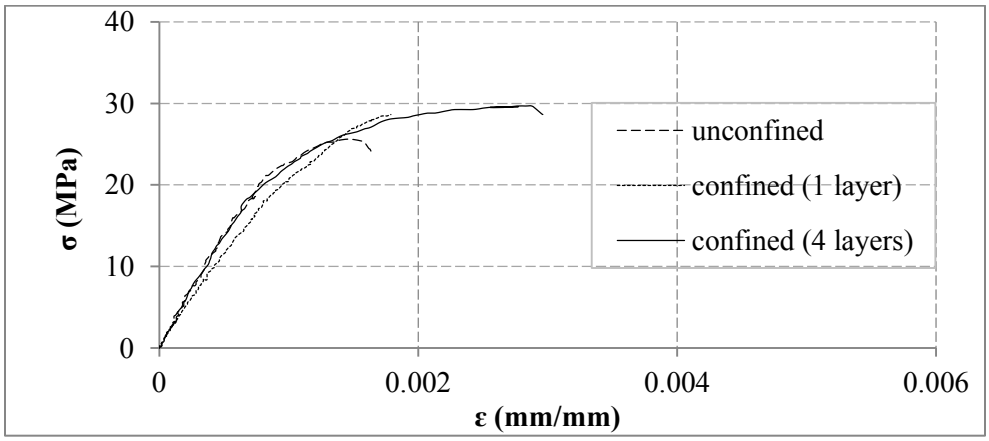

c) Rectangular

Fig. 4-6: Effect of number of PBO-FRCM layers on stress-strain relationships

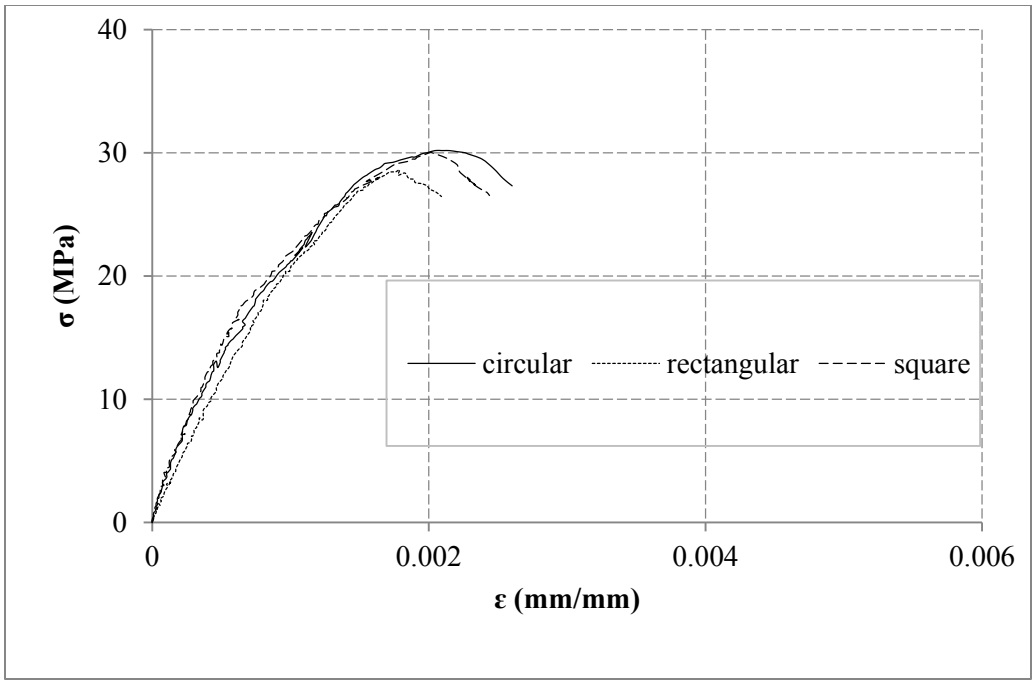

a) 1 Layer

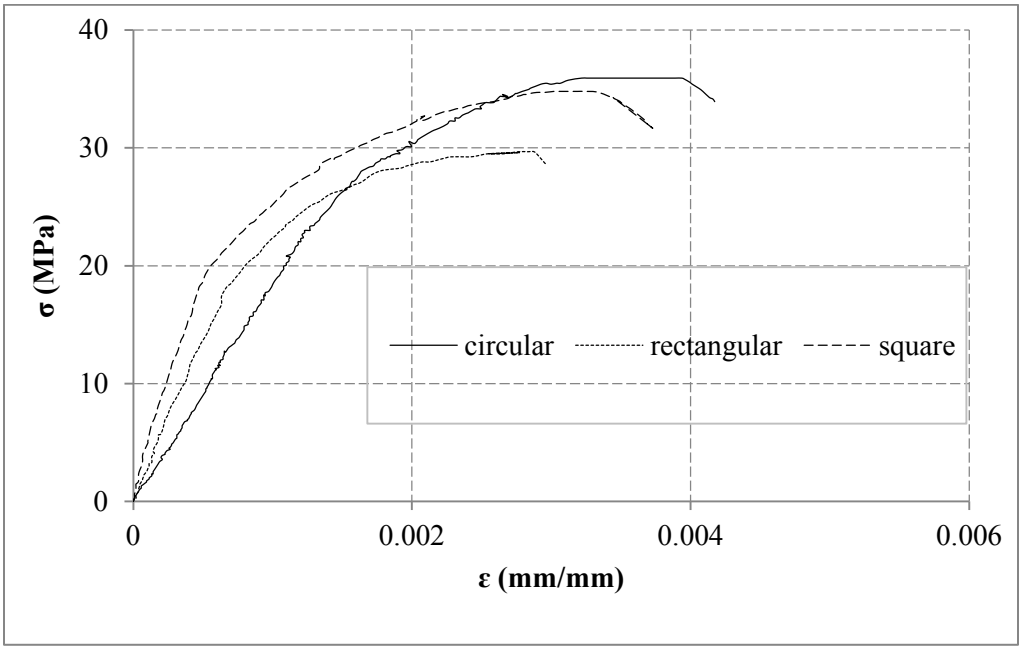

b) 4 layers

Fig. 4-7: Effect of cross-sectional shapes on confinement effectiveness

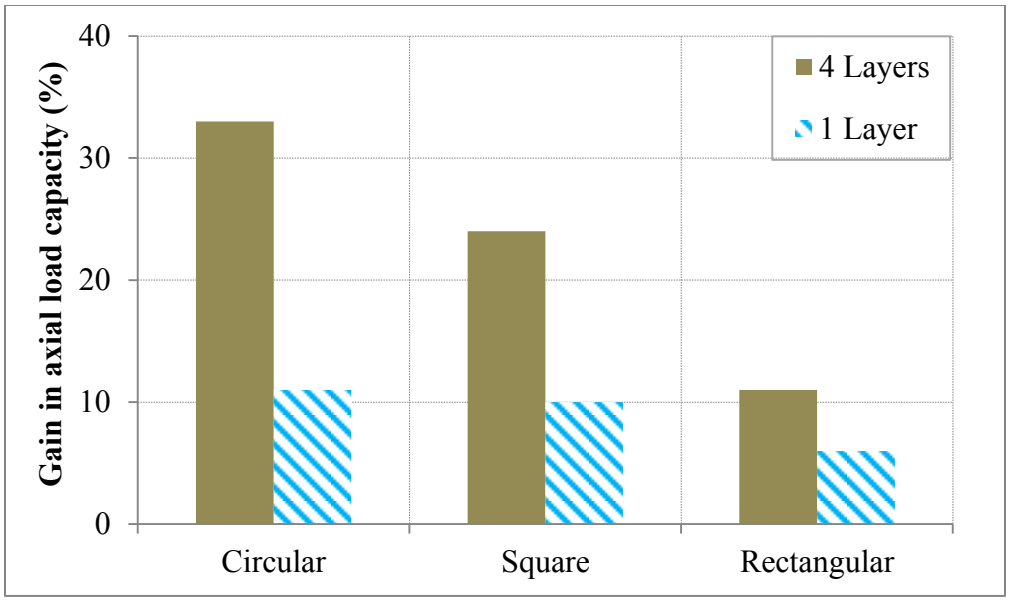

Fig. 4-8: Effect of number of PBO-FRCM layers on the gain in axial load capacity

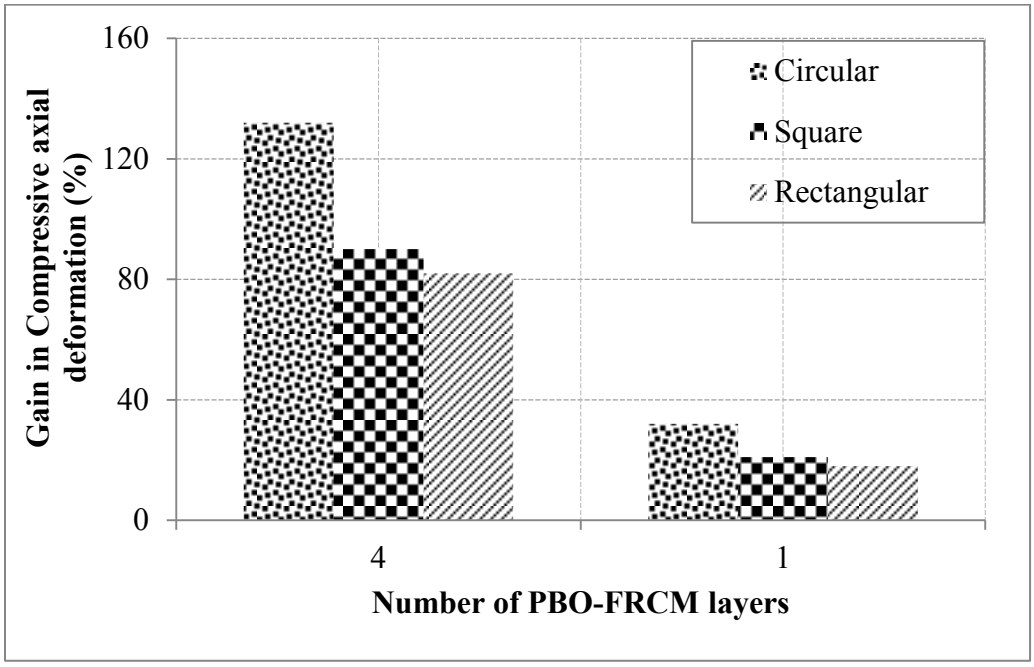

Fig. 4-9: Effect of number of PBO-FRCM and cross-section geometry on axial strain capacity

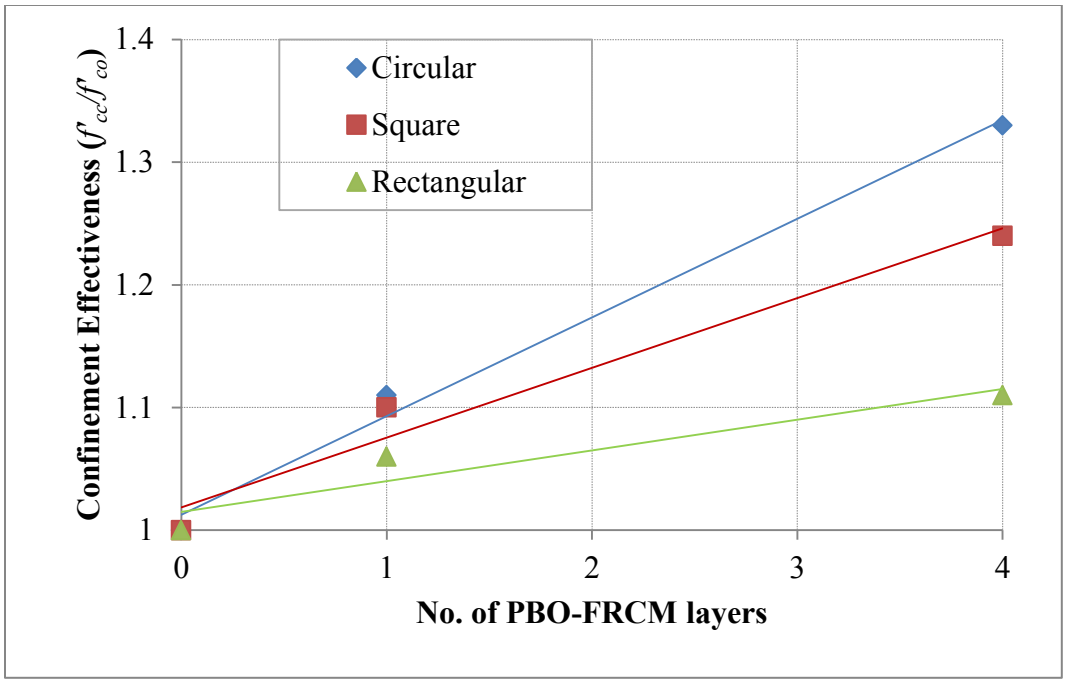

Fig. 4-10: PBO-FRCM confined columns vs. control specimen

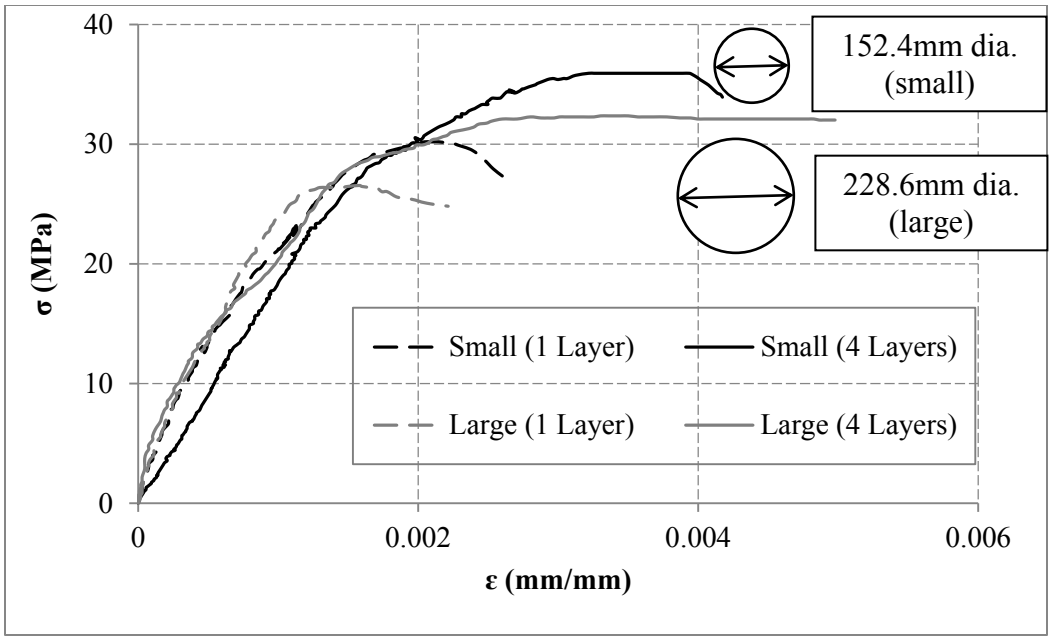

a) Circular

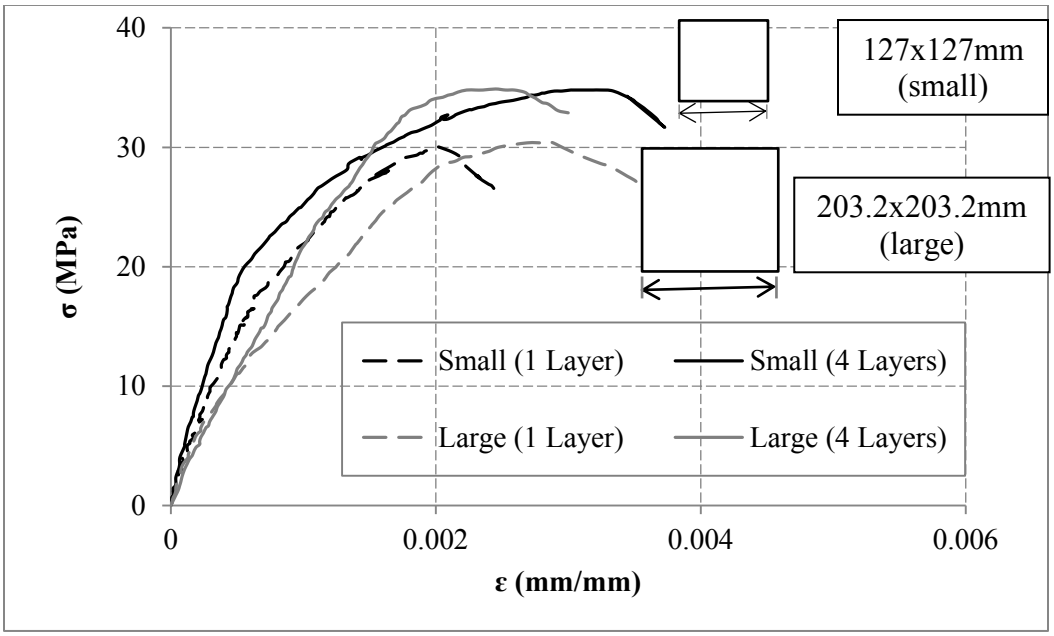

b) Square

Fig. 4-11 Stress-strain relationship, large and small scale specimens compared

a) Circular, b) Square (Loreto et al., (2013))

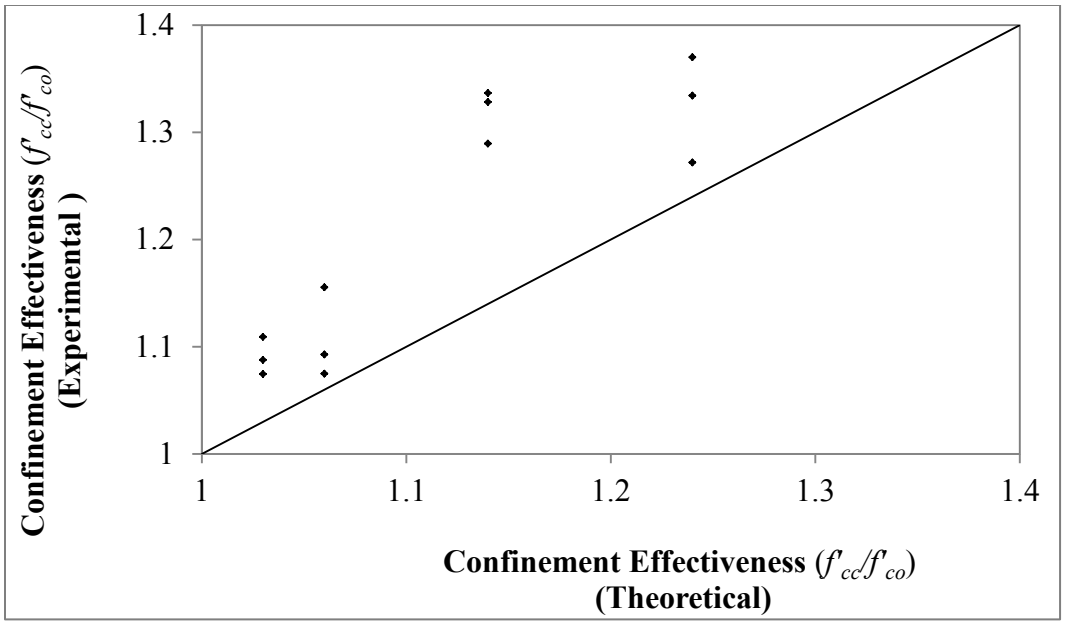

a) Circular

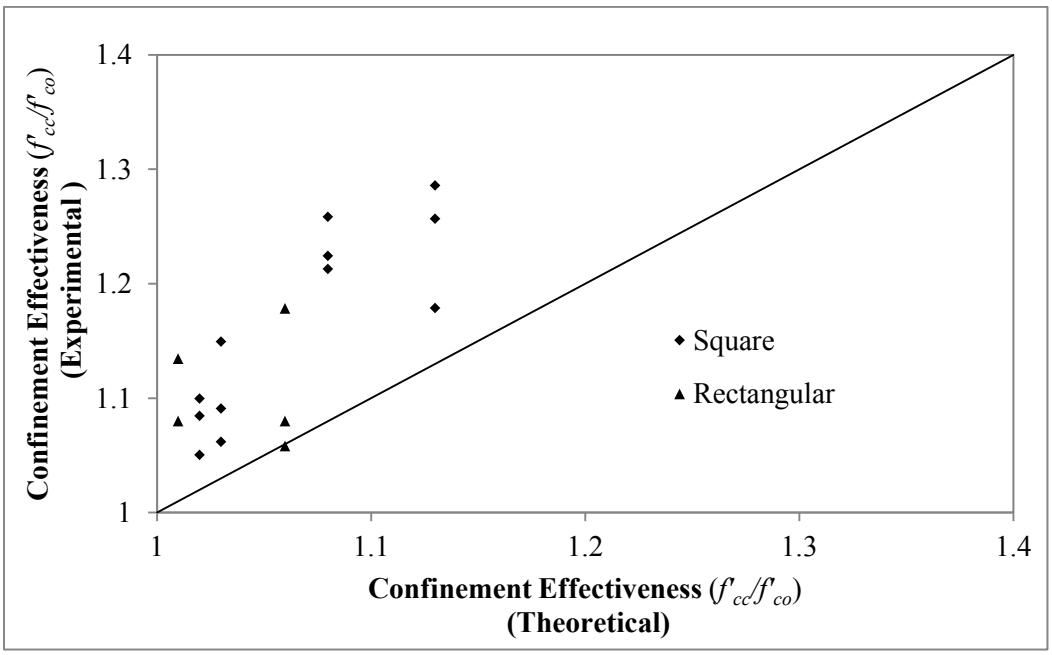

b) Square and rectangular

Fig. 4-12 Experimental vs. theoretical confinement effectiveness ratios (AC434)

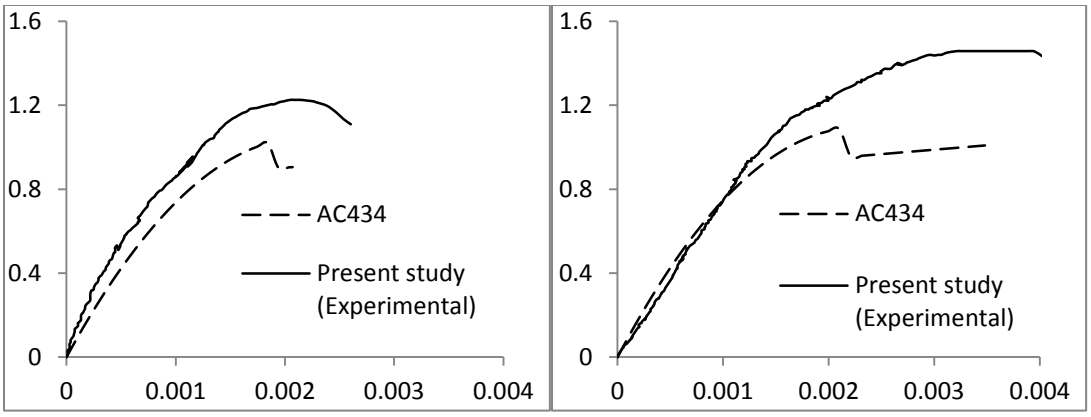

a) Circular 1-layer of PBO-FRCM b) Circular 4 layers of PBO-FRCM

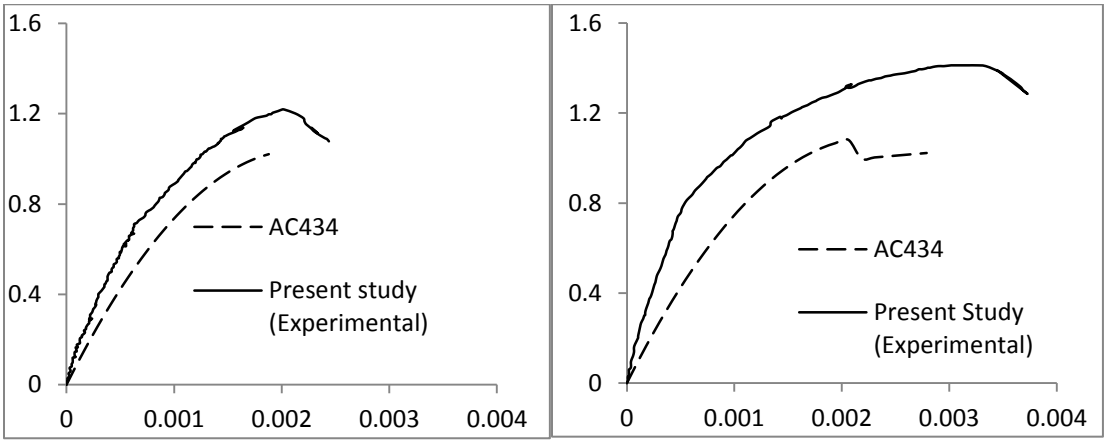

c) Square 1-layer of PBO-FRCM d) Square 4 layers of PBO-FRCM

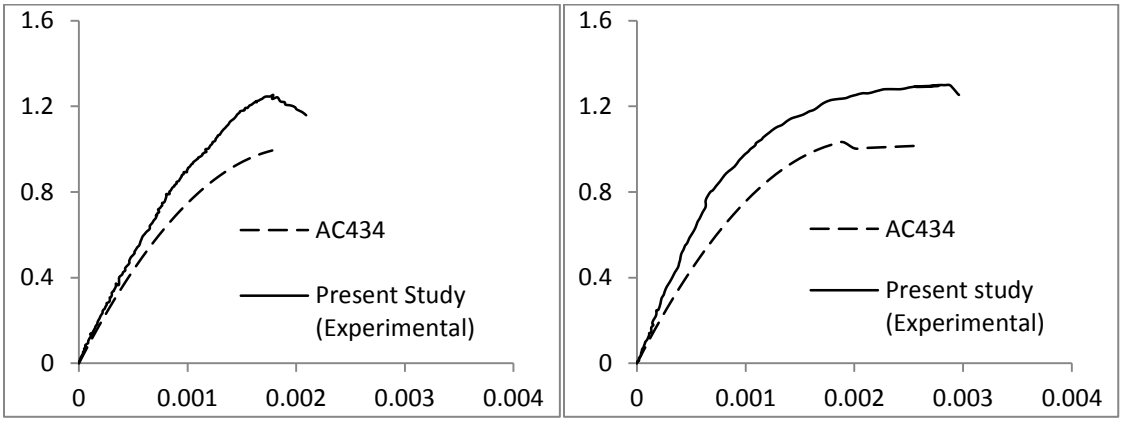

e) Rectangular 1-layer of PBO-FRCM f) Rectangular 4 layers of PBO-FRCM

Fig. 4-13: Confinement effectiveness vs. strain (AC434 model vs. experimental)

CHAPTER V

CONCLUSIONS

The experimental results from the three studies reported in chapter two through four, were used to make the following conclusions for each study.

Study 1 evaluated the performance of non-cylindrical GFRP jackets under hydrostatic loading, and the results were compared with results from flat coupon tests. GFRP jackets of square and rectangular cross-sections with two plies, four plies and six plies were tested and evaluated. A corner radius of 0.5 inches was kept for all the specimens. Based on the experimental evidence in study 1 the following conclusions were made:

- The maximum hoop strains obtained in the tests conducted on two, four and six plies of rectangular and square GFRP jackets have shown considerably smaller values in comparison with their respective flat coupon specimens.
- The ICE methodology appeared to subject the GFRP jackets in a hydrostatic loading which forces the jackets take a circular shape and behave in a very different way than when they are used to confine concrete columns. The methodology also enabled the monitory of the strains in the inner face of the GFRP jacket. It should be noted that the methodology was effectively used in characterizing GFRP laminates with circular cross-section. Further study is thus needed to verify if this methodology is applicable for non-cylindrical jackets.

Eight specimens of RC columns were considered in study 2 to evaluate the performance of GFRP jackets when applied to RC columns of rectangular and square sections. The following conclusions were made based on this experimental investigation:

- GFRP wrapping affected both the axial strength and axial deformation of RC columns.
- GFRP wrapping was more effective in enhancing the axial load carrying capacity of square specimens than rectangular cross-sections.
- The GFRP confinement had a greater impact in enhancing the axial deformation than the axial load bearing capacity for both the square and rectangular columns.
- The confinement effectiveness was found to be more enhanced for smaller scale columns in comparison with the full scale RC columns confined with the same GFRP system and equivalent confining pressure.

The experimental investigation in study 3 evaluates the performance of PBO-FRCM as a confining material for RC columns of different cross-sections. Its effectiveness in enhancing the axial strength and deformation of RC columns with circular, square and rectangular cross-sections were evaluated for one layer and four layers. The results from the 27 specimens in this research were compared with similar study on large column specimens. Design values were also computed and compared with the results from the experimental investigation. The following conclusions can be drawn from the study:

- PBO-FRCM was found to be simpler to apply for wrapping columns as compared to widely used FRP.

- The predominant failure mode observed in PBO-FRCM confined columns was mesh-matrix separation, showing a week bond between the inorganic cementitious matrix and the structural reinforcement PBO mesh. The cementitious matrix was found to be unable to fully impregnate the PBO mesh.
- PBO-FRCM confining was most effective in increasing the load bearing capacity of circular RC columns, followed by square and rectangular columns.
- Ductility is already improved when the column is wrapped by a single layer of PBO-FRCM, regardless of its shape.
- Ductility is increased significantly when the column is wrapped by four layers of PBO-FRCM. With regards to shape, this increase follows the same general trend of increase in strength.
- Increase in axial deformation due to confinement was found to be greater than the increase in axial strength for all the cross sections and number of FRCM layers.
- The Experimental results were comparable with the theoretical design values, thus the design models suggested in AC434 can be used for design of PBO-FRCM confined columns.
- There is no obvious size effect on the modes of failure observed, and the size effect on the confinement effectiveness is also very weak.

Recommendations for future work

- Further research is needed to study the effect of size for GFRP confined columns.
- More study is needed to improve the performance of the PBO-FRCM matrix through improving the matrix properties, so that the PBO mesh is better impregnated to avoid early failure due to mesh-matrix separation.
- PBO-FRCM wrapped large columns should be further studied to determine the effectiveness, and size effect.
- More experimental data are also necessary for a complete validation of the methodology discussed in Study 1 for non-circular cross-sections.
- More experimental and numerical simulation can be performed on non-circular GFRP jackets under hydrostatic pressure to further verify the properties of GFRP laminates especially monitoring the strains on the inner surfaces of the jackets.

APPENDIX A

STUDY 3- Stress-strain relationships and detailed results

A total of 27 specimens of different cross-sections were tested in study 3, and the stress-strain relationship for each specimen is given in Fig. A-1 to Fig. A-9.

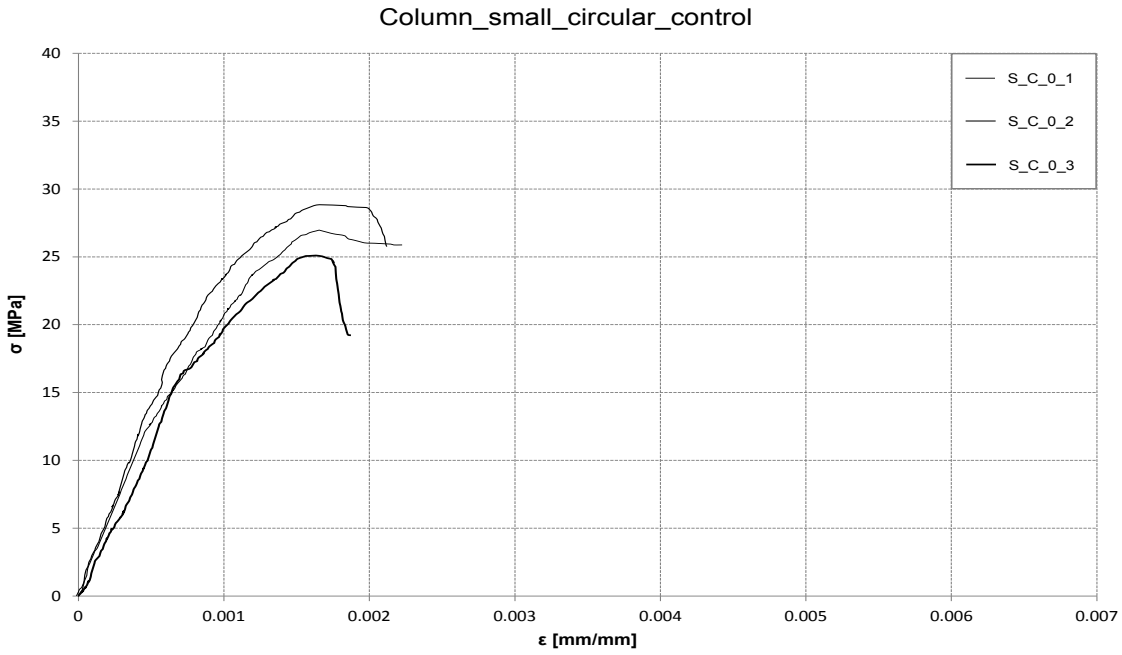

Fig. A-1: Stress vs. strain relationship (S_C_0 specimens)

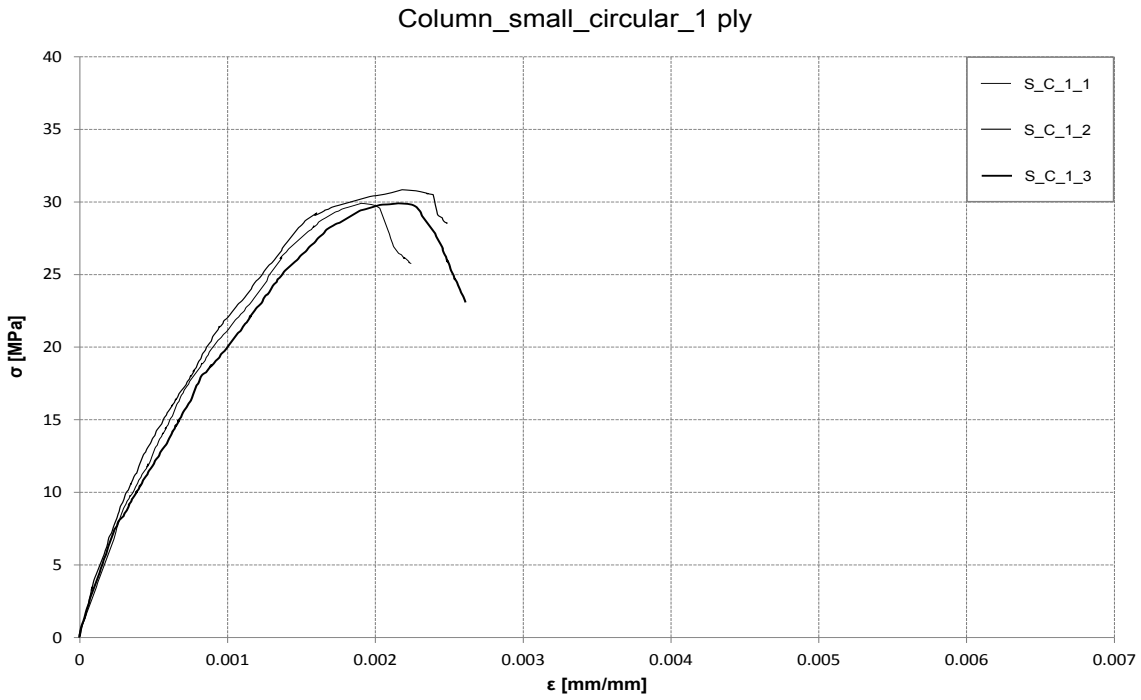

Fig. A-2: Stress vs. strain relationship (S_C_1 specimens)

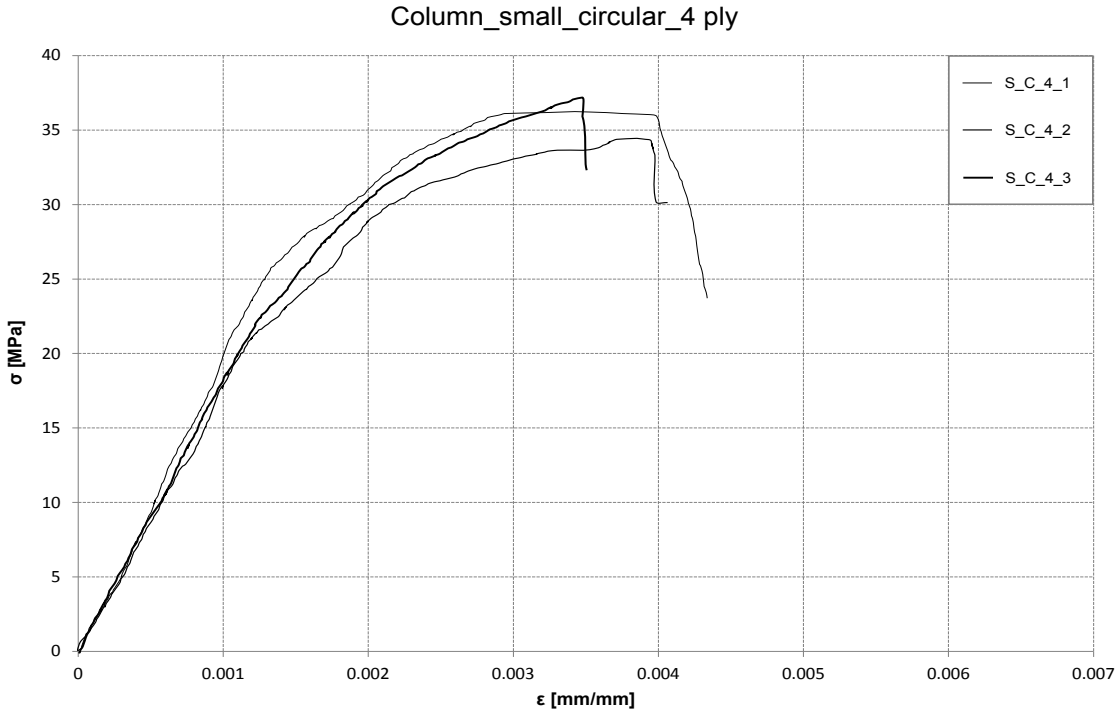

Fig. A-3: Stress vs. strain relationship (S_C_4 specimens)

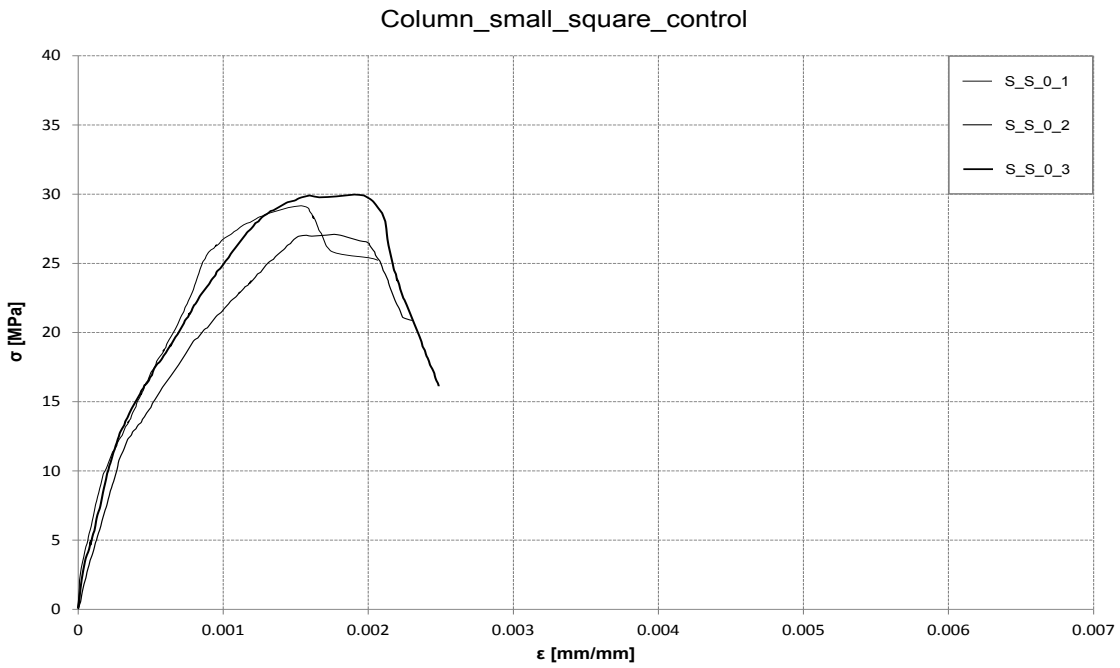

Fig. A-4: Stress vs. strain relationship (S_S_0 specimens)

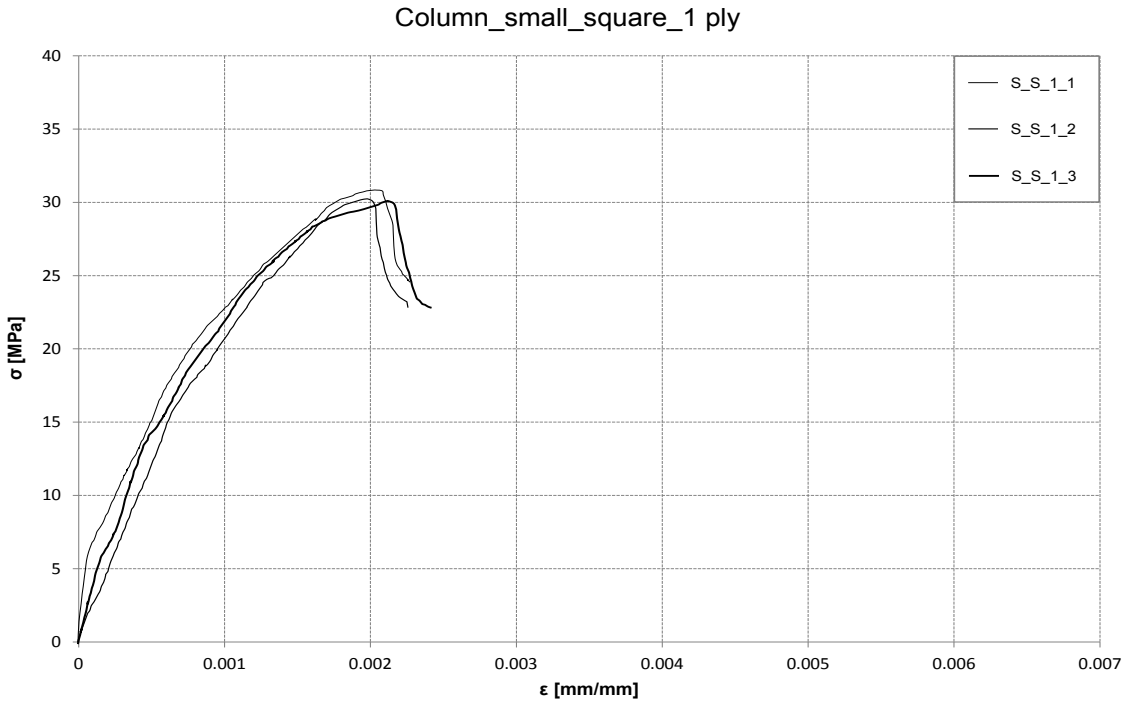

Fig. A-5: Stress vs. strain relationship (S_S_1 specimens)

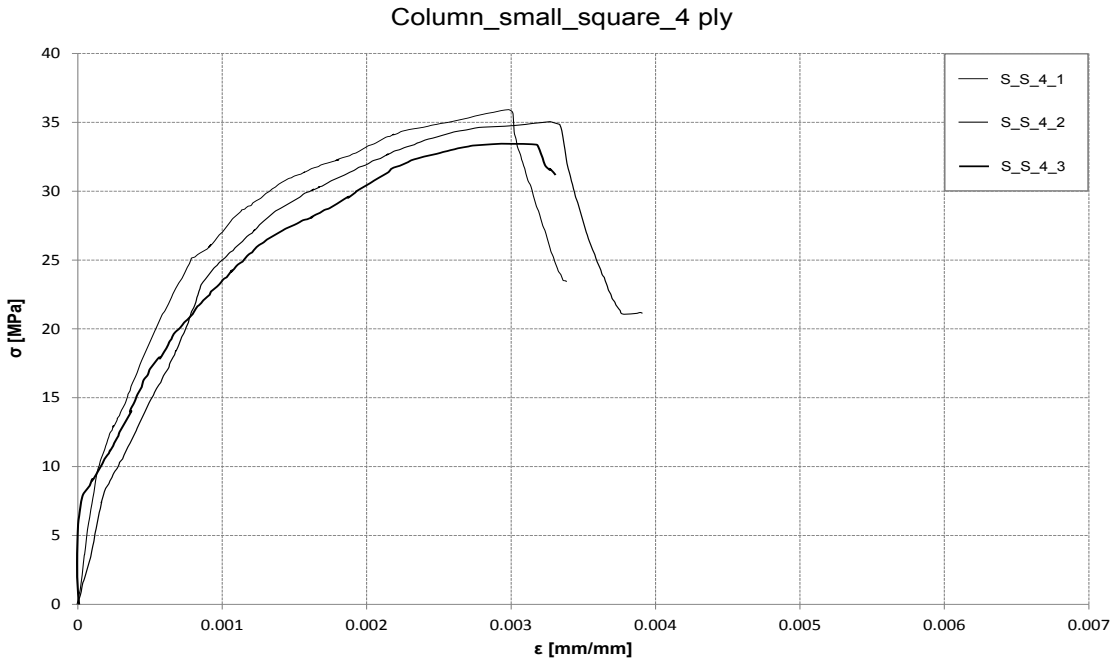

Fig. A-6: Stress vs. strain relationship (S_S_4 specimens)

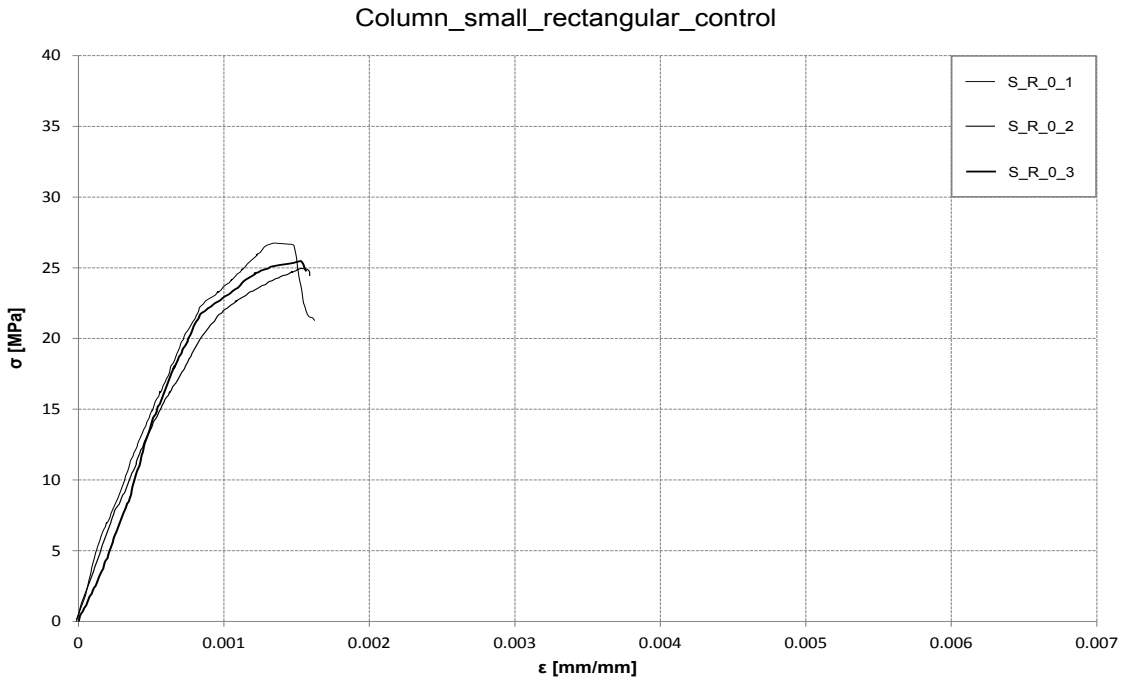

Fig. A-7: Stress vs. strain relationship (S_R_0 specimens)

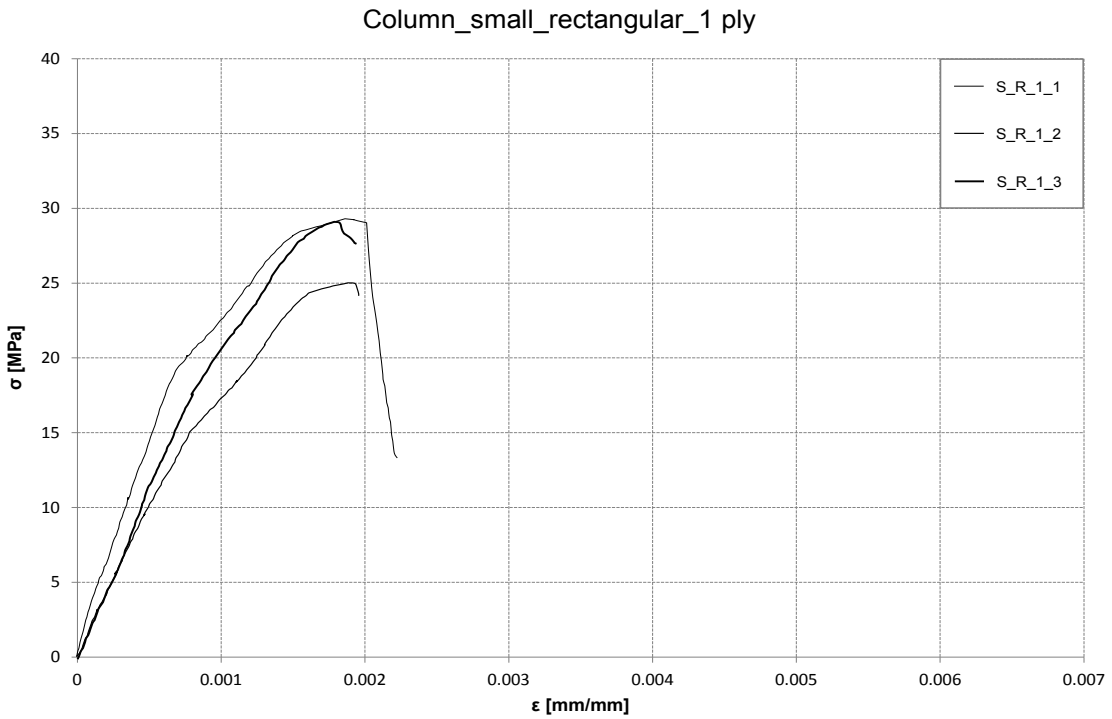

Fig. A-8: Stress vs. strain relationship (S_R_1 specimens)

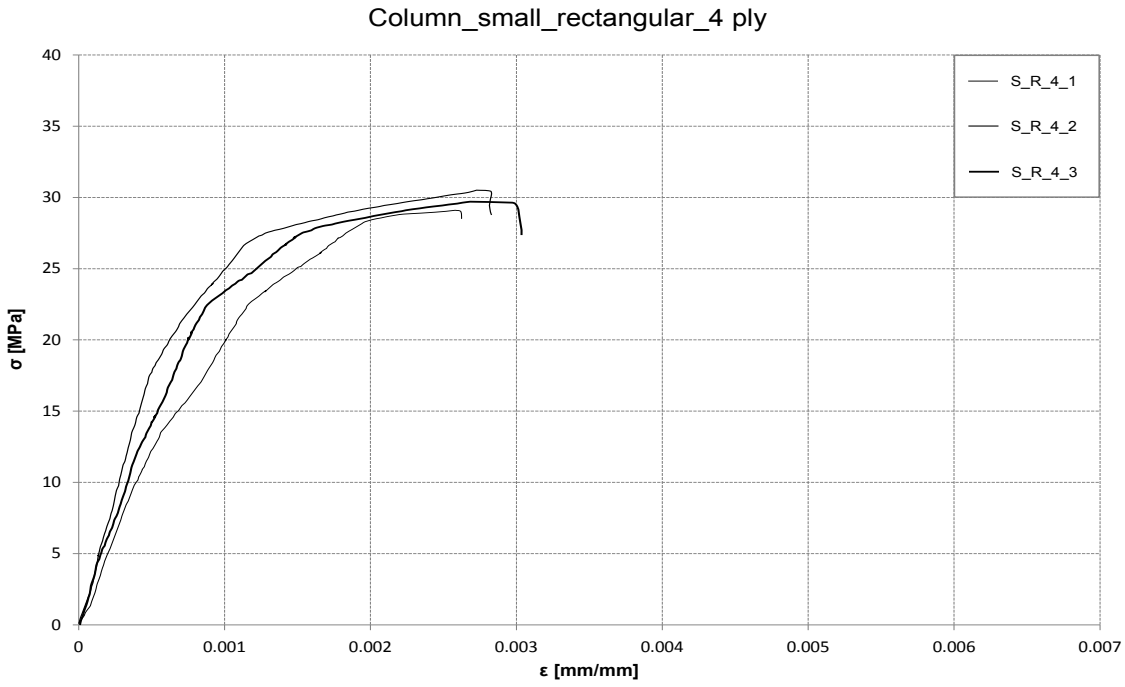

Fig. A-9: Stress vs. strain relationship (S_R_4 specimens)

Table A-1: Theoretical vs. experimental strength enhancement

Specimen ID	Experimental (Exp.) results		Exp. strength enhancement	Th. design criteria		Th. strength enhancement	Exp./Th. ratio
	P_u		$P_{u,avg,strengthed}$ / $P_{u,avg,control}$	$P_{u,Th.}$		$P_{u,Th,strengthed}$ / $P_{u,Th,control}$	$P_{u,avg}/P_{u,Th}$
	kN	kip	-	kN	kip	-	-
S_C_0_1	501	113	1.00	387	87	1.00	1.28
S_C_0_2	519	117					
S_C_0_3	466	105					
Average	495.33	111.67					
SD	26.95	6.11					
COV	5.45	5.45					
S_C_1_1	542	122	1.11	405	91	1.05	1.36
S_C_1_2	574	129					
S_C_1_3	535	120					
Average	550.33	123.67					
SD	20.79	4.73					
COV	3.80	3.80					
S_C_4_1	665	149	1.33	454	102	1.17	1.45
S_C_4_2	631	142					
S_C_4_3	681	153					
Average	659.00	148.00					
SD	25.53	5.57					
COV	3.80	3.80					
S_S_0_1	466	105	1.00	347	78	1.00	1.31
S_S_0_2	423	95					
S_S_0_3	478	108					
Average	455.67	102.67					
SD	28.92	6.81					
COV	6.50	6.50					

Table A-2: Theoretical vs. experimental strength enhancement cont'd...

Specimen ID	Experimental (Exp.) results		Exp. strength enhancement	Th. design criteria		Th. strength enhancement	Exp./Th. ratio
	P_u		$P_{u,avg,strengthed}$ / $P_{u,avg,control}$	$P_{u,Th.}$		$P_{u,Th,strengthed}$ / $P_{u,Th,control}$	$P_{u,avg}/P_{u,Th}$
	kN	kip	-	kN	kip	kN	kip
S_S_1_1	523	118	1.10	360	81	1.04	1.39
S_S_1_2	496	112					
S_S_1_3	483	109					
Average	500.67	113.00					
SD	20.40	4.58					
COV	4.07	4.07					
S_S_4_1	586	132	1.24	391	88	1.13	1.45
S_S_4_2	574	129					
S_S_4_3	538	121					
Average	566.00	127.33					
SD	24.98	5.69					
COV	4.44	4.44					
S_R_0_1	432	97	1.00	320	72	1.00	1.27
S_R_0_2	381	86					
S_R_0_3	408	92					
Average	407.00	91.67					
SD	25.51	5.51					
COV	6.20	6.20					
S_R_1_1	442	99	1.06	325	73	1.01	1.33
S_R_1_2	392	88					
S_R_1_3	460	104					
Average	431.33	97.00					
SD	35.23	8.19					
COV	8.25	8.25					
S_R_4_1	432	97	1.11	338	76	1.06	1.33
S_R_4_2	479	108					
S_R_4_3	442	99					
Average	451.00	101.33					
SD	24.76	5.86					
COV	5.65	5.65					

Table A-3: Theoretical vs. experimental strain enhancement

Specimen ID	Ultimate axial strain, ε'_{cc}		Ultimate axial deflection, δ			
	Th.	Exp.	Th.		Exp.	
	-	-	mm	in	mm	in
S_C_0_1	0.00157	0.00171	0.957	0.038	1.086	0.043
S_C_0_2	0.00157	0.00166	0.957	0.038	1.054	0.042
S_C_0_3	0.00157	0.00158	0.957	0.038	1.003	0.039
Average	0.00157	0.00165	0.957	0.038	1.048	0.041
SD	-	0.00006	-	-	0.042	0.002
COV	-	3.97420	-	-	3.974	3.974
S_C_1_1	0.00207	0.00209	1.262	0.050	1.327	0.052
S_C_1_2	0.00207	0.00221	1.262	0.050	1.403	0.055
S_C_1_3	0.00207	0.00214	1.262	0.050	1.359	0.054
Average	0.00207	0.00215	1.262	0.050	1.363	0.054
SD	-	0.00006	-	-	0.038	0.002
COV	-	2.80794	-	-	2.808	2.807
S_C_4_1	0.00348	0.00398	2.121	0.084	2.527	0.099
S_C_4_2	0.00348	0.00393	2.121	0.084	2.496	0.098
S_C_4_3	0.00348	0.00354	2.121	0.084	2.248	0.089
Average	0.00348	0.00382	2.121	0.084	2.424	0.095
SD	-	0.00024	-	-	0.153	0.006
COV	-	6.31181	-	-	6.312	6.311
S_S_0_1	0.00157	0.00162	0.957	0.038	1.029	0.040
S_S_0_2	0.00157	0.00172	0.957	0.038	1.092	0.043
S_S_0_3	0.00157	0.00165	0.957	0.038	1.048	0.041
Average	0.00157	0.00166	0.957	0.038	1.056	0.041
SD	-	0.00005	-	-	0.033	0.001
COV	-	3.08513	-	-	3.085	3.085

Table A-4: Theoretical vs. experimental strain enhancement cont'd…

Specimen ID	Ultimate strain, ε'_{cc}		Ultimate deflection, δ			
	Th.	Exp.	Th.		Exp.	
	-	-	mm	in	mm	in
S_S_1_1	0.00188	0.0020	1.146	0.045	1.289	0.051
S_S_1_2	0.00188	0.0020	1.146	0.045	1.245	0.049
S_S_1_3	0.00188	0.0022	1.146	0.045	1.403	0.055
Average	0.00188	0.0021	1.146	0.045	1.312	0.052
SD	-	0.0002	-	-	0.082	0.003
COV	-	6.2405	-	-	6.240	6.240
S_S_4_1	0.00279	0.0030	1.701	0.067	1.911	0.075
S_S_4_2	0.00279	0.0034	1.701	0.067	2.165	0.085
S_S_4_3	0.00279	0.0032	1.701	0.067	2.051	0.081
Average	0.00279	0.0032	1.701	0.067	2.042	0.080
SD	-	0.0002	-	-	0.127	0.005
COV	-	6.2280	-	-	6.23	6.228
S_R_0_1	0.00151	0.0016	0.921	0.036	0.98	0.039
S_R_0_2	0.00151	0.0017	0.921	0.036	1.06	0.042
S_R_0_3	0.00151	0.0015	0.921	0.036	0.96	0.038
Average	0.00151	0.0016	0.921	0.036	1.00	0.039
SD	-	0.0001	-	-	0.050	0.002
COV	-	5.0240	-	-	5.020	5.024
S_R_1_1	0.00178	0.0018	1.085	0.043	1.168	0.046
S_R_1_2	0.00178	0.0019	1.085	0.043	1.213	0.048
S_R_1_3	0.00178	0.0019	1.085	0.043	1.187	0.047
Average	0.00178	0.0019	1.085	0.043	1.190	0.047
SD	-	0.000035	-	-	0.022	0.001
COV	-	1.8747	-	-	1.875	1.875
S_R_4_1	0.00256	0.0027	1.561	0.061	1.708	0.067
S_R_4_2	0.00256	0.0028	1.561	0.061	1.797	0.071
S_R_4_3	0.00256	0.0030	1.561	0.061	1.911	0.075
Average	0.00256	0.0028	1.561	0.061	1.805	0.071
SD	-	0.0002	-	-	0.102	0.004
COV	-	5.6418	-	-	5.642	5.642

APPENDIX B

STUDY 3- Specimen preparation, instrumentation and test setup

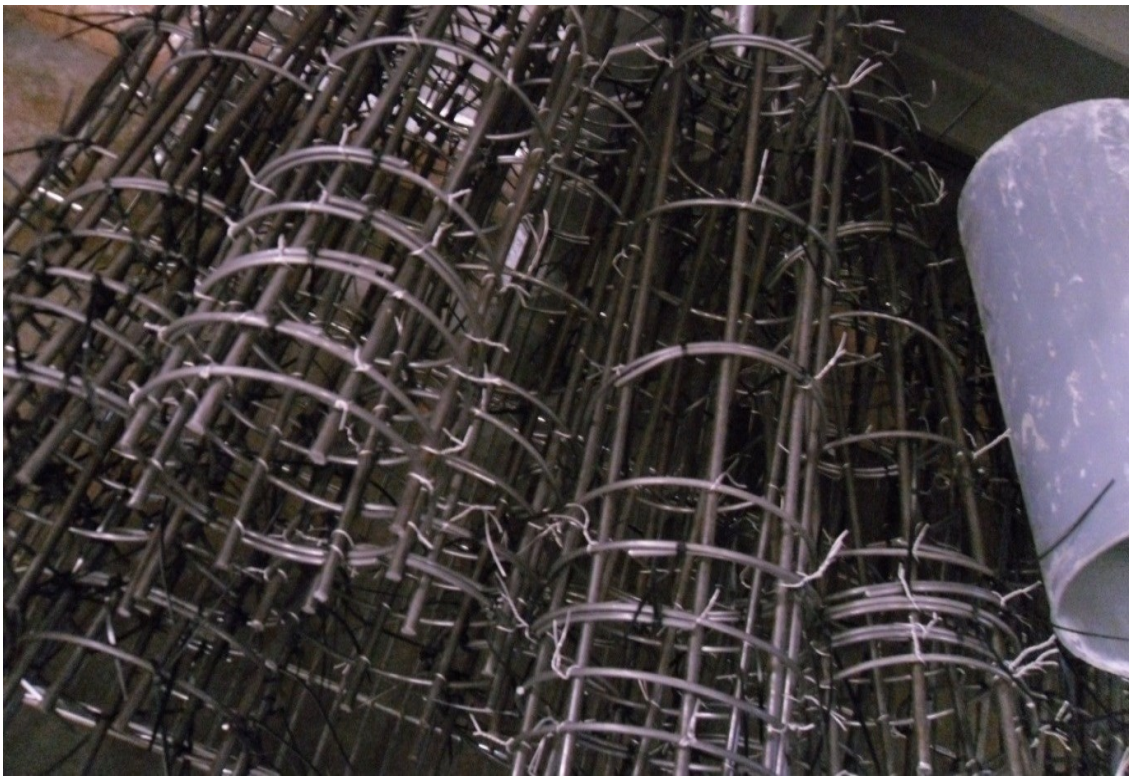

Fig. B-1: Reinforcement bars

Fig. B-2: Formwork

Fig. B-3: Reinforcement bars placed inside formwork

Fig. B-4: square, rectangular and circular RC columns

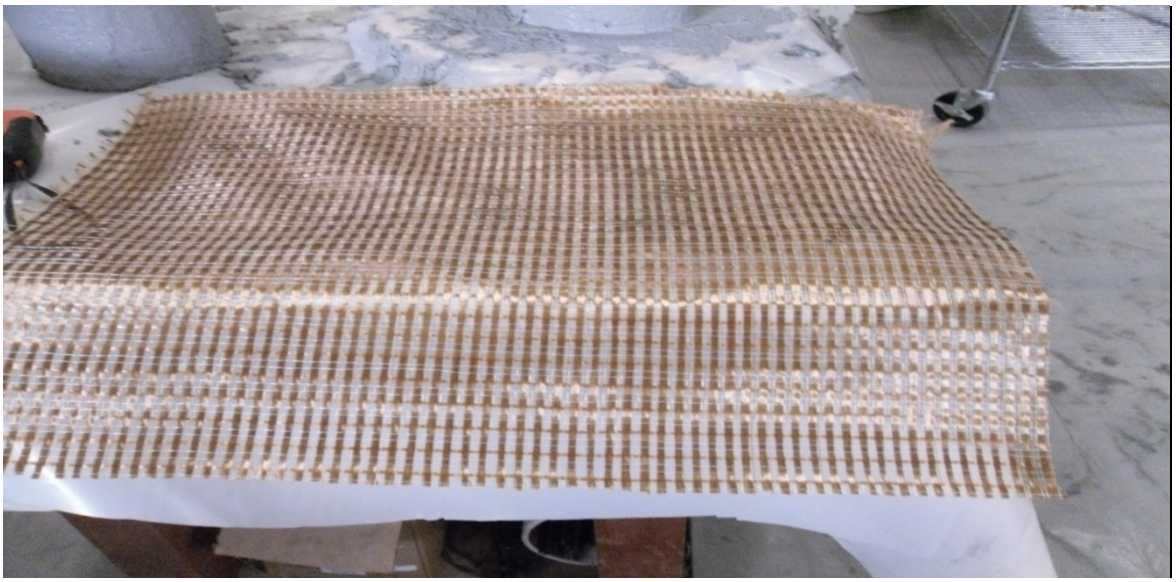

Fig. B-5: PBO mesh

Fig. B-6: Application of the inorganic cementitious matrix

Fig. B-7: Application of the PBO fiber

Fig. B-8: PBO-FRCM wrapped RC columns

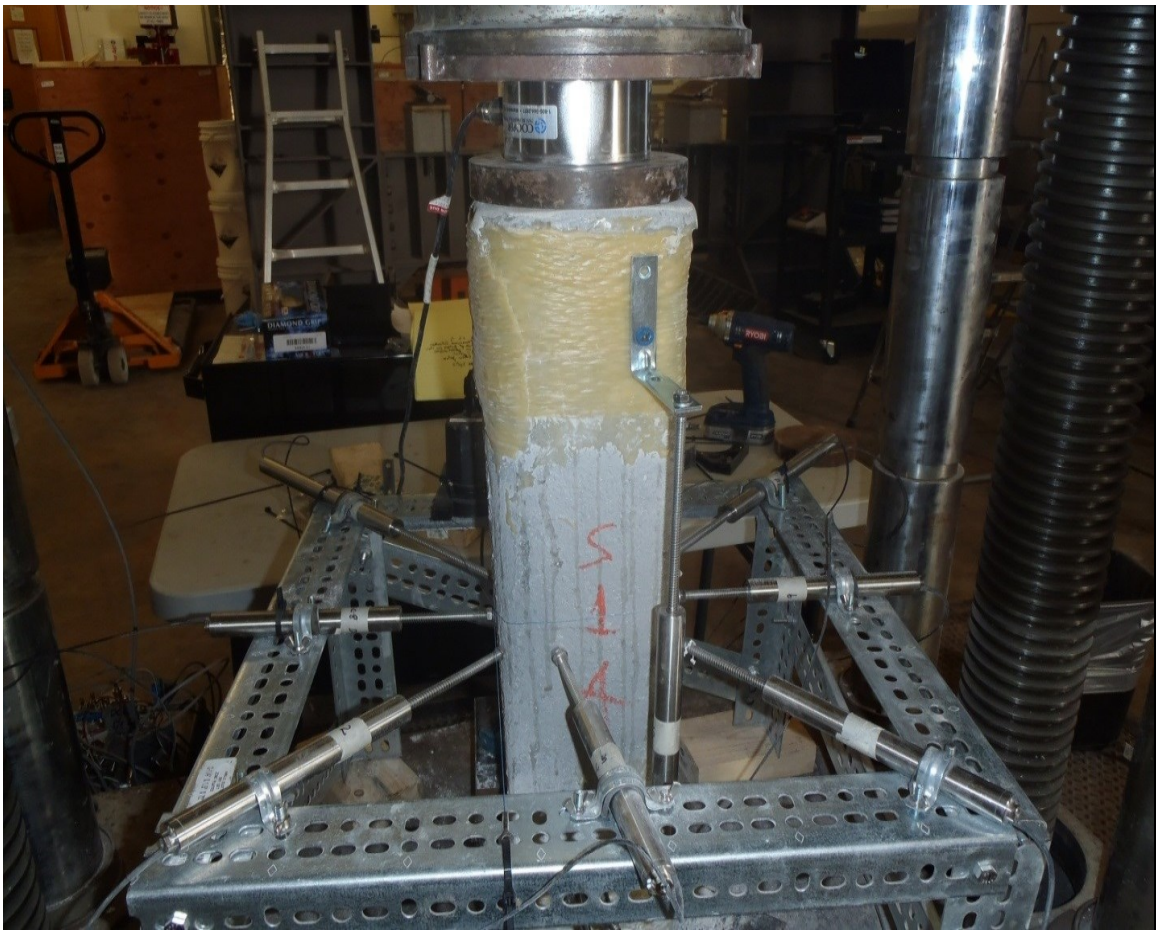

Fig. B-9: PBO-FRCM wrapped square column set up for testing

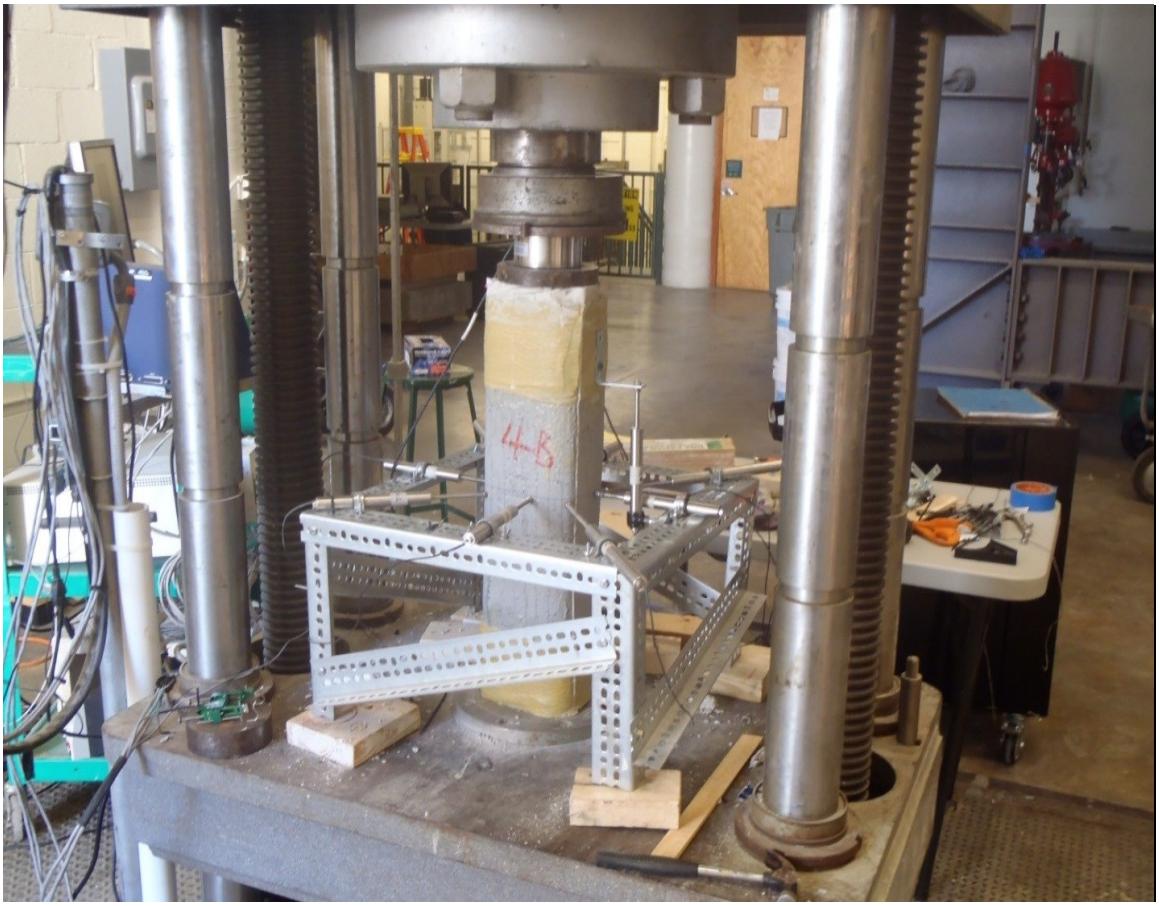

Fig. B-10: PBO-FRCM wrapped rectangular column set up for testing

Fig. B-11: PBO-FRCM wrapped circular column set up for testing

Fig. B-12: Failed PBO-FRCM wrapped circular column

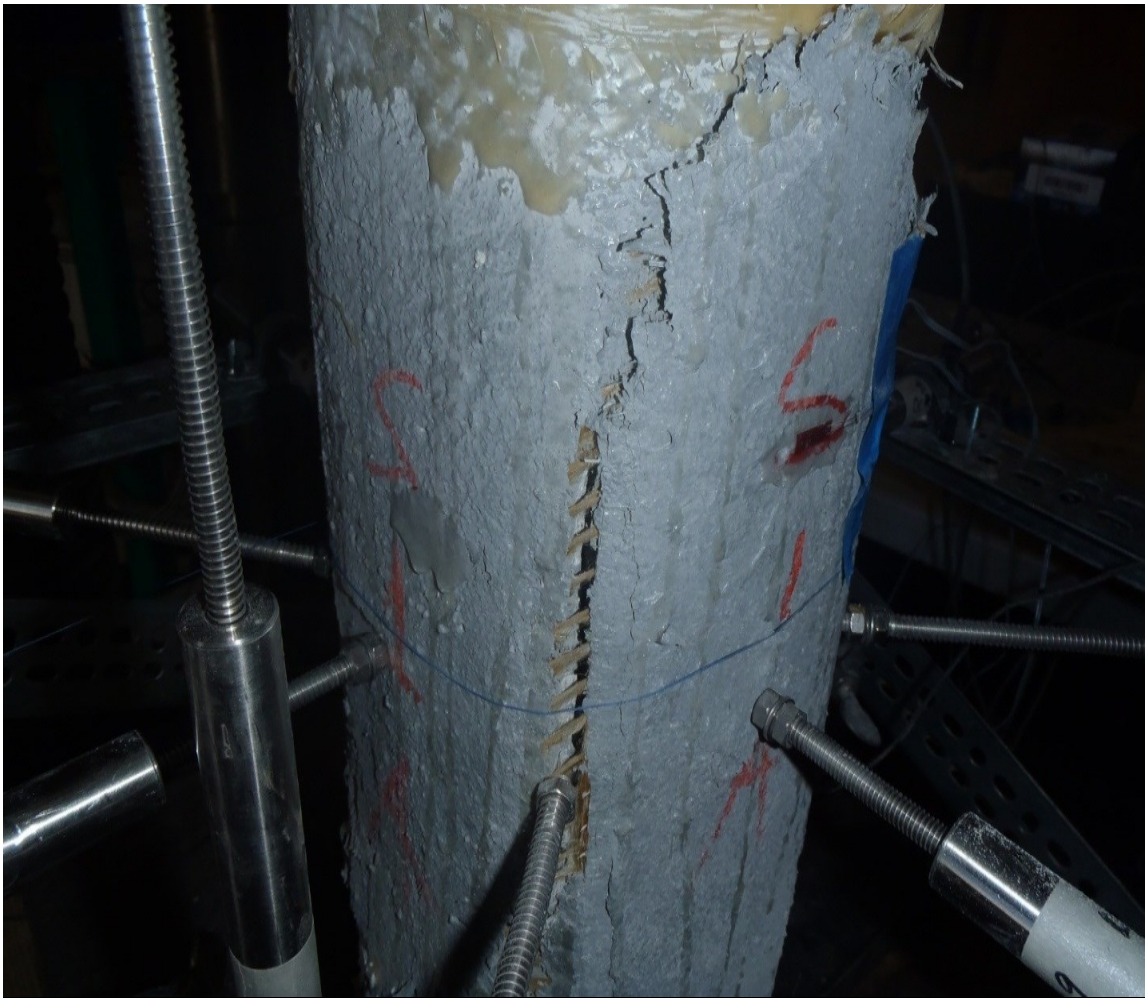

Fig. B-13: Failed PBO-FRCM wrapped square column

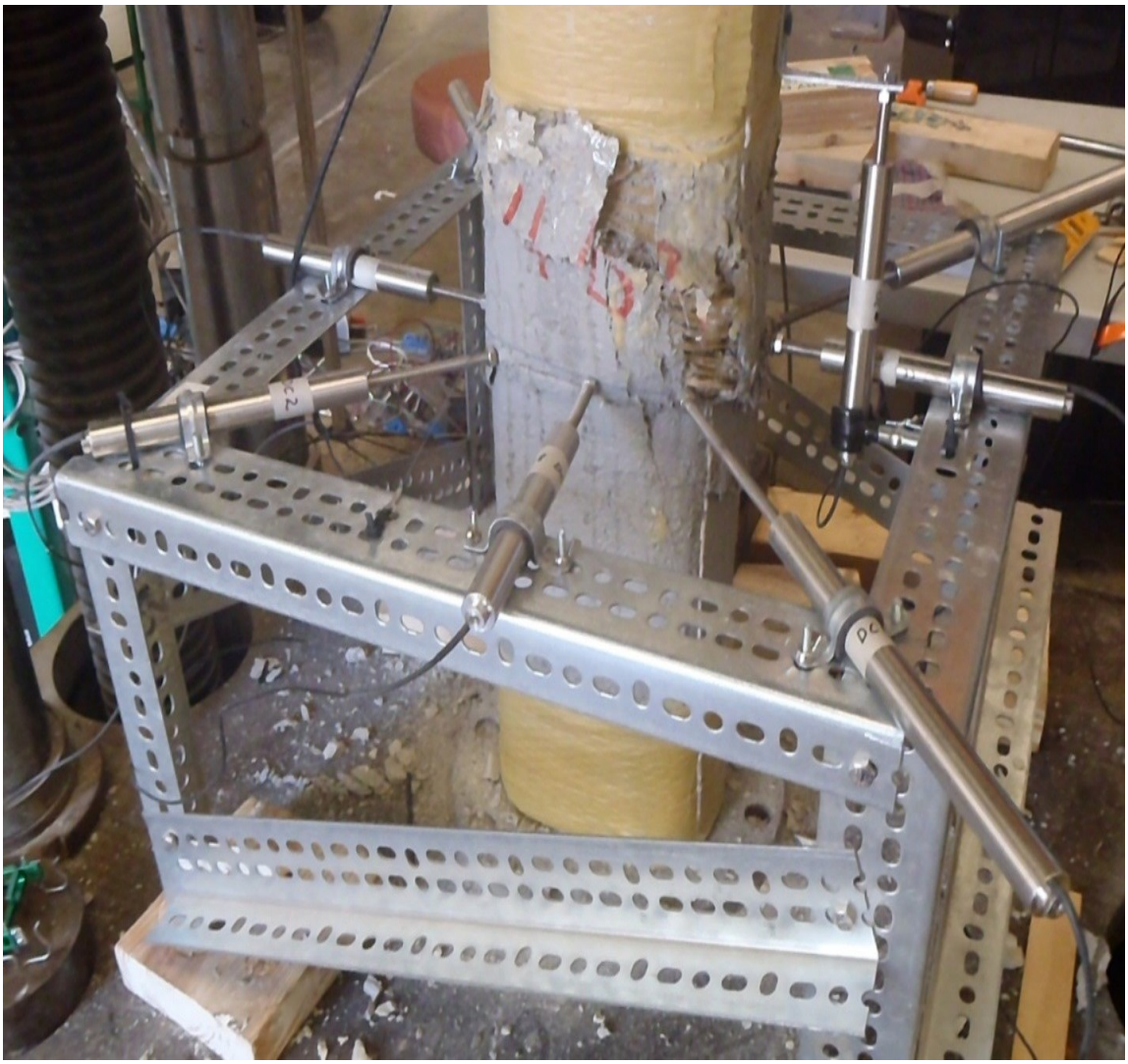

Fig. B-14: Failed PBO-FRCM wrapped rectangular column

Fig. B-15: Failed control column

APPENDIX C

STUDY 1: Specimen preparation, testing and results

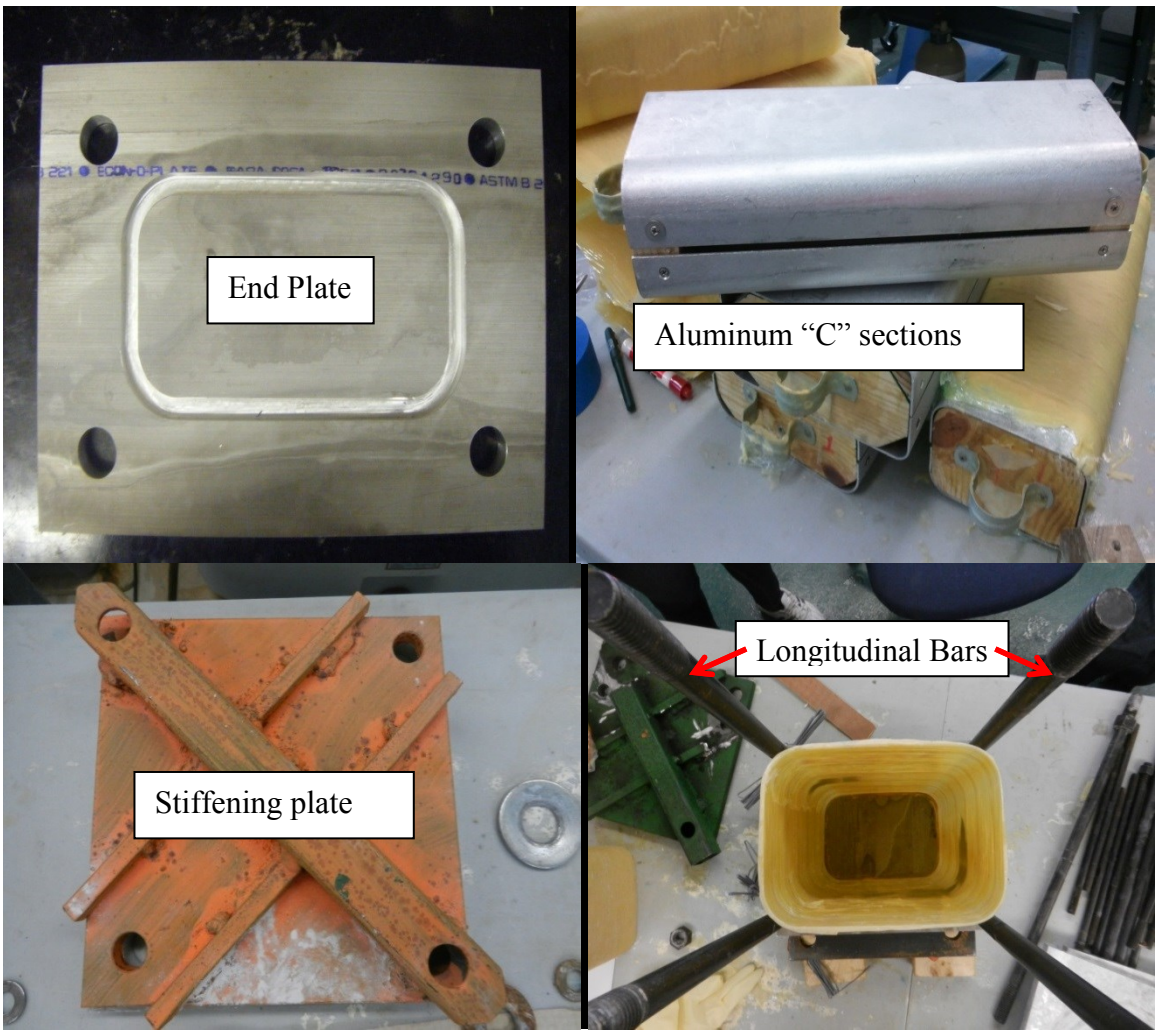

Fig. C-1: ICE methodology test rig components

Fig. C-2: Cutting glass fiber sheets

Fig. C-3: Aluminum "C" sections prepared for wrapping

Fig. C-4: Wet lay-up impregnation of glass fibers and wrapping of the aluminum "C" section

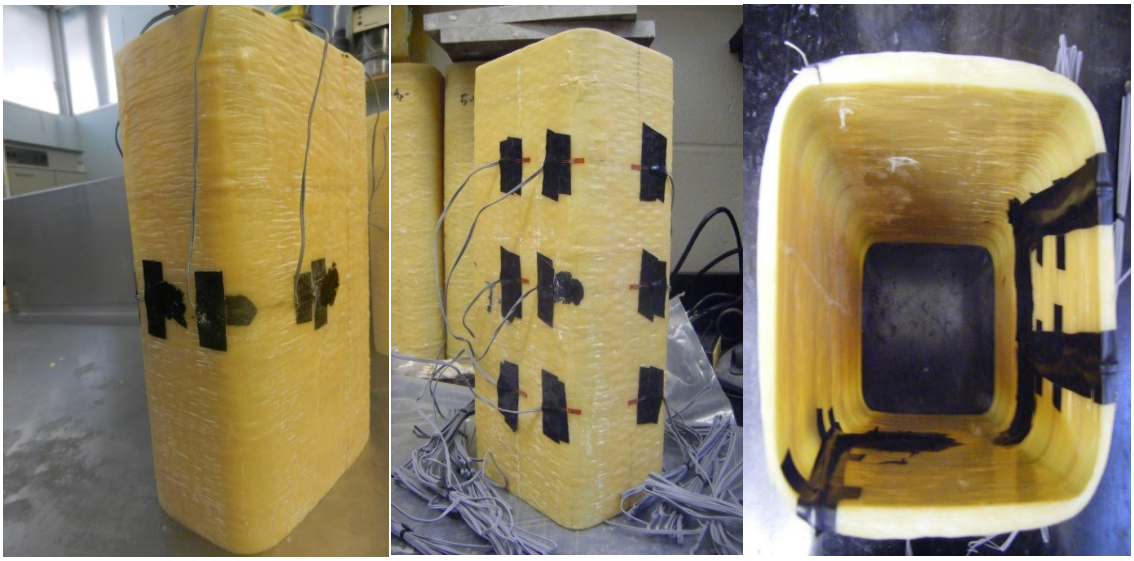

Fig. C-5: Strain gauge configuration for GFRP specimens

a) R_1.5_2_B **b) R_1.5_4_B** **c) R_1.5_6_B**

Fig. C-6: Failed sample 2-ply, 4-ply and 6-ply GFRP jackets

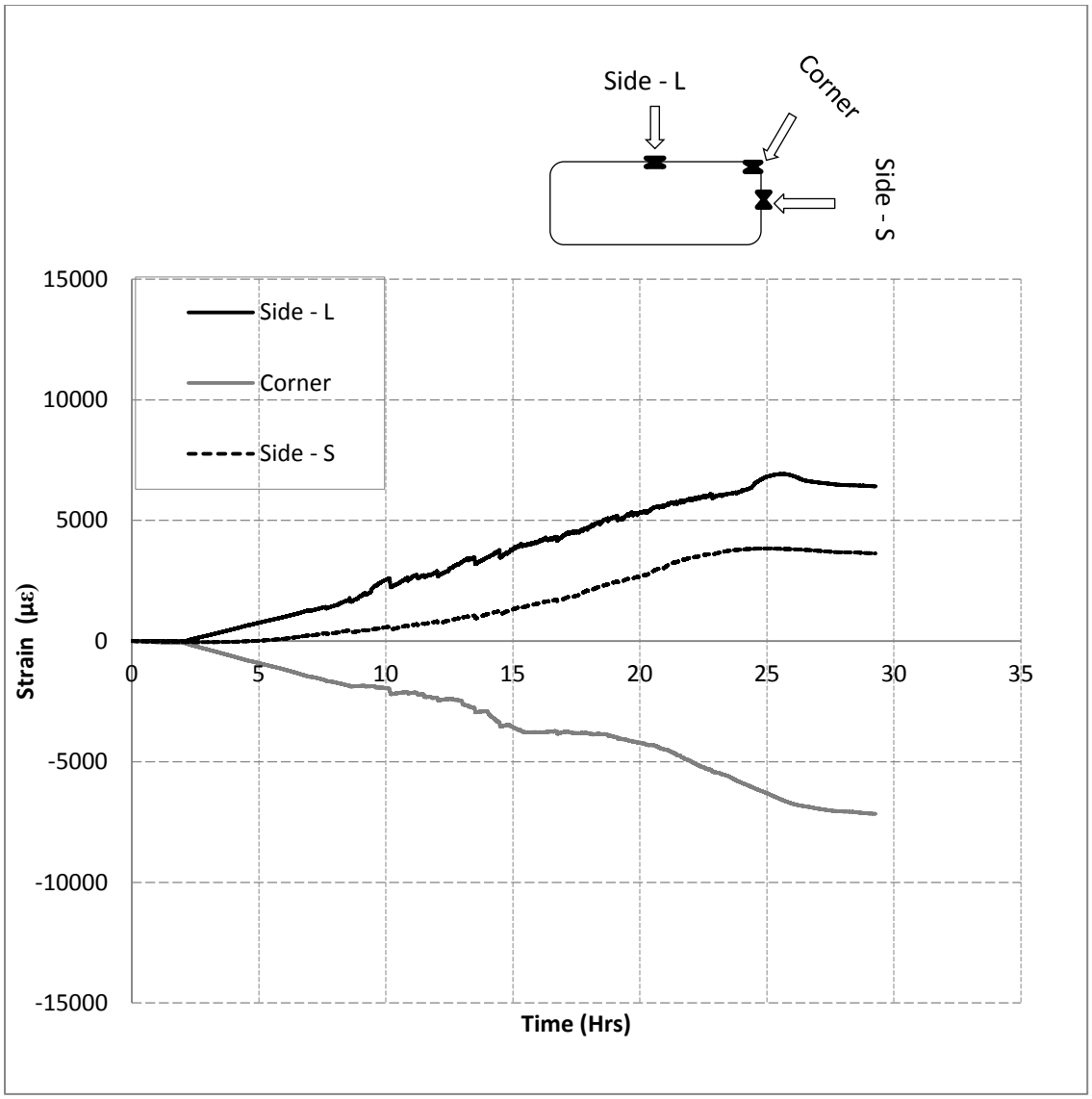

Fig. C-7: Circumferential strain vs. time (R_2.0_4_A)

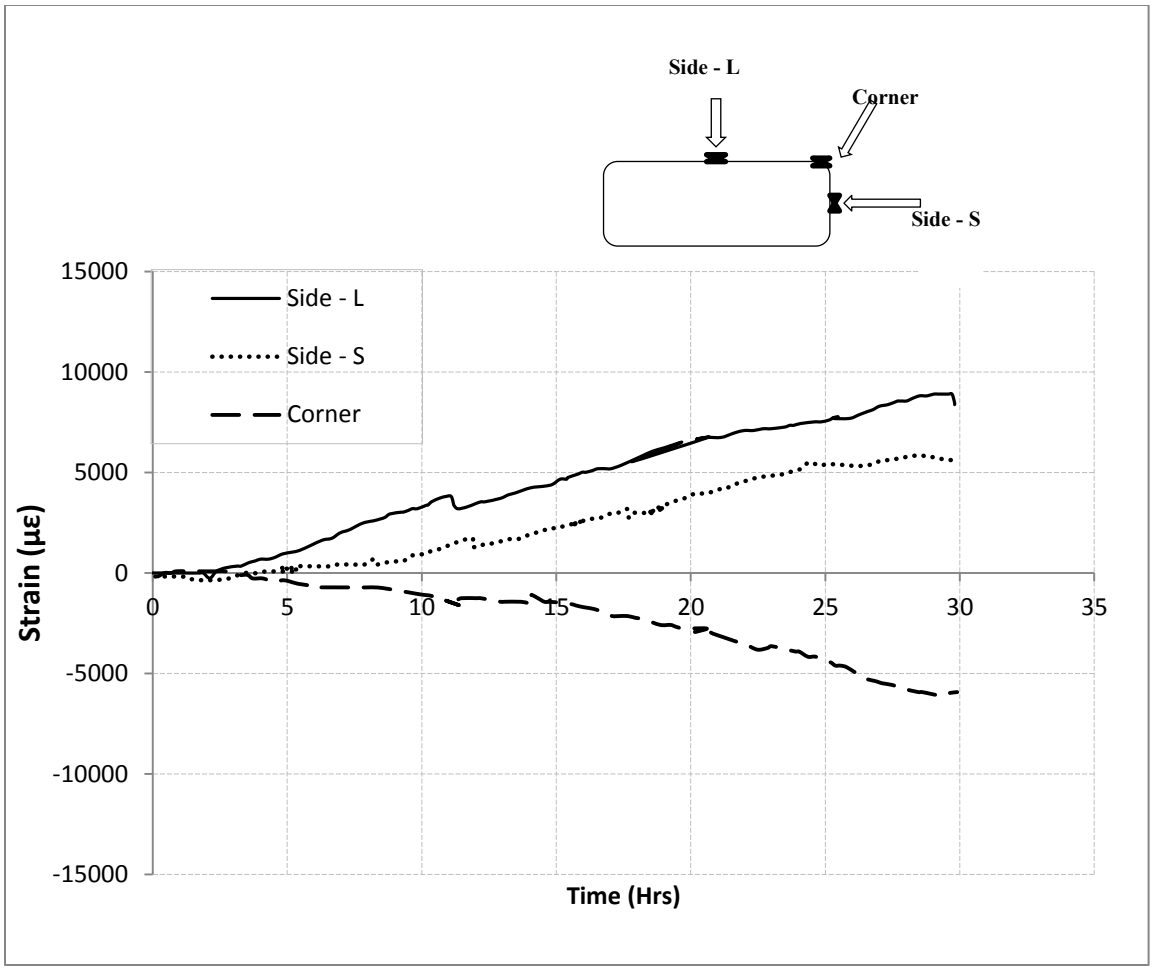

Fig. C-8: Circumferential strain vs. time (R_2.0_6_A)

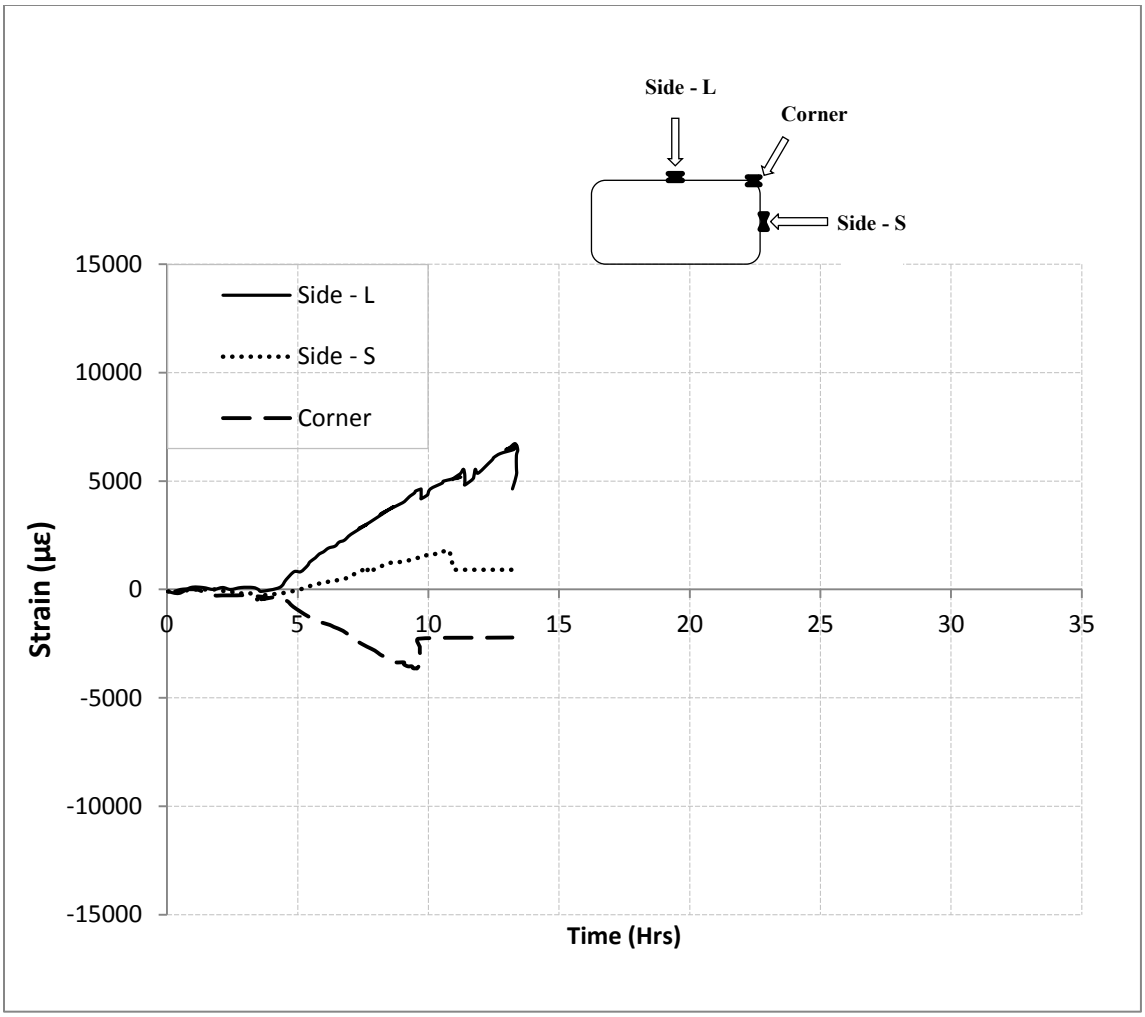

Fig. C-9: Circumferential strain vs. time (R_1.5_2_B)

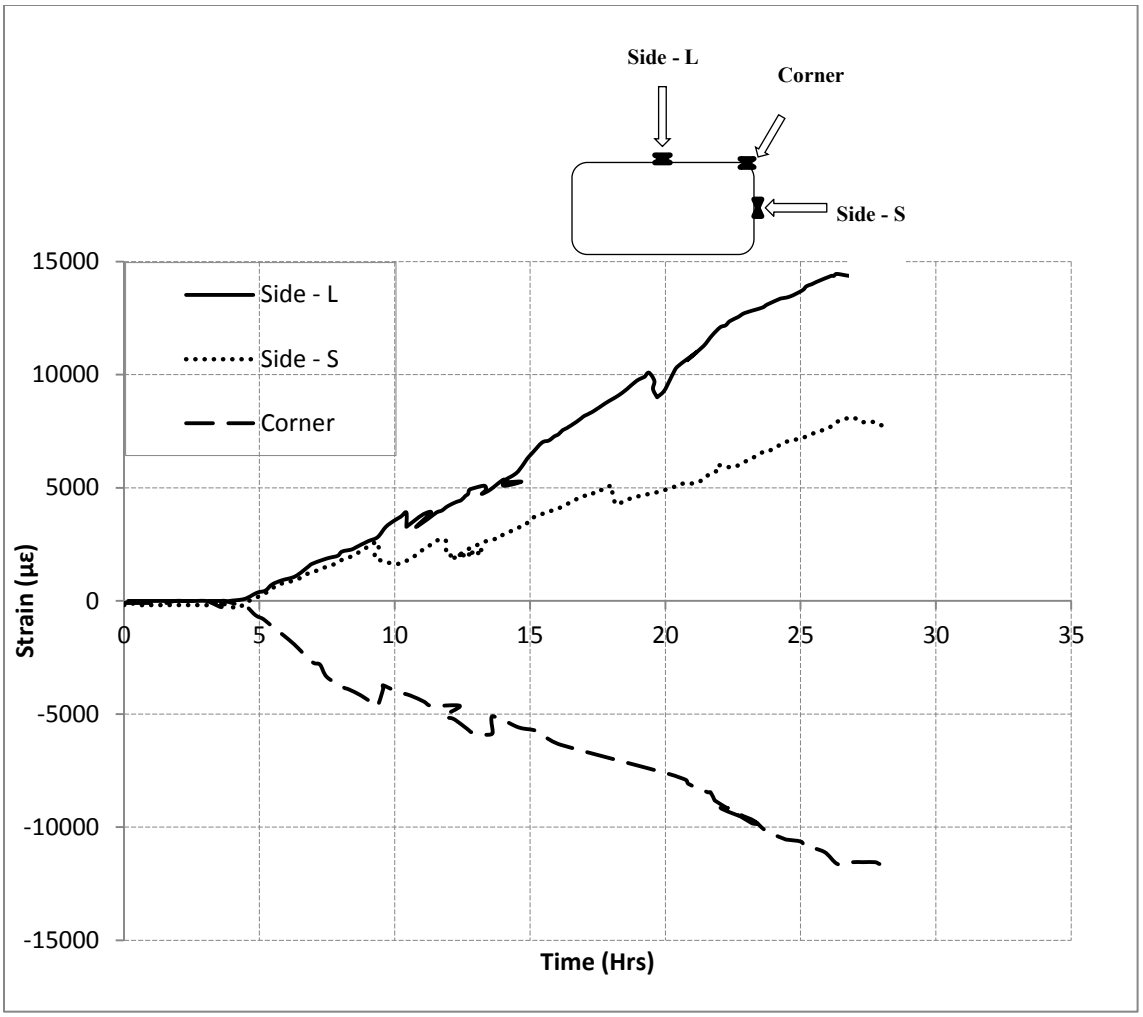

Fig. C-10: Circumferential strain vs. time (R_1.5_6_A)

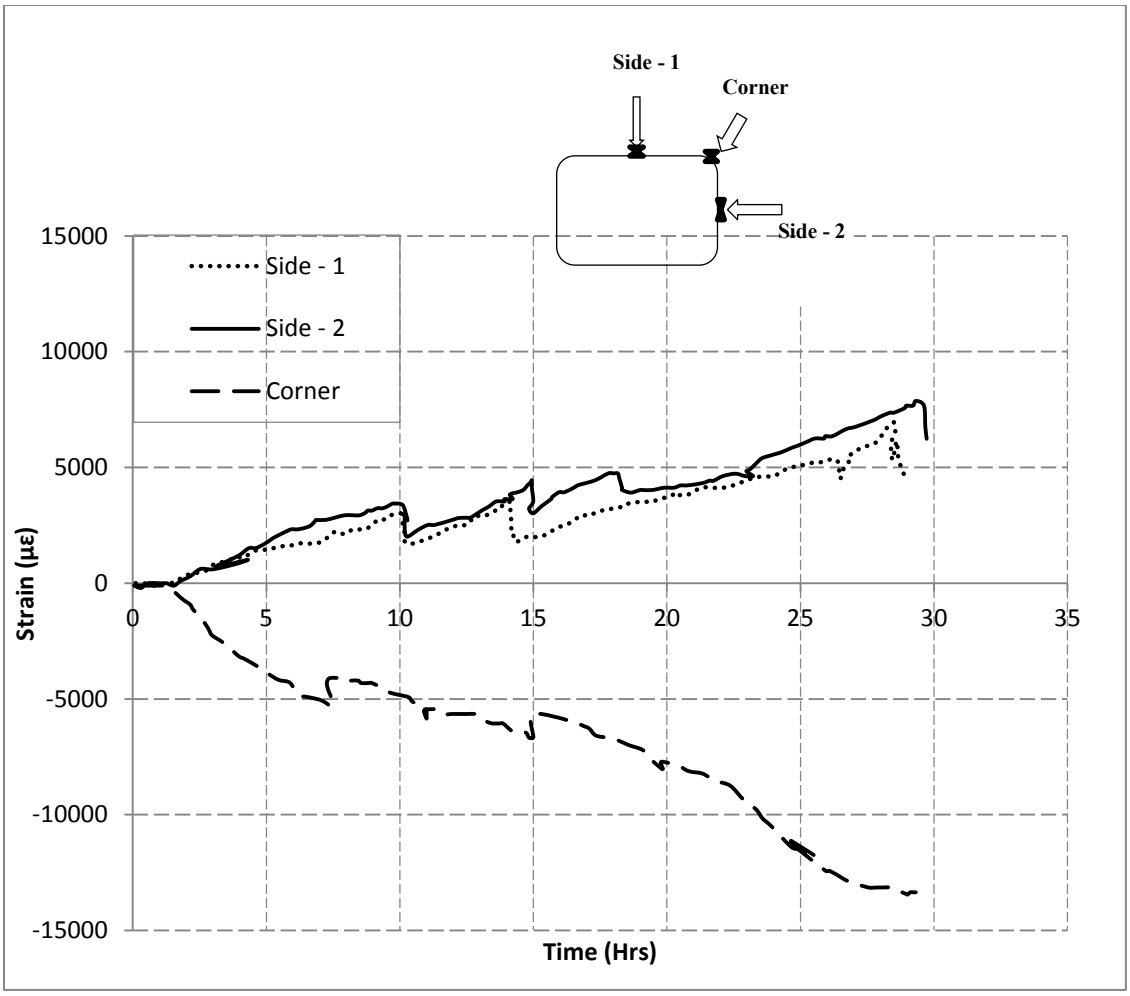

Fig. C-11: Circumferential strain vs. time (R_1.0_4_B)

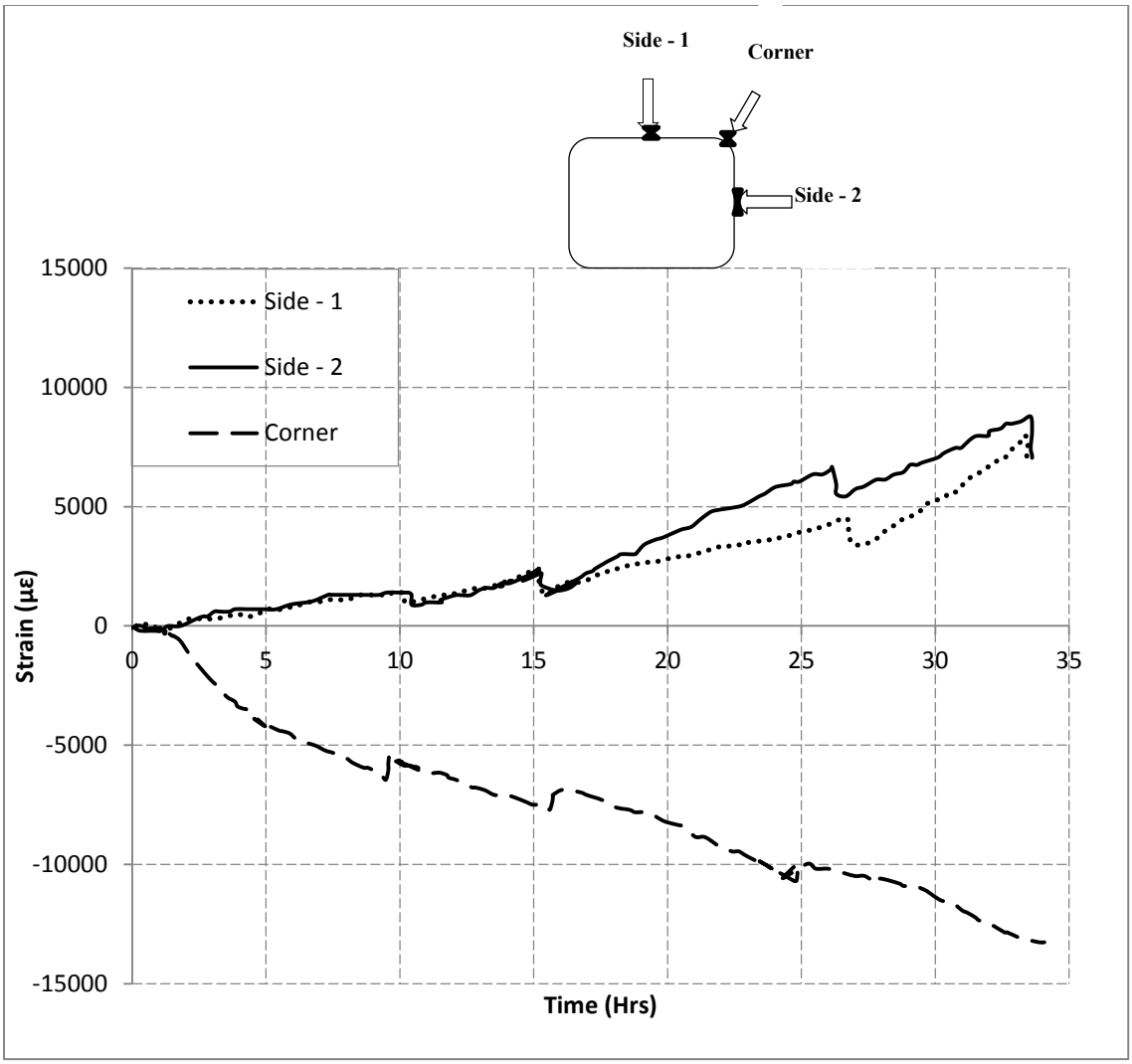

Fig. C-12: Circumferential strain vs. time (R_1.0_6_B)

Fig. C-13: Preparation of GFRP flat coupons

Fig. C-14: Curing of GFRP flat coupons and cutting the flat coupons in to standard sizes

REFERENCES

1. Abegaz A., Suaris W., De Luca A., and Nanni A. (2012). "Fiber reinforced cementitious matrix (FRCM) composites as confining systems for reinforced concrete columns." Proc. 10th International Symp. on Ferrocement and Thin Reinforced Cement Composites (FERRO 10), Havana, Cuba, October 12-17, 2012.

2. AC 434 (2011). "Acceptance criteria for masonry and concrete strengthening using fiber-reinforced cementitious matrix (FRCM) composite systems." ICC-Evaluation Service.

3. American Concrete Institute (ACI) Committee 549 (2013). "Design and construction guide of externally bonded FRCM systems for concrete and masonry repair and strengthening." American Concrete Institute, Farmington Hills, MI.

4. American Concrete Institute (ACI) Committee 440 (2004). "Guide test methods for fiber-reinforced polymers (FRPs) for reinforcing or strengthening of concrete structures." ACI 440.3R-04, Farmington Hills, MI.

5. American Concrete Institute (2008). "Building code requirements for structural concrete." ACI 318-11, Farmington Hills, MI.

6. American Society for Testing and Materials (ASTM) (2007). "Standard test method for compressive strength of hydraulic cement mortars (using 2-in. or [50-mm] cube specimens)." ASTM C 109, West Conshohocken, PA.

7. American Society for Testing and Materials (ASTM) (2005). "Standard test method for splitting tensile strength of intact rock core specimens." ASTM D 3967, West Conshohocken, PA.

8. American Society for Testing and Materials (ASTM) (2008). "Standard test method for apparent hoop tensile strength of plastic or reinforced plastic pipe by split disc method." ASTM D 2290, West Conshohocken, PA.

9. American Society for Testing and Materials (ASTM) (2008). "Properties of polymer matrix composite materials." ASTM D 3039, ASTM International, West Conshohocken, PA.

10. American Society for Testing and Materials (ASTM) (1968). "Standard test method for preparation and tension testing of filament-wound pressure vessels." ASTM D 2585, West Conshohocken, PA.

11. American Society for Testing and Materials (ASTM) (2008). "Standard test method for tensile properties of polymer matrix composite materials." ASTM D 3039, ASTM International, West Conshohocken, PA.

12. Arboleda D., Loreto G., De Luca A., and Nanni A. (2012). "Material characterization of fiber reinforced cementitious matrix (FRCM) composite laminates." Proc., 10th International Symp. on Ferrocement and Thin Reinforced Cement Composite (FERRO 10) , H. W. Rivas, L. P. Seoane and I. G. Castro, eds., Havana, Cuba, 29–37.

13. ASTM International (2005). "Standard test method for compressive strength of cylindrical concrete specimens." ASTM C 39, ASTM International, West Conshohocken, PA.

14. Balaguru P., and Kurtz S. (1998). "Use of inorganic polymer-fiber composites for repair and rehabilitation of infrastructures." In: Silva-Araya WF, deRincon OT, Pumarada O'Neill L, editors. Repair and rehabilitation of reinforced concrete structures: the state of the art, Reston, VA, American Society of Civil Engineers, 155-168.

15. Ballinger C., Maeda T., and Hoshijima T. (1993). "Strengthening of reinforced concrete chimneys, columns and beams with carbon fiber reinforced plastics." Proc. International Symp. Fiber-Reinforced-Plastic Reinforcement for Concrete Structures, Nanni, A., and Dolan, C. W., ed., ACI, SP 138, 233-247.

16. Bank L.C. (2006). "Composites for construction: structural design with FRP materials." John Wiley & Sons, New York, NY.

17. Bazant Z. P. (1984a). "Size effect in blunt fracture: concrete, rock, metal." Journal of Engineering Mechanics, ASCE, 110(4), 518–535.

18. Bazant Z. P., and Kwon Y. K. (1994). "Failure of slender and stocky reinforced concrete columns: Tests of size effect." Materials and Structures, 27, 79–90.

19. Chaallal O., Hassan M., and Shahawy M. (2003). "Confinement model for axially loaded short rectangular columns strengthened with fiber reinforced polymer wrapping." ACI Structural Journal, 100(2), 215–221.

20. Chaplin M. (2007). "Hexagonal ice structure." Water Structure and Science.

21. D'Ambrisi A., and Focacci F. (2011). "Flexural strengthening of RC beams with cement based composites." Journal of Composites for Construction, ASCE, 10.1061 /CC.1943-5614.0000218, 707–720.

22. D'Ambrisi A., Feo, L., and Focacci F. (2012). "Bond-slip relations for PBO-FRCM materials externally bonded to concrete." Composites Part B: Engineering, 43 (8), 2938–2949.

23. De Caso y Basalo F., Matta F., and Nanni A. (2012). "Fiber reinforced cement-based composite system for concrete confinement." Construction and Building Materials, Vol. 32, 55-65.

24. De Caso y Basalo F., Matta F., and Nanni A. (2009). "Fiber reinforced cementitious-matrix composites for infrastructure rehabilitation." Proc., Fiber Reinforced Polymer Reinforcement for Concrete Structures, FRPRCS-9, Sydney, Australia.

25. De Lorenzis L., and Tepfers R. (2003). "Comparative study of models on confinement of concrete cylinders with fiber-reinforced polymer composites." Journal of Composites for Construction, ASCE, 7(3), 219–237.

26. De Luca A., Nardone F., Matta F., Nanni A., Lignola G., and Prota A. (2011). "Structural evaluation of full-scale FRP-confined reinforced concrete columns." Journal of Composites for Construction, 15(1), 112–123.

27. Eisenberg D., and Kauzmann W. (1969). "The structure and properties of water." Oxford, The Clarendon Press, Chapter 3, Ice.

28. Fam A. Z., and Rizkalla S. H. (2001). "Confinement Model for axially loaded concrete confined by circular fiber-reinforced polymer tubes." ACI Structural Journal, 98(4), 451–461.

29. Fardis M. N., and Khalili H. (1982). "FRP-encased concrete as a structural material." Magazine of Concrete Research, 34(121), 191–202.

30. Fardis M. N., and Khalili H. (1981). "Concrete encased in fiberglass-reinforced plastic." ACI Journal of American Concrete Institute, 78(6), 440-446.

31. Fletcher N. H. (1970). "The chemical physics of ice." Cambridge University Press.

32. Fyfe E. R. (1995). "Testing and field performance of the high strength fiber wrapping system." Proc. Structures Congress XIII, ASCE, Boston, MA, 603-606.

33. Hadi M. N. S. (2005). "Behavior of FRP strengthened concrete columns under eccentric compression loading." Composite Structures, Vol. 77, 92-96.

34. Harajli M. H. (2006). "Axial stress-strain relationship for FRP confined circular and rectangular concrete columns." Cement and Concrete Composites, 28(10), 938–948.

35. Harries K. A., and Kharel G. (2002). "Behavior of variably confined concrete." ACI Materials Journal, 99(2), 180-189.

36. ISIS Canada (2006b). "ISIS educational module 3: An introduction to FRP-reinforced concrete." ISIS Canada Resource Centre.

37. Johnson A. K, Cohen D., Hansen M. F., and Toombes Y. T. (1995). "Pressurized ring test for composite pressure vessel hoop strength and stiffness evaluation." Journal of Composites Technology and Research, 17(4), 331-340.

38. Katsumata H., and Yagi K. (1990). "Applications of retrofit method with carbon fiber for existing reinforced concrete structures." Proc. 22nd Joint UJNR Panel Meeting on Repair and Retrofit of Existing Structures, National Institute for Standards and Testing (NIST), Gaithersburg, MD.

39. Kurt C. E. (1978). "Concrete-filled structural plastic columns." Journal of Structural Engineering, ASCE, 104(1), 55-63.

40. Kurtz S., and Balaguru P. (2001). "Comparison of inorganic and organic matrices for strengthening of RC beams with carbon sheets." Journal of Structural Engineering, 127(1), 35-42.

41. Lahlou K., Artin P. C., and Chaallal O. (1992). "Behavior of high-strength concrete under confined stresses." Cement & Concrete Composites, 14, 185-193.

42. Lam L., and Teng J. G. (2003). "Design-oriented stress–strain model for FRP-confined concrete." Journal of Construction and Building Materials, 17(6-7), 471-489.

43. Lam L., and Teng J. G. (2004). "Ultimate condition of fiber reinforced polymer-confined concrete." Journal of Composites for Construction, ASCE, 8(6), 539-548.

44. Lam, L., and Teng J. G. (2003b). "Design-oriented stress-strain model for FRP-confined concrete in rectangular columns." Journal of Reinforced Plastics and Composites, 22(13), 1149–1186.

45. Lignola G. P., Prota A., Manfredi G., and Cosenza E. (2008). "Effective strain in FRP jackets on circular RC columns." Fourth International Conference on FRP Composites in Civil Engineering (CICE), Zurich, Switzerland.

46. Mander J. B., Priestley M. J. N., and Park R. (1988). ''Theoretical stress-strain model for confined concrete.'' Journal of Structural Engineering, 114(8), 1804–1826.

47. Mason B. J., Bryant G. W., and Van den Heuval A. P. (1963). "Growth habits and surface structure of ice crystals." Philosophical Magazine, 8, 505–509.

48. Matthys S., Toutanji H., Audenaert K., and Taerwe L. (2005). "Axial load behavior of large-scale columns confined with fiber-reinforced polymer composites." ACI Structural Journal, 102(2), 258–267.

49. Mirmiran A., Shahawy M., Samaan M., El Echary H., Mastrapa J. C., and Pico O. (1998). "Effect of column parameters on FRP-confined concrete." Journal of Composites for Construction, ASCE, 2(4), 175-185.

50. Mirmiran A. (1997). ‘‘Analytical and experimental investigation of reinforced concrete columns encased in fiberglass tubular jackets and use of fiber jacket for pile splicing.’’ Final Rep., Contract No. B-9135, Florida Dept. of Transportation, Tallahassee.

51. Mirmiran A. (1998). “Length effects on FRP-reinforced concrete columns.” Proc. of the 2nd International Conference on Composites in Infrastructure, Tucson, AZ, 518-532.

52. Mirmiran A., and Shahawy M. (1997). “Behavior of concrete columns confined by fiber composite.” Journal of Structural Engineering, 123(5), 583–590.

53. Mirmiran A., Shahawy M., Samaan, M., El Echary H., Mastrapa J. C., and Pico O. (1998b). “Effect of column parameters on FRP-confined concrete.” Journal of Composites for Construction, ASCE, 2(4), 175–185.

54. Nanni A. (2012). “FRCM strengthening - a new tool in the concrete and masonry repair toolbox.” Concrete International Design and Construction, 34 (4), 43–49.

55. Nanni A., and Bradford N. M. (1995). “FRP jacketed concrete under uniaxial compression.” Construction Building Materials, 9(2), 115–124.

56. Nanni A. (2001). “Relevant applications of FRP composites in concrete structures.” Proceedings Composites in Construction (CCC 2001), J. Figueiras, L. Juvandes and R. Furia, eds., (invited), Porto, Portugal, 661-670.

57. Nanni A., and Dolan C. W., Editors. (1993). “FRP reinforcement for concrete structures.” Proc. ACI SP-138, American Concrete Institute, Detroit, MI.

58. Nielsen L. E., and Landel R. F. (1994). “Mechanical properties of polymers and composites.” Marcel Dekker.

59. Papakonstantinou C., and Balaguru P. (2006). “Bond characteristics and structural behavior of inorganic polymer FRP. In: Measuring, monitoring and modeling concrete properties.” Dordrecht, Netherlands, Springer Netherlands, 735-741.

60. Pessiki S., Harries K. A., Kestner J. T., Sause R., and Ricles J. M. (2001). “Axial behavior of reinforced concrete columns confined with FRP jackets.” Journal of Composites for Construction, ASCE, 5(4), 237–245.

61. Petrenko V. F., and Whitworth R. W. (1995). “Physics of ice.” Oxford University Press.

62. Picher F., Rochette P., and Labossière P. (1996). "Confinement of concrete cylinders with CFRP." Proc. of the 1st International Conference on Composites in Infrastructure, H. Saadatmanesh and M. R. Ehsani, eds., University of Arizona, Tucson, Arizona, 829-841.

63. Richart F. E., Brandtzaeg A., and Brown R. L. (1928). "A study of the failure of concrete under combined compressive stresses." Bulletin No. 185, University of Illinois, Engineering Experimental Station, Urbana, ILL.

64. Rocca S., Galati N., and Nanni A. (2006). "Experimental evaluation of FRP strengthening of large size reinforced concrete columns." Center for Infrastructure Engineering Studies (CIES), Report No. 06-63, University of Missouri-Rolla, Rolla, MO.

65. Rocca S., Galati N., and Nanni A. (2008). "Review of design guidelines for FRP confinement of reinforced concrete columns of non-circular cross sections." Journal of Composites for Construction, ASCE, 12(1), 80-92.

66. Rochette P., and Labossière P. (2000). "Axial testing of rectangular column models confined with composites." Journal of Composites for Construction, ASCE, 4(3), 129-136.

67. Saadatmanesh H., Ehsani M. R., and Jin L. (1996). "Seismic strengthening of circular bridge pier models with fiber composites." ACI Structural Journal, 93(6), 639-647.

68. Saadatmanesh H., Ehsani M. R., and Li M. W. (1994). "Strength and ductility of concrete columns externally reinforced with fiber composite straps." ACI Structural Journal, 91(4), 434-447.

69. Samaan M., Mirmiran A., and Shahawy M. (1998). ''Model of concrete confined by fiber composites.'' Journal of Structural Engineering, ASCE, 124(9), 1025–1031.

70. Seible F., Burgueno R., Abdallah M. G., and Nuismer R. (1996). "Development of advanced composite carbon shell systems for concrete columns in seismic zones." Proc., 11th World Conf. on Earthquake Engineering, Pergamon–Elsevier Science, Paper No. 1375, Oxford, U.K.

71. Seible F., Priestley M. J. N., Hegemier G., and Innamorato D. (1997). "Seismic retrofitting of RC columns with continuous carbon fiber jackets." Journal of Composites for Construction, ASCE, 1(2), 52–62.

72. Shehata L. A. E. M., Carneiro L. A. V., and Shehata L. C. D. (2002). "Strength of short concrete columns confined with CFRP sheets." Materials and Structures, 35, 50–58.

73. Spoelstra M. R., and Monti G. (1999). "FRP-confined concrete model." Journal of Composites for Construction, ASCE, 3(3), 143-150.

74. Taerwe L., ed. (1995). "Non-metallic (FRP) reinforcement for concrete structures." Proc. of the 2nd International RILEM Symposium (FRPRCS-2).

75. Tan K. H. (2002). "Strength enhancement of rectangular RC columns using FRP." Journal of Composites for Construction, ASCE, 6(3), 175–183.

76. Teng J. G., Huang Y. L., Lam L., and Ye L. P. (2007). "Theoretical model for fiber reinforced polymer-confined concrete." Journal of Composites for Construction, ASCE, 11(2), 201-210.

77. Teng J. G., and Lam L. (2004). "Behavior and modeling of fiber reinforced polymer-confined concrete." Journal of Structural Engineering, 130(11), 1713–1723.

78. Teng J. G., Jiang T., Lam, L., and Luo Y. Z. (2009). "Refinement of a design-oriented stress–strain model for FRP-confined concrete." Journal of Composites for Construction, ASCE, 13(4), 269-278.

79. Toutanji H., Han M., Gilbert J., and Matthys S. (2010). "Behavior of large-scale rectangular columns confined with FRP composites." Journal of Composites for Construction, ASCE, 14(1), 62-71.

80. Toutanji H. (1999). "Stress-strain characteristics of concrete columns externally confined with advanced fiber composite sheets." ACI Materials Journal, 96(3), 397-404.

81. Toyobo Co., Ltd. (2005). "PBO fibers - zylon technical information." Osaka, Japan.

82. Triantafillou T. C., and Papanicolaou C. G. (2006). "Shear strengthening of reinforced concrete members with textile reinforced mortar (TRM)." Materials and Structures, 39 (1), 93–103.

83. Walsh E. J., and Adams D. O. (2008). "Development and evaluation of the quadrant ring test method." Journal of Experimental Mechanics, 48(3), 319-326.

84. Wang L. M., and Wu Y. F. (2008). "Effect of corner radius on the performance of CFRP-confined square concrete columns: Test." Journal of Engineering Structures, 30(2), 493-505.

85. Wu H. C., and Sun P. (2005). "Fiber reinforced cement based composite sheets for structural retrofit." In: Chen J. F., Teng J. G., ed. Proc. of the International Symp. on Bond Behavior of FRP in Structures. Hong Kong, PRC: International Institute for FRP in Construction, 343-348.

86. Wu H. C., and Teng J. (2002). "Innovative cement based thin sheet composites for retrofit." In: Proc. of the 3rd International Conference on Composites in Infrastructure (ICCI'02), San Francisco, CA, June 10-12.

87. Xiao Y., and Wu H. (2000). "Compressive behavior of concrete confined by carbon fiber composite jackets." Journal of Materials in Civil Engineering, 12(2), 139–146.

88. Xiao Y., Martin G. R., Yin Z., and Mar R. (1996). "Seismic retrofit of reinforced concrete bridge columns using a prefabricated composites wrapping system." Proc. 1st Int. Conf. Composites in Infrastructure, Saadatmanesh, H., and Ehsani, M. R., ed., Tucson, AZ., 903-916.

89. Yang X., Nanni A., and Chen G. (2001). "Effect of corner radius on performance of externally bonded FRP reinforcement." Non-Metallic Reinforcement for Concrete Structures, FRPRCS-5, Cambridge, 197-204.

90. Yang X., Wei J., Nanni A., and Dharani L. R. (2004). "Shape effect on the performance of carbon fiber reinforced polymer wraps." Journal of Composites for Construction, ASCE, 8(5), 444-451.

91. Yang X., Nanni A., and Chen G. (2001). "Effect of corner radius on performance of externally bonded FRP reinforcement." Non-Metallic Reinforcement for Concrete Structures, FRPRCS-5, Cambridge, UK.